THE SYNTHESIS, REACTIVITY AND APPLICATION OF FUNCTIONALIZED ALKYL TRANSITION METAL COMPLEXES

A thesis submitted to the

University of Cape Town

in fulfilment of the requirements for the degree of

Doctor of Philosophy

by

YI-HSIEN LIAO

B. Sc

Department of Chemistry

University of Cape Town

Rondebosch 7700

South Africa

August 1994

THE SYNTHESIS, REACTIVITY AND APPLICATION OF FUNCTIONALIZED ALKYL TRANSITION METAL COMPLEXES

YI-HSIEN LIAO

Dedicated to my dear father and mother

Ben-Tein and Chen-May

ACKNOWLEDGEMENTS

My sincere thanks and appreciation go to:

My supervisor, Professor John R. Moss, for his intelligent direction and support throughout the study.

My colleagues in the organometallic research group: Dr. Jo-Ann Andersen and Meredith Timme for proof reading this manuscript; Fazlin Waggie and Robyn George for experimental assistance; Oliver Hill for help with computer matters; Earl Starr, Jacques Maré, Renqiang Zeng and Xiaolong Yin for helpful discussion.

I thank all the help from the following people:

Margie Nair and Noel Hendricks for recording many NMR spectra;

Riana Mohamed for recording the DSC traces;

Dr. Boshoff and the University Chemical Laboratory, Cambridge (England) for recording the FAB mass spectra;

The microanalysis laboratory at U.C.T. and the CSIR (Pretoria) for the microanalyses;

Professor G. E. Jackson for some helpful discussion on NMR spectra;

Dr. Alan Hutton for the cyclic voltammetry;

Dr. Charles Marais for the Hyperchem® computer software.

I also thank the Foundation for Research Development (FRD) and the University of Cape Town for the financial support during this work.

ABSTRACT

Haloalkyl transition metal complexes can be precursors for a wide range of useful complexes. In Chapter 1, the bromohexyl iron complex, $[CpFe(CO)_2\{(CH_2)_6Br\}]$ has been prepared and new information on electrochemical and thermal behaviour of $[CpFe(CO)_2\{(CH_2)_6Br\}]$ has been obtained from cyclic voltammetry and differential scanning calorimetry respectively. The chemical reactivity of $[CpFe(CO)_2\{(CH_2)_6Br\}]$ with various reagents including NaOMe, a cobaloxime anion, MeLi, NaN_3, magnesium metal, phenol derivatives (phenol, resorcinol, 4-hydroxybenzyl alcohol and 3,5-dihydroxybenzyl alcohol), trityl salt, PPh_3, and $CO/AgBF_4$ has also been studied. The new complexes that we obtained are namely: $[CpFe(CO)(L)\{C{=}O(CH_2)_6Br\}]$ (L = CO and PPh_3) from the reactions with $CO/AgBF_4$ and PPh_3 respectively, $[CpFe(CO)_2\{CH_2{=}CH(CH_2)_4Br]PF_6$ from the reaction with the trityl salt, and ω-functionalized hexyl iron complexes. All these new complexes have been characterized by standard analytical and spectroscopic methods. The results showed that chemoselective reactions of $[CpFe(CO)_2\{(CH_2)_6Br\}]$ can occur at either the metal centre or the ω-functional group. The results are also compared to those obtained for alkyl and functionalized alkyl iron complexes.

In Chapter 2, a series of new ω-hydroxyalkyl transition metal complexes of the type $[L_mM\{(CH_2)_nOH\}]$ (where $L_mM = CpFe(CO)_2$, $Cp^*Fe(CO)_2$ and $CpRu(CO)_2$; n = 2, 3 and 4), have been prepared. These new complexes have been characterized by microanalysis, IR, ^1H, ^{13}C NMR and mass spectroscopy. The unusually high CO absorption bands of $[CpFe(CO)_2\{(CH_2)_2OH\}]$ in IR spectroscopy are discussed. Also, significantly low chemical shifts of α carbons in ω-hydroxypropyl metal complexes were observed in ^{13}C NMR spectra. This effect has been investigated by comparison with a series of ω-functionalized propyl iron complexes and a new mode of interaction

between iron and ω-functional group is proposed. The mass spectrum of $[CpFe(CO)_2\{(CH_2)_2OH\}]$ shows a new fragmentation pathway and this is discussed.

In Chapter 3, the reactivity of $[CpFe(CO)_2\{(CH_2)_3OH\}]$ with various reagents, including silyl chlorides (Me_3SiCl, *t*-$BuMe_2SiCl$ and *t*-$BuPh_2SiCl$), PPh_3/CBr_4, 4-nonyloxybenzoyl chloride, Ph_3CPF_6 and PPh_3 is described. Cyclic voltammetry and differential scanning calorimetry are also employed to investigate the electrochemical behaviour and the thermal properties of $[CpFe(CO)_2\{(CH_2)_3OH\}]$. The results are compared with those obtained for $[CpFe(CO)_2\{(CH_2)_6Br\}]$.

In Chapter 4, we describe the synthesis of a series of new organometallic dendrimers. These dendrimers have been prepared by the convergent approach and contain organometallic functional groups, namely $CpRu(CO)_2$, which lie exclusively at the surface of the dendritic structure. The construction of theses dendrimers starts from the reaction of haloalkyl metal complexes, $[CpM(CO)_2\{(CH_2)_3Br\}]$ (M = Fe and Ru), with the building block 3,5-dihydroxybenzyl alcohol, followed by the activation reaction with PPh_3/CBr_4 to give the first generation dendritic wedge. Through consecutive reaction cycles, we have prepared a dendritic wedge up to the fourth generation. This reacts with 1,1,1-tris(4-hydroxyphenyl)ethane to give a fourth generation dendrimer. This dendrimer contains 48 ruthenium metal atoms, and has a nominal molecular weight of 18438 amu. As far as we know, this dendrimer is the largest organotransition metal complex ever prepared. The thermal properties of the series of dendrimers have also been studied by differential scanning calorimetry and the results are discussed.

The experimental details are given in Chapter 5.

PUBLICATIONS

Papers:

1. "The synthesis, characterization and properties of long chain alkyl complexes of the type [CpM(CO)$_2$R] (Cp = η^5-C_5H_5; M = Fe or Ru; R = n-C_6H_{13} to n-$C_{12}H_{25}$)" A. Emeran, M. A. Gafoor, J. K. I. Goslett, Y.-H. Liao, L. Pimble and J. R. Moss, *J. Organomet. Chem.*, 1991, 405, 237-246

2. "Synthesis and characterization of some new cobaloximes, including the first members of a new class of heterobimetallic cobaloxime complexes. Crystal structure of [{η^6-$C_6H_5CH_2$Co(DH)$_2$(Py)}Cr(CO)$_3$]" M. R. Domingo, A. Irving, Y.-H. Liao, J. R. Moss and A. Nash, *J. Organomet. Chem.*, 1993, 443, 233-240

3. "Ruthenium-containing Organometallic Dendrimers" Y.-H. Liao and J. R. Moss, *J. C. S. Chem. Commun.*, 1993, 1774-1777

Conference contributions:

1. Poster titled "A study of chemical reactivity of [CpFe(CO)$_2${(CH$_2$)$_6$Br}]' Y.-H. Liao and J. R. Moss, presented at "Catalysis and Catalytic Process" in Gordons Bay, RSA (1990)

2. Short talk and poster titled "Synthesis and characterization of hydroxyalkyl iron complexes [CpFe(CO)$_2${(CH$_2$)$_n$OH}] n = 2, 3, 4" Y.-H. Liao and J. R. Moss, presented at the 31st Convention of the South African Chemical Institute, in Grahamstown, RSA (1991)

3. Poster titled "Synthesis of model complexes for oxygenates formation in Fischer-Tropsch process" Y.-H. Liao and J. R. Moss, presented at "Catalysis and Catalytic Process", in Golden Gate National Park, RSA (1991)

4. Oral presentation titled "Organometallic dendrimers" J. R. Moss and Y.-H. Liao, at XVI International Conference of Organometallic Chemistry, Brighton, England (1994)

ABBREVIATIONS

COSY	correlated spectroscopy
Cp	cyclopentadienyl
Cp*	pentamethylcyclopentadienyl
CV	cyclic voltammetry
DMG	dimethylglyoxime
DSC	differential scanning calorimetry
EI	electron impact
EPR	electron paramagnetic resonance spectroscopy
Et	ethyl
FAB	fast atom bombardment
HETCOR	heteronuclear correlation
IR	infrared spectroscopy
MA	microanalysis
Me	methyl
MS	mass spectrometry
NMR	nuclear magnetic resonance spectroscopy
P^+	parent molecular ion
Ph	phenyl
n-Pr	n-propyl
iso-Pr	iso-propyl
Py	pyridine
TBAP	tetrabutylammonium perchlorate
THF	tetrahydrofuran
trityl	triphenyl carbenium

TABLE OF CONTENTS

CHAPTER 1 A STUDY ON THE CHEMICAL REACTIVITY, ELECTROCHEMICAL BEHAVIOUR AND THERMAL PROPERTIES OF $[CpFe(CO)_2\{(CH_2)_6Br\}]$

1.1 INTRODUCTION

The first known haloalkyl transition metal complexes were reported independently by Green and Pettit in 1966 [1, 2]. Since then many complexes of the type, $[L_mM\{(CH_2)_nX\}]$ (where L_mM = transition metal and its associated ligands, X = halogen), have been synthesized. A comprehensive review on transition metal haloalkyl complexes has been published recently [3].

It has been shown that haloalkyl transition metal complexes can be precursors of a wide range of useful compounds, such as, heterobimetallic hydrocarbon bridged complexes which can serve as models for hydrocarbon intermediates on catalyst surfaces [4 - 9].

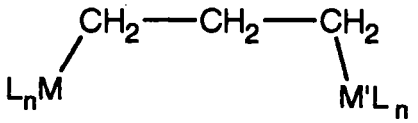

hydrocarbon bridged complex

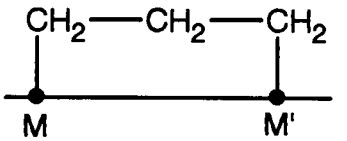

catalyst surface

Also, in some cases, haloalkyl metal complexes can be precursors for cyclic carbene complexes [4, 10 - 13], or decompose to give cycloalkanes [14, 15].

As we know so far, most of the studies on the chemical reactivity of haloalkyl transition metal complexes were carried out on either halomethyl or halopropyl metal complexes.

The longer chain ones, such as bromohexyl metal complexes, are however far less studied. Haloalkyl metal complexes have been a long term project in our laboratories. Previous studies have shown that it is possible to manipulate the functional group on the hydrocarbon chain without affecting the metal group at the other end of chain [16]. Thus a series of iodoalkyl metal complexes has been synthesized in this fashion, as shown in Equation 1.1.

$$[CpFe(CO)_2\{(CH_2)_nBr\}] + NaI \longrightarrow [CpFe(CO)_2\{(CH_2)_nI\}] + NaBr$$

$n = 3 - 10$

Equation 1.1

The haloalkyl metal complexes can simply be regarded either as functionalized alkyl metal complexes or as metal substituted alkyl halides. Thus, reactions of $[CpFe(CO)_2\{(CH_2)_6Br\}]$ **(1)** may take place either at the metal centre or at the other end of hydrocarbon chain. In this Chapter we look into the chemical reactivity of the bromohexyl iron complex **(1)** toward various nucleophiles, and compare the selectivity and reactivity of **(1)** with its various analogues. The effects of hydrocarbon chain length on the chemical reactivities of bromoalkyl iron complexes will also be discussed. Various techniques, such as cyclic voltammetry and differential scanning calorimetry, have also been used to obtain new information about the electrochemical and thermal properties of **(1)**.

1.2 THE CHEMICAL REACTIVITY OF $[CpFe(CO)_2\{(CH_2)_6Br\}]$ (1)

1.2.1 Reaction with sodium methoxide

The complex $[CpFe(CO)_2\{(CH_2)_6Br\}]$ **(1)** reacts with sodium methoxide in the refluxing methanol to give the complex $[CpFe(CO)_2\{(CH_2)_6OCH_3\}]$ **(2)** in 68% yield. The reaction is shown in Equation 1.2.

$$[CpFe(CO)_2\{(CH_2)_6Br\}] + NaOCH_3 \longrightarrow [CpFe(CO)_2\{(CH_2)_6OCH_3\}] + NaBr$$
(2)

Equation 1.2

The resulting complex **(2)** was obtained as a yellow oil. It is stable at room temperature, and can be purified by column chromatography.

In the case of organic alkyl bromides, sodium methoxide acts as a strong base, and under the conditions described above, dehydrobromination would take place to give alkenes [17]. Also, it has been reported that sodium methoxide can react with metal carbonyls, $M(CO)_5$ (M = Fe, Ru, Os), to give methoxycarbonyl derivatives $[M(CO)_4(CO_2CH_3)]^-$ [18]. However we observed none of the above mentioned type of reactions on work-up of the reaction mixture.

The new complex **(2)** was fully characterized by standard spectroscopic methods. The ^1H NMR spectrum of **(2)** showed a singlet and a triplet resonance at δ 3.29 and 3.33 ppm respectively; these resonances indicate that the methoxide group has replaced the bromo group at the end of alkyl chain. The mass spectrum of **(2)** also showed a (P+1) peak at the 293 mass units, which further confirmed the formulation of **(2)**. Further characterization data for **(2)** are given in the experimental section (Chapter 5).

1.2.2 Reaction with the cobaloxime anion

The cobaloxime anion $[Co(DMG)_2(Py)]^-$, regarded as a "supernucleophile" is generated by reduction of $[ClCo(DMG)_2(Py)]$ with $NaBH_4$. It reacts readily with $[CpFe(CO)_2\{(CH_2)_6Br\}]$ **(1)** to give the heterobimetallic complex $[CpFe(CO)_2(CH_2)_6Co(DMG)_2(Py)]$ **(3)** in 61% yield. The reaction is shown in Equation 1.3.

$$[CpFe(CO)_2\{(CH_2)_6Br\}] + [ClCo(DMG)_2(Py)] \xrightarrow{NaBH_4} [CpFe(CO)_2\{(CH_2)_6Co(DMG)_2(Py)\}] \quad \textbf{(3)} \quad + \quad NaBr$$

Equation 1.3

The yellow crystalline complex **(3)** is air stable in the solid state and can be purified by recrystallization from CH_2Cl_2 and hexane.

Previous studies in our laboratory have shown that haloalkyl complexes are good precursors for synthesizing hydrocarbon bridged heterobimetallic complexes [6]. It has also been reported that the incoming nucleophile may attack both the metal site and alkyl bromide end to give, in some cases, homobimetallic complexes [4]. However the cobaloxime nucleophile reacted selectively at the bromo end of **(1)** according to Equation 1.3 and we observed no binuclear cobaloxime complexes.

The heterobimetallic complex **(3)** was characterized by standard spectroscopic methods. The IR showed two υ(CO) bands as expected. The ^{13}C NMR spectrum of **(3)** showed two peaks at δ 3.84 and 30.48 ppm, which correspond to the CH_2 groups directly attached to the iron and cobaloxime group respectively. The mass spectrum of complex **(3)** was not obtained, due to the involatility of sample. Nevertheless, the sharp melting point observed (121 - 124 °C) suggests that the

sample is pure. Satisfactory elemental analysis results were also obtained. The characterization data are given in the experimental section.

1.2.3 Reaction with methyl lithium

The complex **(1)** reacts with methyl lithium to give the known heptyl iron complex $[CpFe(CO)_2\{(CH_2)_6CH_3\}]$ **(4)** in *ca.* 10% yield, as shown in Equation 1.4. Complex **(4)** was obtained as a yellow oil and characterized by IR and ^1H NMR spectroscopy, which were identical to those obtained from an authentic sample.

$$[CpFe(CO)_2\{(CH_2)_6Br\}] + CH_3Li \longrightarrow \underset{\textbf{(4)}}{[CpFe(CO)_2\{(CH_2)_6CH_3\}]} + LiBr$$

Equation 1.4

Methyl lithium acts as a deprotonation reagent in many reactions [19]. It is also known that alkyl lithium reagents may attack the cyclopentadienyl ring of complex $[CpFe(CO)_2(CH_2C_6H_5)]$ to give the anionic product $[(C_5H_4)Fe(CO)_2(CH_2C_6H_5)]^-$, and thus a range of substituted cyclopentadienyl iron complexes, such as $[(C_5H_4CO_2H)Fe(CO)_2(CH_2C_6H_5)]$, can be prepared in this fashion [20]. Also, the well known Fischer carbene complexes are prepared by reacting alkyl or aryl lithium reagents with metal carbonyls [21]. However, under the conditions used here, the only detectable product is **(4)**, extensive decomposition also occurred in the reaction. No further attempts were made to optimize the reaction.

1.2.4 Reaction with sodium azide

The complex **(1)** reacts with sodium azide to give the product $[CpFe(CO)_2\{(CH_2)_6N_3\}]$

(5) in 39 % yield, as shown in Equation 1.5.

$$[CpFe(CO)_2\{(CH_2)_6Br\}] + NaN_3 \longrightarrow \underset{\textbf{(5)}}{[CpFe(CO)_2\{(CH_2)_6N_3\}]} + NaBr$$

Equation 1.5

The reaction took place in a refluxing CH_3CN/H_2O mixture, without a phase transfer catalyst. TLC monitoring of the reaction showed that no starting material remained after 4 hours. The relatively low yield of product can be attributed to the low stability of **(5)**. Indeed, we found that even under nitrogen with protection from light, the pure sample starts decomposing within an hour at room temperature. It has been reported that amines can be obtained *via* azides from alkyl halides under phase transfer catalyst conditions [22]. Attempts have been made to reduce **(5)** under these conditions, but only $[CpFe(CO)_2\{(CH_2)_6H\}]$ was obtained. The new complex **(5)** was characterized by IR, ^1H and ^{13}C NMR and mass spectroscopy. The IR spectrum of **(5)** showed a characteristic absorption of the azide group at 2096 cm^{-1}, and two υ(CO) bands at 1997 and 1937 cm^{-1}. The ^1H NMR spectrum of **(5)** showed a triplet at δ 3.23 ppm, which can be assigned to the CH_2 next to N_3. A mass spectrum of **(5)** shows a molecular ion peak at m/z 303, which further confirmed the formation of **(5)**. Several attempts were made at elemental analyses, however, no satisfactory results could be obtained. This may be due to the unstable nature of complex.

1.2.5 Reaction with lithium aluminiumhydride

Complex **(1)** was reacted with $LiAlH_4$ at room temperature overnight to give the known hexyl iron complex $[CpFe(CO)_2\{(CH_2)_6H\}]$ **(6)** in 20% yield, as shown in Equation 1.6.

$$[CpFe(CO)_2\{(CH_2)_6Br\}] + LiAlH_4 \longrightarrow [CpFe(CO)_2\{(CH_2)_6H\}]$$
(6)

Equation 1.6

The starting material **(1)** was also recovered in *ca.* 60% after column chromatography. It is known that $LiAlH_4$ can cleave the iron carbon bond of $[CpFe(CO)_2R]$ complexes to give $[CpFe(CO)_2H]$ and organic products [23]. However, no such species were observed in this case. The relatively low yield of **(6)**, compared to similar reactions of alkyl bromides [24], suggested that the metal centre and its associated ligands, $CpFe(CO)_2$, may have an influence on the reactivity of the bromo functional group, even though they are separated by six methylene groups.

1.2.6 Reaction with magnesium metal

Several attempts were made to prepare a Grignard reagent by the reaction of **(1)** with magnesium metal. The only observable product is **(6)** in ca. 10% yield. A large portion of starting material **(1)** was recovered after column chromatography. Extensive decomposition occurred when reactions were carried out in refluxing THF.

1.2.7 Reaction with phenol and its derivatives

A series of new phenol derivatives of **(1)** were prepared by the general route at a refluxing acetone solution, as shown in Equation 1.7.

$$[CpFe(CO)_2\{(CH_2)_6Br\}] + C_6H_5OH \xrightarrow[18\text{-crown-6}]{K_2CO_3} [CpFe(CO)_2\{(CH_2)_6OC_6H_5\}]$$
(7)

Equation 1.7

Related complexes **(8)**, **(9)** and **(10)** were prepared in the similar manner by reacting **(1)** with resorcinol, 4-hydroxybenzylalcohol and 3,5-dihydroxybenzylalcohol respectively. The time taken for reactions of **(1)** with phenol and 4-hydroxybenzyl alcohol is 24 hours, but the reactions with resorcinol and 3,5-dihydroxybenzyl alcohol take 48 hours to go to completion. TLC was used routinely to monitor the reactions. Literature reports indicate that the combination of 18-crown-6 and K_2CO_3 in the refluxing acetone gives optimum yields for this type reactions [25]. Furthermore, we found that light protection is essential for achieving highest yields for **(7)** - **(10)**. The yields of the reaction products are variable and relatively low, **(7)** (71%), **(8)** (7%), **(9)** (51%), and **(10)** (36%), when compared to the alkyl bromides (where yields of other derivatives are often >90%). We believe that this is mainly due to the low stabilities of **(7)** - **(10)**.

Generally speaking, the mononuclear complexes **(7)** and **(9)** are more thermally stable than their dinuclear analogues **(8)** and **(10)**. This is in contrast to our previous experiences on the series $[CpFe(CO)_2R]$ [26] and $[CpFe(CO)_2(CH_2)_nFe(CO)_2Cp]$ [27], where $[CpFe(CO)_2(CH_2)_nFe(CO)_2Cp]$ complexes are more stable than $[CpFe(CO)_2R]$. Also, the benzyl alcohol derivatives **(9)**, **(10)** are found to be less stable than **(7)**, **(8)** respectively. However, we were able to purify **(7)** - **(10)** by column chromatography, and handle them at room temperature in air for a short time.

The complexes **(7)** - **(10)** were characterized by standard analytical and spectroscopic methods. The ^1H NMR spectra of **(7)** - **(10)** are particularly informative (see experimental section): all show a triplet at δ 3.95 ppm which corresponds to the CH_2 attached to phenoxy group, and this indicated the formation of the anticipated products. Mass spectra also show either molecular ion peak (P^+), or (P^+ - CO) for

(7) - (10) which further confirmed the formulation of products.

These reactions are important model reactions for the assembly of a series of new organometallic dendritic polymers (or dendrimers). The details of the construction of the dendrimers will be given in Chapter 4. The results described here show that the iron carbon bond between $CpFe(CO)_2$ and the alkyl group is stable under these reaction conditions. Also, they gave us an insight into the properties of phenyl ether complexes, which is crucial in the reaction sequences required for the construction of dendrimers.

1.2.8 Reaction with trityl salt

Triphenyl carbenium (trityl) salts are well known reagents for hydride abstraction and dehydrogenation reactions in organic chemistry. Green and Nagy reported the first hydride elimination reactions, using trityl salt, with a series of iron alkyl complexes of the type $[CpFe(CO)_2R]$ (R = Et, n-Pr, iso-Pr) [28]. The reaction is shown in Equation 1.8.

$$[CpFe(CO)_2(CHR'CH_2R'')] + Ph_3CPF_6 \longrightarrow [CpFe(CO)_2(CHR'=CHR'')]^+PF_6^-$$

Equation 1.8

Similar reactions have also been reported for $[CpRu(CO)_2R]$ [29], $[CpM(CO)_3R]$ (M = Mo and W) [30], $[Mn(CO)_5R]$ [28], $[(\eta^5\text{-cycloheptadienyl})Mn(CO)_3]$ [32] and $[(\eta^4\text{-cycloheptadiene})Fe(CO)_3]$ [31] (R: alkyl, except methyl). It is believed that these reactions go *via* a bimolecular mechanism, and the carbonium ion intermediates are stabilized by the iron metal, as shown in Scheme 1.1 [28].

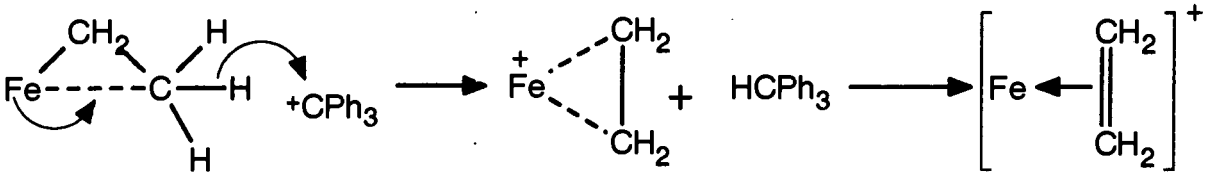

Scheme 1.1

Baird *et al.* later made a detailed study of these cationic iron complexes and demonstrated that the η^2-olefin iron complexes can liberate free olefins on reaction with NaI, as shown in Equation 1.9 [33].

$$[CpFe(CO)_2(\eta^2\text{-olefin})]^+ + NaI \longrightarrow [CpFe(CO)_2I] + \text{olefin}$$

Equation 1.9

It has also been reported that the iron complexes $[CpFe(CO)_2\{(CH_2)_2CN\}]$ and $[CpFe(CO)_2(CF_2CF_2H)]$ gave no reaction with trityl salt in THF [28].

The complex **(1)** was reacted with trityl salt and we found it to give $[CpFe(CO)_2\{CH_2{=}CH(CH_2)_4Br\}]^+PF_6^-$ **(11)** in 77% yield. The reaction is shown in Equation 1.10.

$$[CpFe(CO)_2\{(CH_2)_6Br\}] + Ph_3CPF_6 \longrightarrow \underset{\textbf{(11)}}{[CpFe(CO)_2\{CH_2{=}CH(CH_2)_4Br\}]^+PF_6^-} + Ph_3CH$$

Equation 1.10

However, in the case of $[CpFe(CO)_2\{(CH_2)_3Br\}]$, no β-hydride elimination was observed. Thus, after stirring $[CpFe(CO)_2\{(CH_2)_3Br\}]$ with Ph_3CPF_6 at room temperature for 24 hours, a deep green solution was obtained which suggested the

formation of a 17 e⁻ cationic species [34]. No hydride abstraction product could be detected from the IR spectra of the reaction mixture. These results thus suggest that reactivity of the bromoalkyl iron complexes toward trityl salt is affected by the length of hydrocarbon chain.

The new complex **(11)** was fully characterized by standard spectroscopic methods. The ^1H NMR spectrum of **(11)** showed two separate multiplets, at δ 1.65 and 2.58 ppm for the γ-CH_2 protons. This is because the γ-CH_2 group is prochiral and an iron chiral centre is generated when an asymmetric olefin is η^2-bonded to the iron centre. Such effects were also observed in the ^{13}C NMR spectrum of **(11)**, in which the two carbonyl groups exhibited two separate resonances at δ 209.78 and 212.03 ppm. Faller and Johnson have already reported the prochiral effect of $[CpFe(CO)_2(\eta^2$-olefin$)]^+$ complexes in their NMR spectra, and further suggested that the preferred orientation of the carbon-carbon double bond toward the iron centre is parallel to cyclopentadienyl ring with substituent pointing away from the cyclopentadienyl ring, as shown in Figure 1.1 [29].

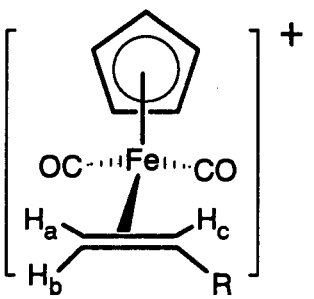

Figure 1.1 The preferred conformation of $[CpFe(CO)_2(\eta^2$-olefin$)]^+$ complexes

1.2.9 Carbonyl insertion reactions

The carbonyl insertion or alkyl migration reaction is one of the most studied reactions in organometallic chemistry.

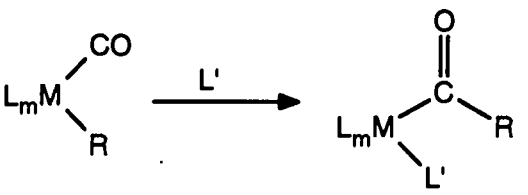

It is fundamentally important to some catalytic processes, such as the hydroformylation reaction [35] and the Fischer-Tropsch process [36]. Basically, there are two ways to facilitate the carbonyl insertion reaction: one is by reacting with strong donor ligands (L), such as tertiary phosphines; the other is by use of oxidizing agents, such as trityl or silver salts. Both of these approaches were investigated with **(1)** and are described below:

Reaction with PPh_3 **(1)** was reacted with PPh_3 in the refluxing benzene to give $[CpFe(CO)(PPh_3)(C{=}O(CH_2)_6Br)]$ **(12)** in 93% yield. The reaction is shown in Equation 1.11.

$$[CpFe(CO)_2\{(CH_2)_6Br\}] + PPh_3 \longrightarrow [CpFe(CO)(PPh_3)\{C{=}O(CH_2)_6Br\}]$$
(12)

Equation 1.11

It has previously been reported that $[CpFe(CO)_2(CH_2Cl)]$ reacts with PPh_3 in methanol to give $[CpFe(CO)_2(CH_2PPh_3)]Cl$ [37], and that $[CpFe(CO)_2\{(CH_2)_3Br\}]$ reacts with PPh_3 to give a cyclic carbene complex [4]. However, we found neither ylide nor carbene complexes in the reaction with **(1)**. Thus, the length of alkyl chain is important in determining the type of product formed. It is also worth noting that no disubstituted phosphine iron complex was observed in the reaction even with five times excess of

PPh_3 in refluxing benzene for two days.

A chiral centre is present in **(12)**, when PPh_3 is coordinated to iron. We are aware of the existence of optical isomers for **(12)**, however no attempt was made to separate these isomers in this study. Davies has made extensive studies on the chiral auxiliary, $Cp(CO)(PPh_3)Fe$, and found that high stereospecificity of organic transformations can be achieved with this metal chiral centre [38].

The orange crystalline complex **(12)** is stable in the solid state, and was characterized by IR, ^1H and ^{13}C NMR, and microanalysis. The IR spectrum of **(12)** showed two bands at 1920, 1614 cm^{-1}, which corresponded to terminal and acyl carbonyls respectively. In the ^1H NMR spectrum of **(12)**, two magnetically non-equivalent protons in α-CH_2 were observed at δ 2.52, 2.85 ppm. This is because the α-CH_2 group is prochiral. Similar effects have been observed before [39 - 41]. The mass spectrum of **(12)** was not obtained due to the involatility of the sample. Nevertheless, microanalysis results confirmed the formula of **(12)**.

Reaction with $AgBF_4$/CO **(1)** converts readily to $[CpFe(CO)_2\{C{=}O(CH_2)_6Br\}]$ **(13)** in 21% yield *via* oxidatively catalysed carbonyl insertion reaction when CO was bubbled through the reaction. The reaction is shown in Equation 1.12.

$$[CpFe(CO)_2\{(CH_2)_6Br\}] + CO \xrightarrow{AgBF_4} \underset{\textbf{(13)}}{[CpFe(CO)_2\{C{=}O(CH_2)_6Br\}]}$$

Equation 1.12

Even though 1 mole equivalent of $AgBF_4$ was used in this study, previous reports have shown the reaction to be catalytic [42]. Several other oxidising agents, such as the

ferrocenium cation [42] and cerium ammonium nitrate [43] have also been reported. Although $AgBF_4$ can abstract halide in some cases [44], we observed no such reaction here. Interestingly, Casey and Smith have reported reactions of $[CpFe(CO)_2\{(CH_2)_nX\}]$ (n = 3 - 5; X = Br, Cl) with $AgBF_4$ to give cycloalkanes [15]. Their results showed that cyclopropane formed much more readily than the other cycloalkanes from their respective complexes. The low yields of cyclobutane and cyclopentane suggested to these authors that the longer chain iron complexes may react *via* a different route to the (3-halopropyl)iron complexes. Indeed, in a separate ^1H NMR experiment, we have also found a trace of cyclohexane in the reaction of **(1)** with $AgBF_4$ in a CD_2Cl_2 solution.

The mechanism of the oxidative carbonylation reaction has been reported by Giering from a series of electrochemical studies on $[CpFe(CO)_2CH_3]$ and the details are given in Section 1.3.

The yellow oil **(13)** was purified by column chromatography and fully characterized by standard spectroscopic methods. The IR spectrum of **(13)** showed two υ(CO) bands at 2015 and 1955 cm^{-1} for terminal carbonyls and an absorption band at 1641 cm^{-1} for the acyl carbonyl. The ^1H NMR spectrum of **(13)** gave two characteristic triplets at δ 2.88, 3.38 ppm, which corresponds to the CH_2 groups attached to the acyl carbonyl and bromo groups respectively. The mass spectrum of **(13)** also gave a molecular ion peak at m/e 368, which further confirmed the formula of **(13)**. Satisfactory elemental analysis results for **(13)** were also obtained.

1.3 ELECTROCHEMICAL BEHAVIOUR OF $CpFe(CO)_2\{(CH_2)_6Br\}$ (1)

Electron transfer reactions are of fundamental importance in the homogeneous catalytic reactions [45]. In addition, cyclic voltammetry (CV) has been recognized as the most powerful tool in studying electron transfer processes and transient redox species [46]. Because of the relatively short life time of the reactive species at ambient condition; CV provides an excellent opportunity to study the redox processes, particularly for organo-transition metal complexes.

Complex **(1)** was studied by CV at room temperature in acetonitrile solution. The cyclic voltammogram of **(1)**, as shown in Figure 1.2, gives an irreversible oxidation peak at *ca.* 0.62 V, followed by a quasi-reversible redox couple at -0.15 V which can only be seen after oxidation at *ca.* 0.6 V. This indicates that a new species is formed on the electrode surface after the oxidation reaction.

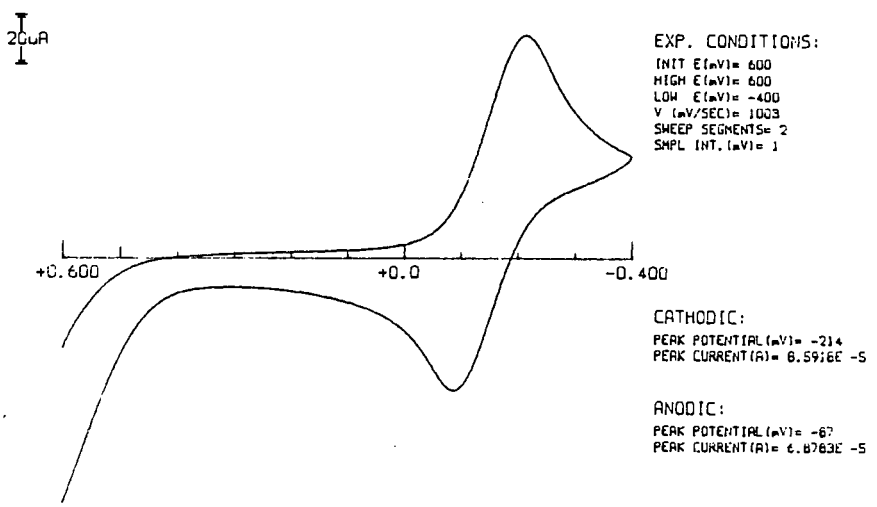

Figure 1.2 A cyclic voltammogram of $[CpFe(CO)_2\{(CH_2)_6Br\}]$

Comparing these results with previous studies in this laboratory on $[CpFe(CO)_2\{(CH_2)_6H\}]$ **(6)** [47], both **(1)** and **(6)** show very similar electrochemical

behaviour and redox potentials. Thus, these results indicate that the terminal bromo group on the alkyl chain has no significant effect on the electrochemical behaviour of complexes of the type $CpFe(CO)_2R$, and the electroactive site of **(1)** is the metal centre.

Giering *et al.* have reported a series of CV studies on $[CpFe(CO)_2(CH_3)]$ in various solvents and temperatures [48, 49]. They also obtained cyclic voltammograms similar to **(1)**, and assigned this quasi-reversible couple to the solvent assisted carbonyl insertion product $[CpFe(solvent)(CO)(COR)]^+$, which was formed just after the oxidation reaction. The mechanism is shown in Scheme 1.2.

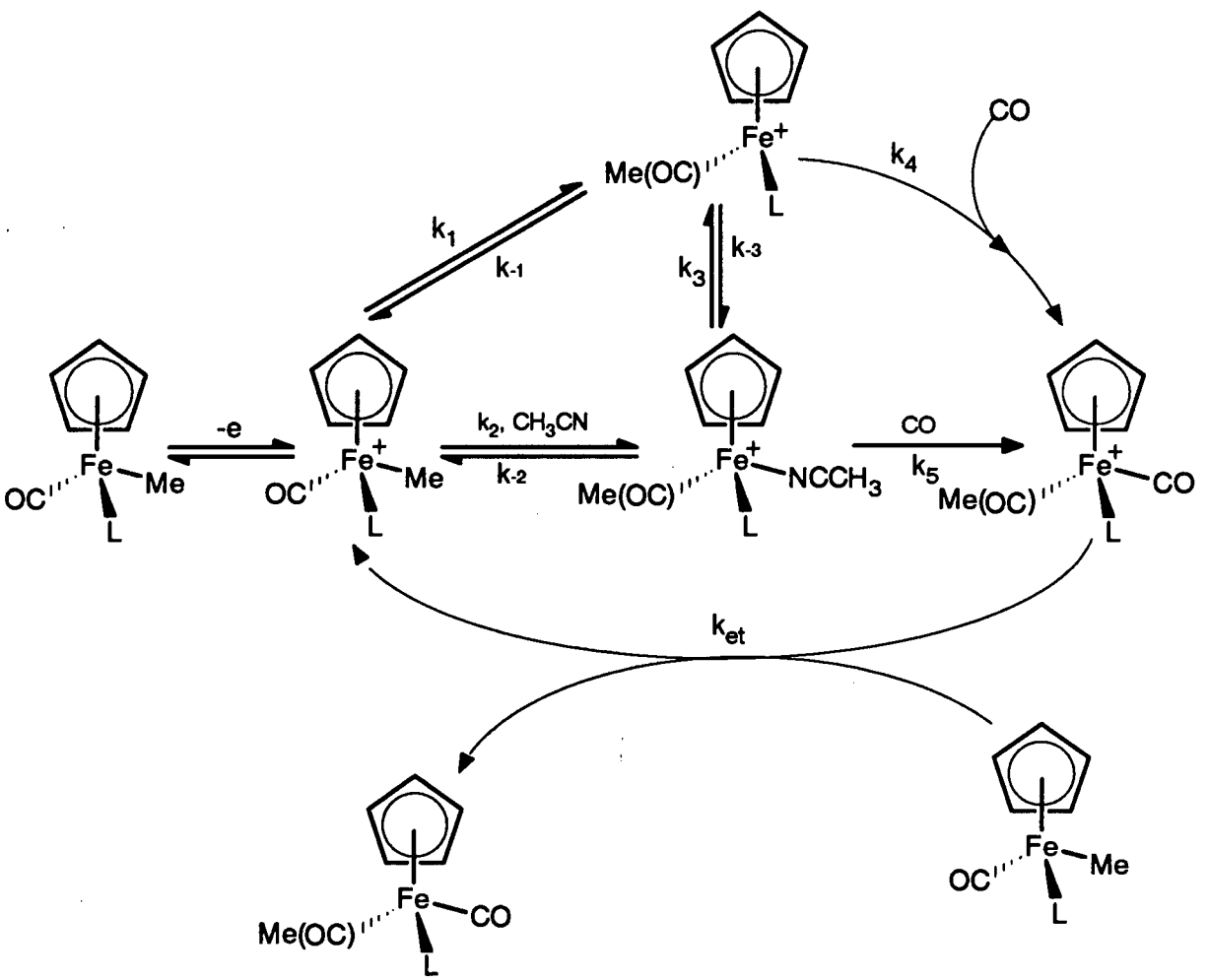

Scheme 1.2

In order to further demonstrate this oxidatively assisted carbonyl insertion reaction, we mixed excess of PPh_3 with **(1)** in the electrolyte solution. The resulting voltammogram (Figure 1.3) showed similar behaviour, except a shift of the redox potential of the quasi-reversible couple from -0.15 to +0.037 V. We can attribute this redox couple to the formation of $[CpFe(CO)(PPh_3)\{CO(CH_2)_6Br\}]^+$ on the electrode surface. Further confirmation of this was obtained from the voltammogram of an authentic sample $[CpFe(CO)(PPh_3)(COC_6H_{12}Br)]$ (Figure 1.4) which gives a quasi-reversible redox couple at +0.043 V.

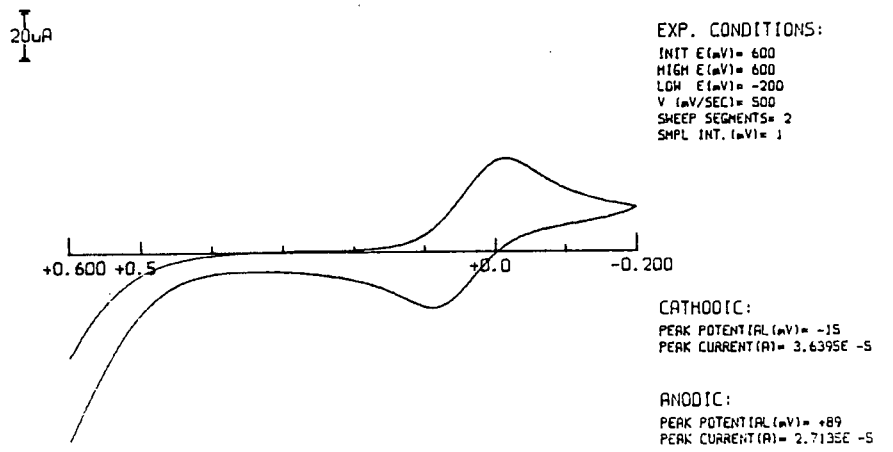

Figure 1.3 A cyclic voltammogram of mixture of $[CpFe(CO)_2\{(CH_2)_6Br\}]$ and PPh_3

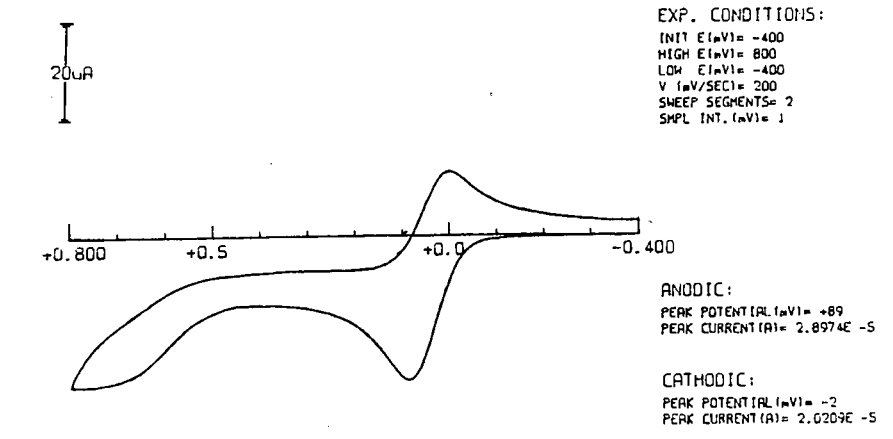

Figure 1.4 A cyclic voltammogram of $[CpFe(CO)(PPh_3)\{C{=}O(CH_2)_6Br\}]$

Thus, we suggest that the new species formed on the surface of electrode in the case of **(1)** without PPh_3 should be $[CpFe(CH_3CN)(CO)(COC_6H_{12}Br)]^+$. Also **(1)** probably follows the same mechanism (Scheme 1.2) as for $[CpFe(CO)_2(CH_3)]$. This study is preliminary, nevertheless we can draw the following conclusions:

1) the alkyl chain length and bromo substituent have little effect on the electrochemical behaviour and oxidation potential of $[CpFe(CO)_2R]$ complexes.

2) the difference in redox potentials between $[CpFe(CO)(CH_3CN)(COR)]$ and $[CpFe(CO)(PPh_3)(COR)]$ may reflect the different electron donating abilities of the incoming ligands.

1.4 THERMAL DECOMPOSITION OF $CpFe(CO)_2\{(CH_2)_6Br\}$

Differential scanning calorimetry (DSC) is the simplest and the most widely used thermal analysis technique. It provides both qualitative and quantitative results about thermal behaviour, which can serve as the fingerprint for a specific material [50]. The DSC trace of complex **(1)** recorded over the range of 30 - 400 °C under N_2, is shown in Figure 1.5.

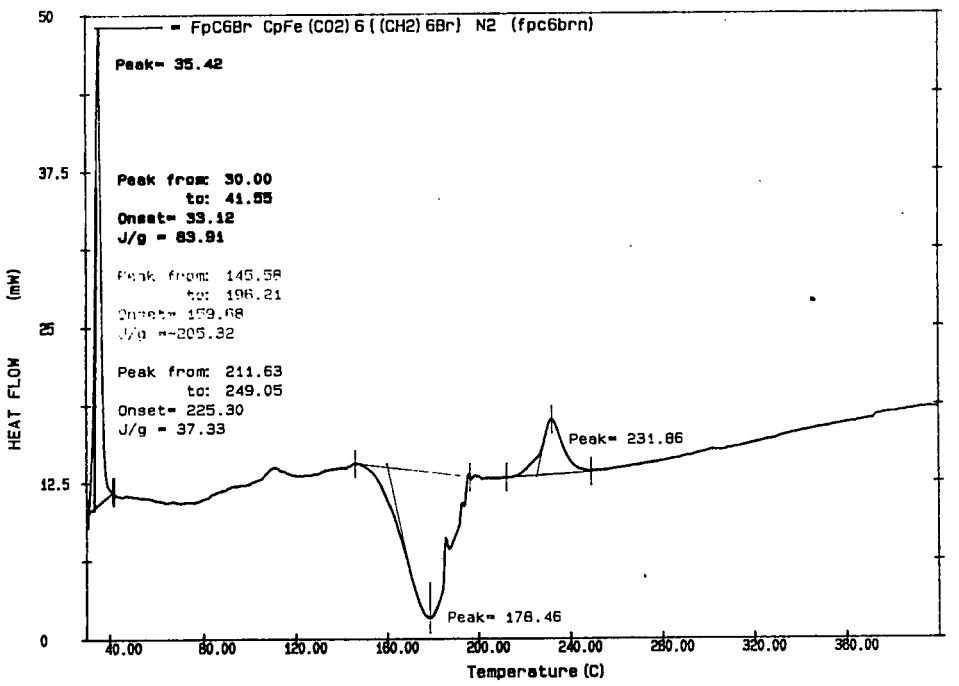

Figure 1.5 A DSC trace of $[CpFe(CO)_2\{(CH_2)_6Br\}]$

The trace shows two endothermic peaks at 35 °C and 232 °C with an exothermic peak at 178 °C. The first endothermic peak can be assigned to the melting of the crystalline sample, by comparison with the hot-stage microscope result. The exothermic peak in the DSC trace should correspond to decomposition of the complex **(1)**. This was confirmed by comparing with previous studies on the series of $[Cp(CO)_2Fe(CH_2)_nFe(CO)_2Cp]$ (n = 4 - 12) [27] and $[CpFe(CO)_2\{(CH_2)_6H\}]$ **(6)** [47]. They all showed very similar decomposition exotherms within the temperature range

of 160 - 200 °C. This may be the characteristic thermal decomposition range for this type of iron complexes, and the bromo functional group of **(1)** seems to have little effect on the decomposition temperature. The high temperature endothermic peak in the DSC trace of **(1)** is identified as ferrocene. This was confirmed by comparison with the DSC trace of an authentic ferrocene sample. The relatively broad endothermic peak of ferrocene is due to sublimation of the sample.

The formation of ferrocene is also seen in the decomposition of **(1)** in toluene solution. A toluene solution of **(1)** was heated at 110 °C under N_2. The reaction was monitored by IR spectroscopy, and showed no υ(CO) absorption bands after 73 hours. The resulting decomposition products were then characterized by ^{1}H NMR spectroscopy which indicated that ferrocene and cyclohexane are the two major products. The decomposition of $[CpFe(CO)_2]_2$ can also produce ferrocene; no $[CpFe(CO)_2]_2$ was observed from the IR spectra when **(1)** decomposed in toluene solution.

It has been reported that the β-hydride elimination reaction dominated when complexes of the type $[CpFe(CO)(PPh_3)R]$ were heated, to give alkenes and the hydride complex $[CpFe(CO)(PPh_3)H]$ [51]. However, we observed no hydride species in the decomposition of **(1)** from IR spectra either.

The results obtained here thus imply that the thermal decomposition of **(1)** may have followed a different route to $[CpFe(CO)(PPh_3)R]$, and that both the bromo and the PPh_3 groups may play important roles on the thermal decomposition mechanism of this type of complex. The decomposition mechanism of **(1)** appears to be complicated, and since this study is preliminary, further investigation is needed to establish the mechanism with certainty.

1.5 CONCLUSION

In this chapter, we have demonstrated that it is possible to direct reactions selectively in **(1)**. The various reactions and their resulting products mentioned in this chapter are summarized in Table 1.1.

Reactants	Products
NaOMe	$[CpFe(CO)_2\{(CH_2)_6OCH_3\}]$ **(2)**
$Na[Co(DMG)_2(Py)]$	$[CpFe(CO)_2(CH_2)_6Co(DMG)_2(Py)]$ **(3)**
MeLi	$[CpFe(CO)_2\{(CH_2)_6CH_3\}]$ **(4)**
NaN_3	$[CpFe(CO)_2\{(CH_2)_6N_3\}]$ **(5)**
$LiAlH_4$	$[CpFe(CO)_2\{(CH_2)_6H\}]$ **(6)**
Mg	$[CpFe(CO)_2\{(CH_2)_6H\}]$ **(6)**
phenol	$[CpFe(CO)_2(C_6H_{12}OC_6H_5)]$ **(7)**
resorcinol	$[\{CpFe(CO)_2(C_6H_{12}O)\}_2C_6H_4]$ **(8)**
4-hydroxybenzyl alcohol	$[CpFe(CO)_2(C_6H_{12}OC_6H_4CH_2OH)]$ **(9)**
3,5-dihydroxybenzyl alcohol	$[\{CpFe(CO)_2(C_6H_{12}O)\}_2C_6H_3CH_2OH]$ **(10)**
Ph_3CPF_6	$[CpFe(CO)_2\{CH_2=CH(CH_2)_4Br\}]PF_6$ **(11)**
PPh_3	$[CpFe(CO)(PPh_3)(C=O(CH_2)_6Br)]$ **(12)**
$CO/AgBF_4$	$[CpFe(CO)_2\{C=O(CH_2)_6Br\}]$ **(13)**

Table 1.1 Summary of reactions of **(1)** described in Chapter 1

In our experience, the bromo group in **(1)** is less reactive than that in alkyl bromides, whereas the reactivity of $CpFe(CO)_2$ in **(1)** seems to be affected little by bromo group. Interestingly, the hydrocarbon chain length did affect the reactivities of **(1)** and $[CpFe(CO)_2\{(CH_2)_3Br\}]$ toward trityl salt. The CV results of **(1)** indicated that the bromo functional group and the alkyl chain length have no effect on the electrochemical

behaviour of complexes [$CpFe(CO)_2R$]. However the thermal decomposition study of **(1)** revealed that both the bromo and PPh_3 groups may affect the decomposition pathway of haloalkyl iron complexes, since we obtained different decomposition products. The thermal decomposition mechanism appears to be complicated, and further studies need to be carried out to establish the mechanism.

1.6 REFERENCES

1. P. W. Jolly and R. Pettit, *J. Am. Chem. Soc.*, **1966**, *88*, 5044.
2. M. L. H. Green, M. Ishaq and R. N. Whiteley, *J. Chem. Soc.* (A), **1967**, 1508.
3. H. B. Friedrich and J. R. Moss, *Adv. Organomet. Chem.*, **1991**, *33*, 235.
4. J. R. Moss, *J. Organomet. Chem.*, **1982**, *231*, 229.
5. K. P. Finch and J. R. Moss, *J. Organomet. Chem.*, **1988**, *346*, 253.
6. H. B. Friedrich, J. R. Moss and B. K. Williamson, *J. Organomet. Chem.*, **1990**, *394*, 313.
7. S. J. Archer, K. P. Finch, H. B. Friedrich, J. R. Moss and A. M. Crouch, *Inorg. Chim. Acta*, **1991**, *182*, 145.
8. J. D. Scott and R. J. Puddephatt, *Organometallics*, **1986**, *5*, 1538.
9. P. K. Monaghan and R. J. Puddephatt, *J. Chem. Soc. Dalton Trans.*, **1988**, 595.
10. F. A. Cotton and C. M. Lukehart, *J. Am. Chem. Soc.*, **1971**, *93*, 2672.
11. V. A. Osborn and M. J. Winter, *Polyhedron*, **1986**, *5*, 435.
12. H. Adams, N. A. Bailey, M. Grayson, C. Ridgway, A. J. Smith, P. Taylor and M. J. Winter, *Organometallics*, **1990**, *9*, 2621.
13. R. L. Trace, J. Sanchez, J. Yang, J. Yin and W. M. Jones, *Organometallics*, **1992**, *11*, 1440.
14. C. P. Casey and L. J. Smith, *Organometallics*, **1988**, *7*, 2419.
15. C. P. Casey and L. J. Smith, *Organometallics*, **1992**, *11*, 738.
16. H. B. Friedrich, P. A. Makhesha, J. R. Moss and B. K. Williamson, *J. Organomet. Chem.*, **1990**, *384*, 325.
17. L. F. Fieser and M. Fieser Ed., *Reagent for Organic Synthesis*, Vol. 1, pp 1091 - 1095, New York, Wiley, **1967**.

18. R. J. Trautman, D. C. Gross and P. C. Ford, *J. Am. Chem. Soc.*, **1985**, *107*, 2355.

19. L. F. Fieser and M. Fieser Ed., *Reagents for Organic Synthesis*, Vol. 1, pp 686 - 689, New York, Wiley, **1967**.

20. T. Y. Orlova, V. N. Setkina, V. F. Sizoi and D. N. Kursanov, *J. Organomet. Chem.*, **1983**, *252*, 201.

21. E. O. Fischer and A. Maasböl, *Chem. Ber.*, **1967**, *100*, 2445.

22. F. Rolla, *J. Org. Chem.*, **1982**, *47*, 4327.

23. A. Wong and J. D. Atwood, *J. Organomet. Chem.*, **1981**, *210*, 395.

24. S. Krishnamurthy, *J. Org. Chem.*, **1980**, *45*, 2551.

25. C. J. Hawker and J. M. J. Fréchet, *J. Am. Chem. Soc.*, **1990**, *112*, 7638.

26. A. Emeran, M. A. Gafoor, J. K. I. Goslett, Y.-H. Liao, L. Pimble and J. R. Moss, *J. Organomet. Chem.*, **1991**, *405*, 237.

27. J. R. Moss and L. G. Scott, *J. Organomet. Chem.*, **1985**, *282*, 255.

28. M. L. H. Green and P. L. I. Nagy, *J. Organomet. Chem.*, **1963**, *1*, 58.

29. J. W. Faller and B. V. Johnson, *J. Organomet. Chem.*, **1975**, *88*, 101.

30. M. Cousins and M. L. H. Green, *J. Chem. Soc.*, **1963**, 889.

31. A. J. Pearson, S. L. Kole and T. Ray, *J. Am. Chem. Soc.*, **1984**, *106*, 6060.

32. A. J. Pearson and M. N. I. Khan, *J. Org. Chem.*, **1985**, *50*, 5276.

33. D. E. Laycock, J. Hartgerink and M. C. Baird, *J. Org. Chem.*, **1980**, *45*, 291.

34. R. H. Magnuson, S. Zulu, W.-M. T'sai and W. P. Giering, *J. Am. Chem. Soc.*, **1980**, *102*, 6887.

35. F. A. Cotton and G. Wilkinson, *Advanced Inorganic Chemistry*, 5th Ed., pp 1233 Wiley, New York, **1988**.

36. C. K. Rofer-DePoorter, *Chem. Rev.*, **1981**, *81*, 447.

37. S. Pelling, C. Botha and J. R. Moss, *J. Chem. Soc. Dalton Trans.*, **1983**, 1495.

38. S. G. Davies, *Chem. Brit.*, **1989**, *25*, 268.

39. J. W. Faller and A. S. Anderson, *J. Am. Chem. Soc.*, **1969**, *91*, 1550.

40. S. G. Davies, I. M. Dordor-Hedgecock, K. H. Sutton and M. Whittaker, *J. Am. Chem. Soc.*, **1987**, *109*, 5711.

41. J. R. Moss and L. G. Scott, *J. Organomet. Chem.*, **1989**, *363*, 351.

42. R. H. Magnuson, R. Meirowltz, S. J. Zulu and W. P. Giering, *Organometallics*, **1983**, *2*, 460.

43. C. Amiens, G. Balavoine and F. Guibé, *J. Chem. Soc., Chem. Commun.*, **1991**, 1458.

44. R. J. Kulawiec, J. W. Faller and R. H. Crabtree, *Organometallics*, **1990**, *9*, 745.

45. B. C. Gates, *Catalytic Chemistry*, Wiley, New York, **1992**.

46. A. J. Bard and L. R. Faulkner, *Electrochemical Methods - Fundamental and Applications*, Wiley, New York, **1980**.

47. R. O. Hill, Bsc Honours project report, University of Cape Town, **1990**.

48. D. C. Woska, J. Bartholomew, J. E. Greene, K. Eriks, A. Prock and W. P. Giering, *Organometallics*, **1993**, *12*, 304.

49. A. A. Tracey, K. Eriks, A. Prock and W. P. Giering, *Organometallics*, **1990**, *9*, 1399.

50. M. E. Brown, *Introduction to Thermal Analysis - Techniques and Applications*, Chapman and Hall, London, **1988**.

51. D. L. Reger and E. C. Culbertson, *J. Am. Chem. Soc.*, **1976**, *98*, 2789.

CHAPTER 2 SYNTHESIS AND CHARACTERIZATION OF ω-HYDROXY ALKYL METAL COMPLEXES OF THE TYPE $[L_mM\{(CH_2)_nOH\}]$ (WHERE $L_mM = CpFe(CO)_2$, $Cp^*Fe(CO)_2$, $CpRu(CO)_2$; n = 2, 3,4)

2.1 INTRODUCTION

A long term study in this laboratory has been the synthesis and characterization of transition metal complexes containing functionalized alkyl ligands which may serve as models for intermediates on catalyst surfaces or as precursors for some important complexes, such as organometallic dendrimers (see Chap 4).

Hydroxyalkyl metal complexes can be regarded as a new class of functionalized alkyl metal complexes, in which the metal center and the hydroxy functional group are bridged by a polymethylene chain, as shown in figure 1.

Figure 2.1 An ω-hydroxyalkyl metal complex

2.1.1 α-Hydroxyalkyl metal complexes

It has been recognized that α-hydroxyalkyl metal complexes can serve as model complexes for intermediates on catalyst surfaces [1 - 5]. In particular, hydroxymethyl complexes have often been proposed as a model complex for one of the key intermediates in CO hydrogenation reactions. It is generally believed that the hydrogenation of CO to give oxygenates, over a catalyst surface, involves a series of

intermediates. These include formyl and hydroxymethyl species in the reaction sequence, as shown in Scheme 2.1.

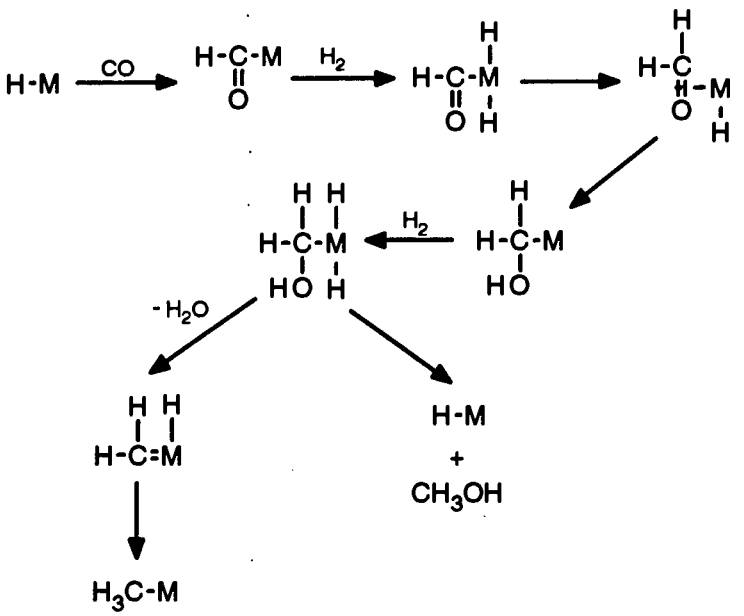

Scheme 2.1

Thus, many hydroxymethyl complexes have been synthesized and studied. A brief summary of known α-hydroxyalkyl transition metal complexes is given in Table 2.1. The general synthetic approaches to α-hydroxyalkyl transition metal complexes can be categorized as depicted in the following text.

Method (A): oxidative addition of aldehydes or ketones

This approach was developed by Stone *et al.* in 1970 [6]. The $[CpFe(CO)_2]^-$ anion was reacted with fluoroacetones to give stable α-hydroxyalkyl metal complexes after acidic treatment, and a series of α-hydroxyalkyl iron complexes were prepared in this manner, as shown in Equation 2.1.

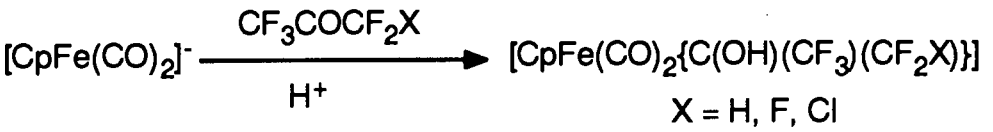

Equation 2.1

It has also been reported that the stability of α-hydroxyalkyl iron complexes can be greatly enhanced by the fluoro substituents on the methyl groups.

An alternative approach to α-hydroxyalkyl metal complexes in this catogrory is the direct reaction of metal hydrides with aldehydes, which avoids the severe acidic treatment. This method was first reported in 1981 by Vaughn and Gladysz, as shown in Equation 2.2 [8].

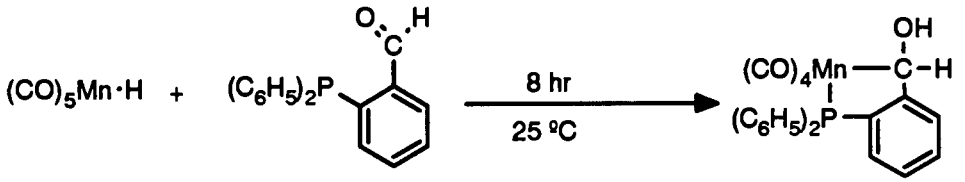

Equation 2.2

In this example, the substitution (replacement of CO by phosphine) and the manganese-carbon bond formation reactions were accomplished in one step to give an isolable α-hydroxyalkyl manganese complex in high yield.

The synthesis of α-hydroxyalkyl complexes *via* these routes seems to be available for many aldehydes and ketones. However, this approach suffers from the low stability of resulting products and many complexes could not be isolated from the reactions.

Method (B): acidolysis of η^2-formaldehyde metal adducts

η^2-Formaldehyde transition metal complexes have also been proposed as model

compounds for the CO hydrogenation reaction (see Scheme 2.1). They react readily with one equivalent of hydrogen halides to give the hydroxymethyl complexes, as shown in Equation 2.3.

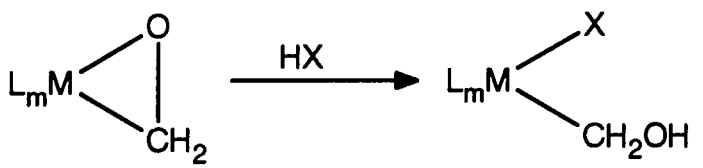

Equation 2.3

The first examples of hydroxymethyl complexes prepared *via* this route were reported in 1980 by Roper *et al.* [10]. It has also been reported that the hydroxymethyl osmium complexes will react further with hydrogen halides and sodium borohydride to give halomethyl and hydride complexes respectively, as shown in Scheme 2.2.

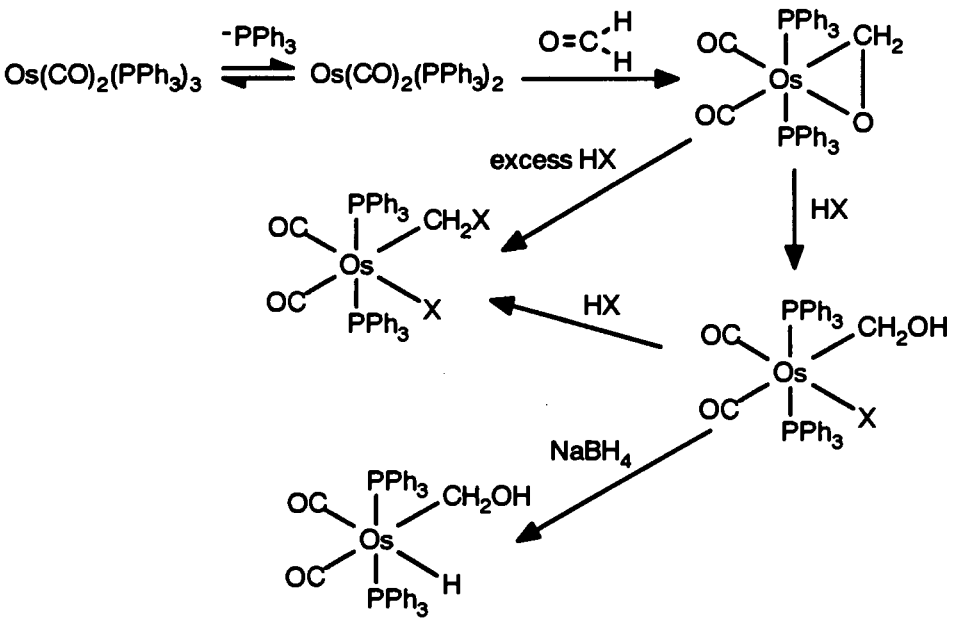

Scheme 2.2

Method (C): free radical reactions

A series of aquo α-hydroxyalkyl metal complexes were prepared by reacting metal cations with aqueous α-hydroxyalkyl radicals [12]. The α-hydroxyalkyl radicals were

readily generated *in situ* by irradiation or from another radical source. A typical example is given in Scheme 2.3.

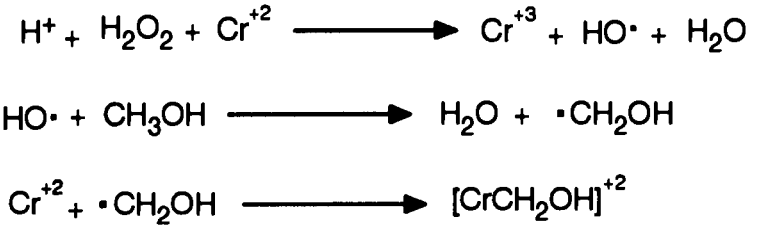

Scheme 2.3

In this case, the hydroxyl radical was generated from hydrogen peroxide in an acidic chromous solution. The radical chain reaction was then carried on to give the hydroxymethyl radical which was *in situ* trapped by the chromous cation to yield the $[CrCH_2OH]^{+2}$ complex. Generally speaking, complexes of this type are short-lived in aqueous solution and can only be observed by UV spectroscopy. However, $[(H_2O)_5Cr(CH_2OH)]^{+2}$ can be purified by ion-exchange chromatography and is stable in aqueous solution at 5 °C.

Method (D): reduction of metal carbonyls

This is one of the most popular routes to prepare formyl or hydroxymethyl transition metal complexes. The most important feature of this route is its relevance to the catalytic CO hydrogenation reaction, which offered organometallic chemists an excellent opportunity to model intermediates on the catalyst surface.

As stated before, the CO hydrogenation reaction is believed to involve formyl, hydroxymethyl, and alkyl species on the catalyst surface. Also, on the organometallic chemistry side, it has long been known that metal carbonyls can be readily converted

to methyl metal complexes by $NaBH_4$, as shown in Equation 2.4.

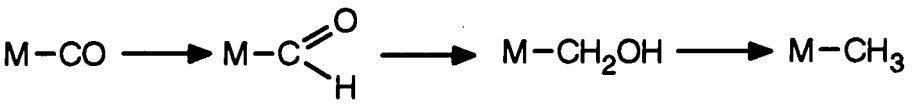

Equation 2.4

It was suspected that these reactions went through the intermediacy of formyl and hydroxymethyl complexes, which are similar intermediates to those proposed in the catalytic CO hydrogenation reaction. However, niether the formyl nor the hydroxymethyl complexes could be isolated at that time. It was not until 1979 when Graham and Casey independently isolated the first hydroxymethyl rhenium complex, $[CpRe(NO)(CO)(CH_2OH)]$ [16, 17], through consecutive reduction reactions of $[CpRe(NO)(CO)_2]^+$. All possible reduction reactions and intermediates from $[Re\text{-}CO]^+$ to $[Re\text{-}CH_3]$ have been studied and isolated, as shown in Scheme 2.4.

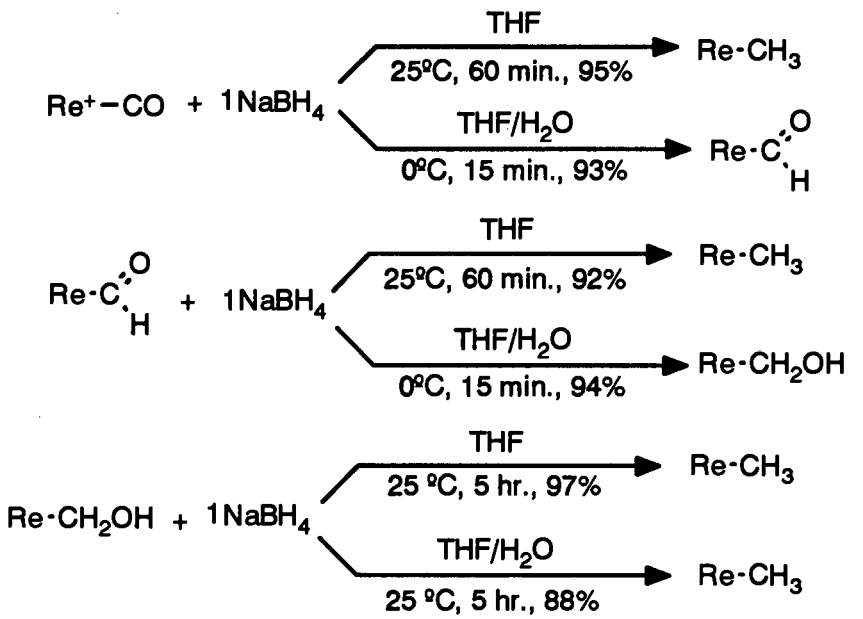

Seheme 2.4

This reaction sequence was regarded as the first model reaction for the catalytic CO hydrogenation reaction, and thereafter became a general reaction of metal carbonyls. Many other hydroxymethyl complexes prepared *via* this route can also be found in Table 2.1.

Table 2.1 A summary of known α-hydroxyalkyl transition metal complexes

Complexes	Preparation	Characterization	Reference
$CpFe(CO)_2C(OH)(CF_3)R$			
$R = CF_3$, CF_2H	A	IR, MS, NMR, MA	6
$R = CF_2Cl$	A	IR	6
$(CO)_4CoCH_2OH$	A	intermediate	7
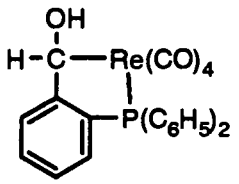	A	IR, NMR, MS, MA	8
Rh(OEP)(CHMeOH)	A	NMR	9
OEP = octaethylporphyrin			
$Os(CH_2OH)X(CO)_2(PPh_3)_2$			
$X = Cl, Br, H, CF_3CO_2^-$	B	IR, NMR, MA	10
$Fe(CH_2OH)(CO)_2L_2Cl$	B	IR, NMR	11
$L = P(OMe)_3$			
$[(H_2O)_5CrCHROH]^{2+}$			
$R = H, CH_3, C_2H_5$	C	UV	12
$R = CF_3$	C	UV	13

$L(Co^{III})$-CHROH R = H, CH_3, CF_3, CH_2OH L = 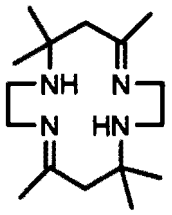	C	UV	14
$(CO)_5MCH(OH)(C_6H_5)$ M = Mn, Re	D	intermediate	15
$(C_5H_5)Re(CO)(NO)(CH_2OH)$	D	IR, NMR, MS, MA	16, 17
$[IrH(CH_2OH)(PMe_3)_4]^+$	D	IR, NMR, MA	18
$[(C_5Me_5)M(CO)_2CH_2OH]$			
M = Fe	D	IR, NMR, MA	19
M = Ru	D	IR, NMR, MA	20
M = Os	D	IR, NMR, MA	21
$[(C_5H_5)M(CO)_2CH_2OH]$			
M = Fe	D	IR, NMR, MS	22
M = Ru	D	IR, NMR, MS, MA	22

2.1.2 β-Hydroxyalkyl metal complexes

β-Hydroxyalkyl transition metal complexes have also been proposed as intermediates in the hydroxypalladation process, or the so called Wacker process [23]. It is believed that the oxidation of ethene to acetaldehyde by palladium(II) chloride in aqueous solution must have gone through a β-hydroxyethyl palladium intermediate. The individual reaction steps of the catalytic mechanism are summarized in Scheme 2.5.

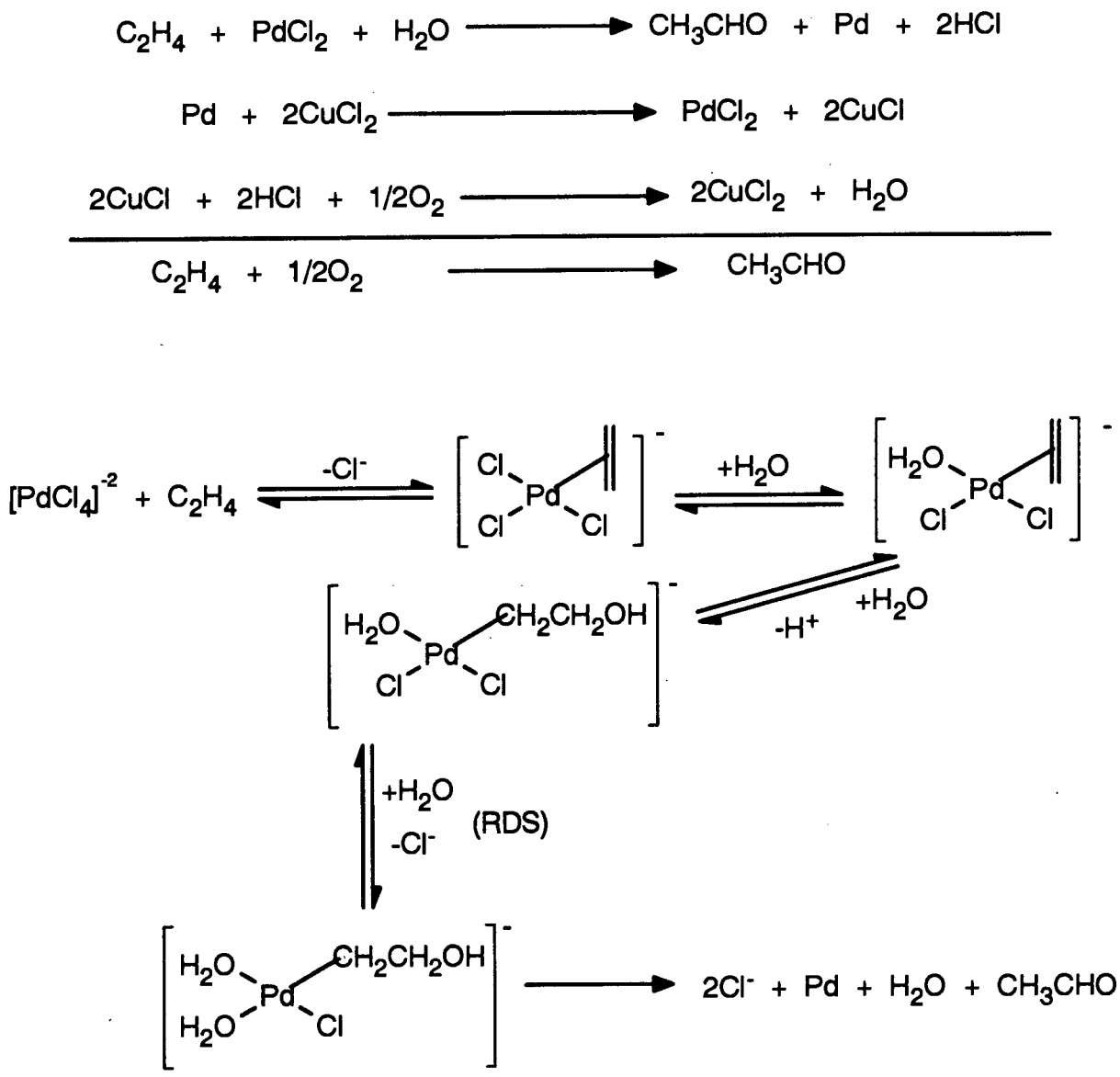

Scheme 2.5

Although the key intermediate, *i.e.* the β-hydroxyethyl palladium complex, has never been isolated, a model complex, $[Cl_5Pt(CH_2CH_2OH)]^{-2}$, has been prepared from Zeise's salt in the presence of chlorine as oxidant in aqueous solution [24]. The reaction sequence is shown in Scheme 2.6.

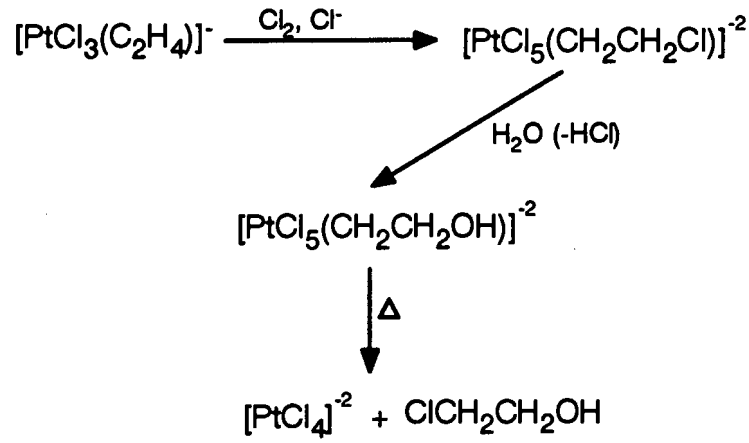

Scheme 2.6

Recently, Bercaw *et al.* reported an alternative route to $[Cl_5Pt(CH2CH2OH)]^-$, *via* oxidative addition reaction of ICH_2CH_2OH to $[PtCl_4]^{-2}$, as shown in Equation 2.5 [25].

$$[PtCl_4]^{-2} + ICH_2CH_2OH \longrightarrow [Cl_5Pt(CH_2CH_2OH)]^{-2} + [PtI_2]_x + KCl$$

Equation 2.5

Although the importance of β-hydroxyethyl metal complexes has been recognized, not many complexes of this type have been studied so far. Perhaps the first known β-hydroxyalkyl complexes can be traced back to 1900 [26]. The β-hydroxyethyl mercury complexes are prepared by the addition reaction of mercury halides (HgX_2) to the ethylene, followed by hydrolysis, as shown in Equation 2.6.

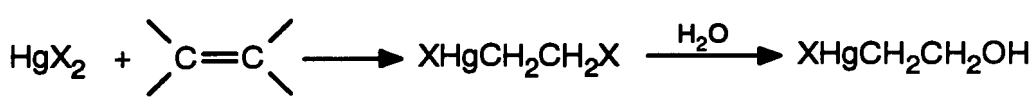

Equation 2.6

In contrast to most of the β-hydroxyethyl transition metal complexes, complexes like $XHgCH_2CH_2OH$ are stable in the solid state but decompose on acidic treatment to give ethanol, as shown in Equation 2.7.

$$XHgCH_2CH_2OH + HCl \longrightarrow XHgCl + CH_3CH_2OH$$

Equation 2.7

This whole reaction sequence is well known to organic chemists as the oxymercuration-demercuration reaction which is highly regiospecific, and yields Markovnikov addition products of alcohols from alkenes [27]. Many β-hydroxyethyl mercury complexes have been prepared in this manner and no intention is made here to cover all the complexes of this type.

There are also a few aquo β-hydroxyethyl chromium complexes, of the type $[(H_2O)_5Cr^{III}\text{-}CHR^1CHR^2OH]^{2+}$; where R^1 = H, CH_3; R^2 = H, CH_3 [14, 28]. Basically, these complexes are prepared in a similar manner to their hydroxymethyl analogues (Method (C), Section 2.1.1), and they can only be observed by UV spectroscopy.

A general synthetic methodology to β-hydroxyethyl metal complexes was reported in 1967 by Schrauzer and Windgassen [29]. The cobaloxime(II) was reacted with ethylene oxide under hydrogen (as reducing agent) to give an air-stable β-hydroxyethyl cobaloxime complex in high yield, as shown in Equation 2.8.

$$2[Co^{II}] + 2\ \underset{H_2C\text{—}CH_2}{\overset{O}{\diagup\!\diagdown}} + H_2 \longrightarrow 2[Co]\text{-}CH_2CH_2OH$$

Equation 2.8

Other reported β-hydroxyethyl complexes synthesized by this route are $[L_mM(CH_2CH_2OH)]$, where L_mM = $CpFe(CO)_2$ [30, 31], $CpFe(CO)(L)$ (L = PPh_3, $P(OPh)_3$) [32], $CpM(CO)_3$ (M = Mo, W) [33]. Basically, the metal anions are reacted with ethylene oxide, and β-hydroxyethyl metal complexes are obtained after acidic treatment. However, $[CpFe(CO)_2(CH_2CH_2OH)]$ could not be isolated by this route, because of the high sensitivity of complex to acidic treatment. The cationic η^2-ethylene iron complex was the only isolated product, as shown in Scheme 2.7.

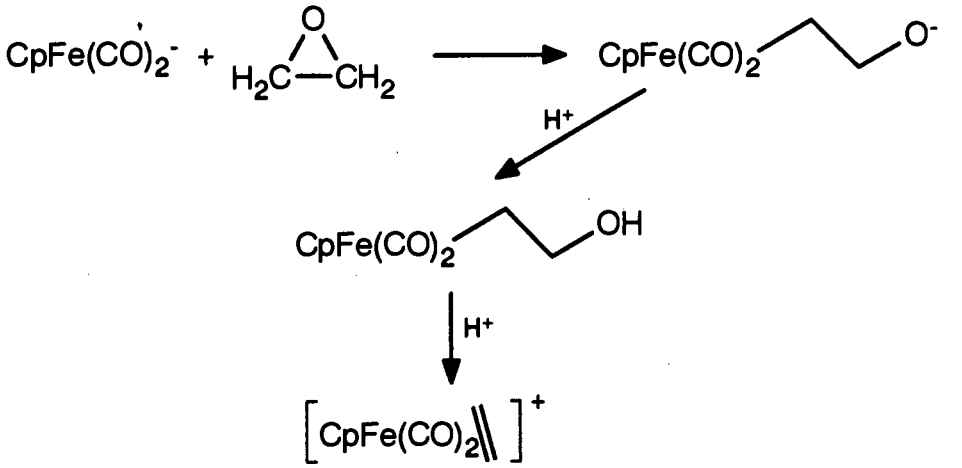

Scheme 2.7

In this present study, we have successfully synthesized and isolated $[CpFe(CO)_2(CH_2CH_2OH)]$, as a yellow crystaline product *via* a different method. Thus $CpFe(CO)_2^-$ was reacted with ICH_2CH_2OH to give $[CpFe(CO)_2(CH_2CH_2OH)]$ directly without acid treatment, as shown in Equation 2.9.

$$Na^+CpFe(CO)_2^- + ICH_2CH_2OH \longrightarrow [CpFe(CO)_2(CH_2CH_2OH)] + NaI$$

Equation 2.9

This reaction goes in good yield (55 %), and analytically pure crystaline $[CpFe(CO)_2(CH_2CH_2OH)]$ was fully characterized by standard spectroscopic methods. Details of this reaction can be seen in Section 2.2.

2.1.3 ω-Hydroxyalkyl complexes of the type, $[L_mM\{(CH_2)_nOH\}]$, where n > 2

ω-Hydroxyalkyl complexes, $[L_mM\{(CH_2)_nOH\}]$ (n > 2), are far less well known, compared to hydroxymethyl and hydroxyethyl complexes. The first series of ω-hydroxyalkyl complexes were repoted in 1967 by Schrauzer and Windgassen [29]. The cobaloxime anion was reacted with hydroxyalkyl halides to give hydroxyalkyl cobaloxime complexes, as shown in Equation 2.10.

$$2[Co^{II}] + 2X(CH_2)_nOH + H_2 \longrightarrow 2[Co^{II}]\text{-}(CH_2)_nOH + 2HX$$

X = halogen
n = 3, 4

Equation 2.10

Also, a mixture of $(CO)_9Co_3C(CH_2)_nOH$ (n = 4, 5) was reported as thermal decomposition products of $(CO)_4CoBH_2$•THF [34]. In this case, the C-O bond of THF was cleaved by $(CO)_4CoBH_2$, and the hydroxypentyl complex was formed after CO insertion. The mechanism for the formation of products was also reported, and is shown in Scheme 2.8.

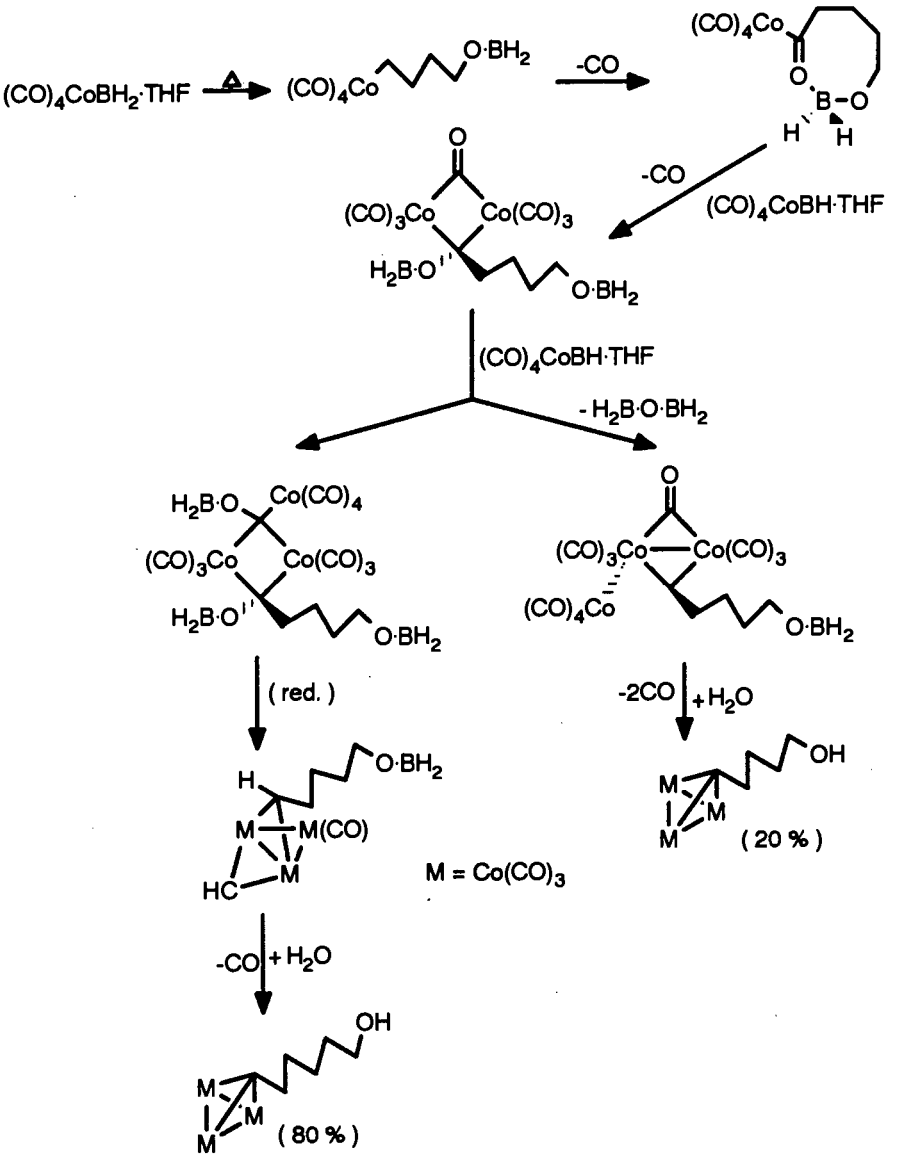

Scheme 2.8

2.1.4 Scope of this study

In this chapter, we report the synthesis of a series of new ω-hydroxyalkyl transition metal complexes of the type, $[L_mM\{(CH_2)_nOH\}]$ (where L_mM = $CpFe(CO)_2$, $Cp^*Fe(CO)_2$, $CpRu(CO)_2$; n = 2, 3, 4). These complexes have been fully characterized by standard spectroscopic methods, and the results will be discussed in the following sections.

2.2 PREPARATION OF ω-HYDROXYALKYL TRANSITION METAL COMPLEXES

A series of new ω-hydroxyalkyl transition metal complexes has been prepared by the general method, shown in Equation 2.11.

$$Na^+L_mM^- + X(CH_2)_nOH \longrightarrow [L_mM\{(CH_2)_nOH\}] + NaX$$

X = I, n = 2
X = Br, n = 3
X = Cl, n = 4

$L_mM^- = CpFe(CO)_2^-,\ Cp^*Fe(CO)_2^-,\ CpRu(CO)_2^-$

Equation 2.11

The following complexes have been prepared in this manner:

$[CpFe(CO)_2\{(CH_2)_2OH\}]$	**(14)**	$[Cp^*Fe(CO)_2\{(CH_2)_2OH\}]$	**(17)**
$[CpFe(CO)_2\{(CH_2)_3OH\}]$	**(15)**	$[Cp^*Fe(CO)_2\{(CH_2)_3OH\}]$	**(18)**
$[CpFe(CO)_2\{(CH_2)_4OH\}]$	**(16)**	$[Cp^*Fe(CO)_2\{(CH_2)_4OH\}]$	**(19)**
$[CpRu(CO)_2\{(CH_2)_2OH\}]$	**(20)**		
$[CpRu(CO)_2\{(CH_2)_3OH\}]$	**(21)**		

Prior to this study, the only known series of ω-hydroxyalkyl complexes were the cobaloxime complexes of the type, $[(Py)(DMG)_2Co\{(CH_2)_nOH]$ (n = 2, 3, 4), which have been made by a similar method [29]. Those authors suggested that ethylene oxide is a better alkylation reagent than 2-hydroxyalkyl halides. Indeed a few β-hydroxyethyl complexes were prepared and isolated in that manner, as shown in Section 2.1.2. However, **(14)** was reported as an intermediate and could not be isolated from ethylene oxide. It is believed that the required protonation reaction causes the decomposition of **(14)** to give the cationic η^2-ethylene iron complex, as shown in Scheme 2.7.

In this present study we have used 2-iodoethanol instead of ethylene oxide, so as to avoid the protonation reaction. Thus, we were able to isolate three β-hydroxyethyl metal complexes **(14)**, **(17)** and **(20)** which were recrystallized from CH_2Cl_2/hexane at -15 °C. The reaction temperatures and times used for the preparation of **(14)** - **(21)** vary considerably. They depend very much on the nucleophilicities of metal anions and the alkyl halides used (see experimental section). In the reaction of $[CpRu(CO)_2]^-$ with 4-chlorobutanol, no anticipated 4-hydroxybutyl ruthenium complex was obtained after stirring the reaction mixture at room temperature for 24 hours. Presumably this is due to the weak nucleophilicity of $[CpRu(CO)_2]^-$ towards 4-chlorobutanol. More vigorous reaction conditions or the use of better leaving groups may be needed to facilitate this reaction. The yields for **(14)** - **(21)** are shown in Table 2.2. Generally speaking, the yields for the $CpFe(CO)_2$ series of complexes **(14)** - **(16)** are the highest, followed by the complexes of the $Cp^*Fe(CO)_2$ series **(17)** - **(19)**. The $CpRu(CO)_2$ series of complexes **(20)** and **(21)** give the lowest yields.

2.3 GENERAL PROPERTIES OF COMPLEXES (14) - (21)

The complexes **(14)** - **(19)** are all isolated as yellow crystalline products, and complexes **(20)**, **(21)** are white crystals. Although, in some cases, **(20)** was obtained as light brown crystals, characterization data showed no differences between them, and the colour may be due to minute traces of ruthenium metal or oxide. The melting points of **(14)** - **(21)** are given in Table 2.2. It is found that the $Cp^*Fe(CO)_2$ series of complexes give the highest melting points, and the melting points of complexes are generally decreased as alkyl chain length increased, which is very similar to those results on complexes $[CpFe(CO)_2(CH_2)_nFe(CO)_2Cp]$ [35] and $[CpFe(CO)_2\{(CH_2)_nX]$ (

where X = Br, I,) [36]. The complexes **(14)** - **(21)** are soluble in common organic solvents, except hexane. It is also found that **(14)** - **(21)** are insoluble in water, although the cobaloxime hydroxypropyl complex was found to be soluble in water.

2.4 IR SPECTRA OF COMPLEXES (14) - (21)

The IR spectra of **(14)** - **(21)** were recorded in the CH_2Cl_2 solution between 2200 and 1600 cm^{-1}. The data are shown in Table 2.2. Basically, there is no change of υ(CO) between 3-hydroxypropyl and 4-hydroxybutyl complexes. However, a significant shift in υ(CO) from 3-hydroxypropyl to 2-hydroxyethyl complexes was observed, Particularly in the $CpFe(CO)_2$ series of complexes, there is a shift of *ca.* 20 cm^{-1} between **(14)** and **(15)**. The shift in υ(CO) is much less in the $Cp^*Fe(CO)_2$ and $CpRu(CO)_2$ series of complexes (7 cm^{-1} between **(17)** and **(18)**; 4 cm^{-1} between **(20)** and **(21)**). The shift in υ(CO) in 2-hydroxyethyl complexes is not solely due to the effect of alkyl chain length, since there is almost no change in υ(CO) between $[CpFe(CO)_2(C_2H_5)]$ and $[CpFe(CO)_2(C_3H_7)]$. Also the υ(CO) of **(15)** is the same as for $[CpFe(CO)_2(C_3H_7)]$, which implies that the hydroxy group has no effect on the υ(CO) of **(15)**, whereas hydroxy group has a significant effect on υ(CO) of **(14)**. We believe that the shift of υ(CO) in 2-hydroxyethyl complexes is due to the contribution of a possible resonance form (B), as shown in Scheme 2.9.

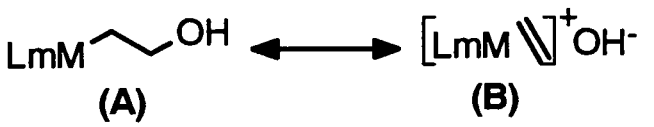

(A) **(B)**

Scheme 2.9

The cationic η^2-ethylene transition metal complexes are known to give higher υ(CO)

than the ethyl transition metal complexes, due to the positive charge on the metal centre. For example, υ(CO) for $[CpFe(CO)_2(\eta^2\text{-ethylene})]^+PF_6^-$ are 2078, 2041cm^{-1}, whereas υ(CO) for $[CpFe(CO)_2(C_2H_5)]$ are 2000, 1938 cm^{-1}. Thus, if we took $[CpFe(CO)_2(\eta^2\text{-ethylene})]^+PF_6^-$ and $[CpFe(CO)_2(C_2H_5)]$ as the model complexes for the resonance forms (B) and (A) respectively in **(14)**, the IR results obtained here could indicate that there is about a 20% contribution of (B) form to the overall structure of **(14)**. This may have significant consequences on the chemical reactivity of **(14)**. Thus, **(14)** may be expected to react with the proton to give $[CpFe(CO)_2(\eta^2\text{-ethylene})]^+$, whereas the iron carbon bond is cleaved when $[CpFe(CO)_2(C_2H_5)]$ is treated with acids.

The hydrogen bonding of the hydroxy group in **(15)** was also studied by IR spectroscopy. A sample of **(15)** was dissolved in dry toluene and spectra were recorded in the region of 4000 and 3000 cm^{-1}. The spectra showed a sharp strong absorption band at 3595 cm^{-1} which was assigned as non-hydrogen bonded hydroxy group. In addition, a broad strong absorption band at 3459 cm^{-1} was assigned to the hydrogen bonded hydroxy group. The type of hydrogen bonding in **(15)** was also established by measuring spectra at different concentrations of samples. It is found that the position of absorption band at 3459 cm^{-1} is concentration dependent and was shifted to higher wavenumber as the concentration decreased. This implies that the absorption band at 3459 cm^{-1} is due to the intermolecular hydrogen-bonded hydroxy group, which is common in most organic alcohols [37].

Table 2.2 Some characterization data for the ω-hydroxyalkyl transition metal complexes

Complexes	Yield%	Melting point °C	IR υ(CO) cm^{-1} CH_2Cl_2		Molecular ion in mass spectra	Microanalysis Calc. % (Found %)	
						C	H
[CpFe(CO)$_2${(CH$_2$)$_2$OH}] (14)	55	57-58	2013	1960	222 (P)	48.7 (48.7)	4.5 (4.3)
[CpFe(CO)$_2${(CH$_2$)$_3$OH}] (15)	74	43-44	2002	1942	236 (P)	50.9 (50.5)	5.1 (4.9)
[CpFe(CO)$_2${(CH$_2$)$_4$OH}] (16)	32	24-26	2000	1940	250 (P)	52.8 (53.0)	5.6 (5.9)
[Cp*Fe(CO)$_2${(CH$_2$)$_2$OH}] (17)	27	75 (dec)	1983	1922	292 (P)	57.6 (57.7)	6.9 (6.9)
[Cp*Fe(CO)$_2${(CH$_2$)$_3$OH}] (18)	59	74-76	1978	1915	306 (P)	58.7 (58.2)	7.2 (7.2)
[Cp*Fe(CO)$_2${(CH$_2$)$_4$OH}] (19)	19	69-71	1978	1915	320 (P)	60.0 (59.7)	7.6 (7.6)
[CpRu(CO)$_2${(CH$_2$)$_2$OH}] (20)	15	40 (dec)	2014	1951	268 (P)		
[CpRu(CO)$_2${(CH$_2$)$_3$OH}] (21)	24	44-46	2012	1947	254 (P-CO)		

2.5 ^{1}H NMR SPECTRA OF COMPLEXES (14) - (21)

The ^{1}H NMR data for complexes **(14)** - **(21)** are summarized in Table 2.3. Since these complexes are relative simple, most of the assignments for these data are made by integration and comparisons with analogous complexes. However the assignments for complex **(15)** were further confirmed by COSY and HETCOR experiments.

In general, the alkyl chain length has no effects on the δ value of Cp ring. It is found that the solvents used in the NMR experiments have a significant effect on the δ value of the Cp ring, but have much less effect on the δ value of MCH_2. The chemical shift of MCH_2 shows an unusual shift between 2-hydroxyethyl and 3-hydroxypropyl complexes. It is observed that the δ value for MCH_2 of **(14)** is lower than that of **(15)**, whereas in the cases of **(17)** and **(20)** the δ values for MCH_2 are higher than for **(18)** and **(21)** respectively. We believe that this rather unusual shift toward low frequency for **(14)** is due to the contribution of resonance form (B) (Scheme 2.9), in which a significant amount of π electron density (*ca.* 20% according to IR results) was accumulated along the carbon carbon bond. Thus the protons on the α-carbon are shielded and go to low frequency.

The assignment of the hydroxy proton was achieved with the aid of D_2O wash experiments. It is found that the chemical shift of the hydroxy proton varies, between 0.5 and 1.6 ppm, depending on the concentrations of samples. This should give us further confirmation of the intermolecular hydrogen bonding in these hydroxyalkyl metal complexes.

Table 2.3 ^{1}H NMR data for the hydroxyalkyl metal complexes **(14) - (21)**

Complexes	Solvent	Cp ring	M-CH_2	CH_2	CH_2O	OH
[$CpFe(CO)_2\{(CH_2)_2OH\}$] (14)	C_6D_6	4.03	1.44	N/A	3.65	1.18
[$CpFe(CO)_2\{(CH_2)_3OH\}$] (15)	$CDCl_3$	4.68	1.62	1.34	3.49	*a*
	C_6D_6	4.05	1.69	1.38	3.46	1.01
[$CpFe(CO)_2\{(CH_2)_4OH\}$] (16)	$CDCl_3$	4.76	1.52		3.66	1.73
	C_6D_6	4.06	1.54		3.48	0.68
[$Cp^*Fe(CO)_2\{(CH_2)_2OH\}$] (17)	C_6D_6	1.35	1.11	N/A	3.83	*b*
[$Cp^*Fe(CO)_2\{(CH_2)_3OH\}$] (18)	$CDCl_3$	1.71	0.81	*c*	3.55	1.38
[$Cp^*Fe(CO)_2\{(CH_2)_4OH\}$] (19)	$CDCl_3$	1.71	0.98	*c*	3.62	1.28
[$CpRu(CO)_2\{(CH_2)_2OH\}$] (20)	C_6D_6	4.48	1.71	N/A	3.66	1.21
[$CpRu(CO)_2\{(CH_2)_3OH\}$] (21)	$CDCl_3$	5.23	1.61	1.81	3.53	1.43

a: signal overlaps with CH_2 resonance *b*: signal overlaps with MCH_2 resonance *c*: signal overlaps with Cp* resonance
chemical shifts are in ppm

2.6 ^{13}C NMR SPECTRA OF COMPLEXES (14) - (21)

The ^{13}C NMR data for complexes **(14)** - **(21)** are given in Table 2.4. In contrast to the proton NMR spectra, there is no significant change of ^{13}C chemical shift in different solvents. It is also found that the alkyl chain length has no effect on the δ values of the Cp ring or the CO. However the δ value of CH_2O showed a shift toward low frequency as the alkyl chain length increased.

An unusually low δ value for M-CH_2 in the 3-hydroxypropyl metal complexes **(15)**, **(18)** and **(21)** was seen in the ^{13}C NMR spectra. A similar effect was also observed in the analogous series of bromopropyl metal complexes. It was suspected that the remote interaction between the metal centre and the functional group on alkyl chain caused this unusual chemical shift of MCH_2 in the ^{13}C NMR spectra. This remote interaction between the metal centre and the functional group was believed to be a result of the formation of a sterically favoured five member ring, as shown in Figure 2.2.

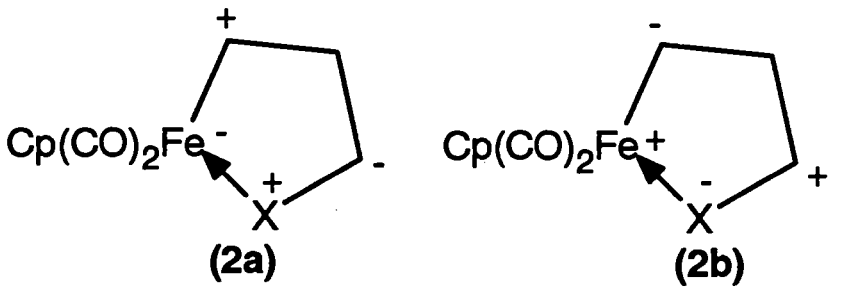

Figure 2.2 The remote interaction between metal and functional group X

In the present study, we investigated this remote interaction by comparing the ^{13}C δ values of M-CH_2 between [$CpFe(CO)_2\{(CH_2)_3X\}$] and [$CpFe(CO)_2\{(CH_2)_4X\}$]. The results are summarized in Table 2.5.

Table 2.4 ^{13}C NMR data for the ω-hydroxyalkyl metal complexes **(14) - (21)**

Complexes	Solvent	Cp ring		$M-CH_2$	CH_2		CH_2O	CO
$[CpFe(CO)_2\{(CH_2)_2OH\}]$ (14)	C_6D_6	84.89		5.08	N/A		69.52	217.45
$[CpFe(CO)_2\{(CH_2)_3OH\}]$ (15)	$CDCl_3$	85.36		-2.69	40.89		66.07	217.36
	C_6D_6	85.37		-1.76	41.57		66.01	218.06
$[CpFe(CO)_2\{(CH_2)_4OH\}]$ (16)	$CDCl_3$	85.41		3.11	37.88	34.23	62.72	217.67
	C_6D_6	85.38		3.61	38.43	34.76	62.51	218.24
$[Cp^*Fe(CO)_2\{(CH_2)_2OH\}]$ (17)	C_6D_6	95.74	9,61	16.28	N/A		70.24	219.44
$[Cp^*Fe(CO)_2\{(CH_2)_3OH\}]$ (18)	$CDCl_3$	94.89	9.31	6.98	40.47		66.87	219.24
$[Cp^*Fe(CO)_2\{(CH_2)_3OH\}]$ (19)	$CDCl_3$	94.91	9.28	13.28	38.81	33.54	63.01	219.51
$[CpRu(CO)_2\{(CH_2)_2OH\}]$ (20)	C_6D_6	87.62		-1.27	N/A		69.64	202.18
$[CpRu(CO)_2\{(CH_2)_2OH\}]$ (21)	$CDCl_3$	88.53		-9.53	42.31		66.18	202.13

chemical shifts are in ppm

Table 2.5 ^{13}C NMR data for ($Fe-CH_2$) in functionalized propyl iron complexes

Complexes	δ ($Fe-CH_2$)		$\Delta\delta(C_3-C_4)$	EN (X)	ΔEN (X-C)	Reference
	C3	C4		2.5 (C)		
$[CpFe(CO)_2(C_3H_6OH)]$	-2.7	3.1	-5.8	3.5 (O)	1.0	*a*
$[CpFe(CO)_2(C_3H_6Br)]$	-0.8	1.3	-2.2	2.7 (Br)	0.2	[36]
$[CpFe(CO)_2(C_3H_6I)]$	1.9	1.1	0.8	2.2 (I)	-0.3	[36]
$[CpFe(CO)_2(C_3H_7)]$	6.5	3.3	3.1	2.2 (H)	-0.3	*b*
$[CpFe(CO)_2(C_3H_6)Fe(CO)_2Cp]$	7.8	3.8	4.0	1.6 (Fe)	-0.9	[38]
$[CpFe(CO)_2(C_3H_6)Ru(CO)_2Cp]$	7.7	3.7	4.0	1.4 (Ru)	-1.1	[39]
$[CpFe(CO)_2(C_3H_6)Mo(CO)_3Cp]$	8.4	3.3	5.1	1.3(Mo)	-1.2	[40]
$[CpFe(CO)_2(C_3H_6)W(CO)_3Cp]$	9.1	3.9	5.2	1.4 (W)	-1.1	[40]
$[CpFe(CO)_2(C_3H_6)Re(CO)_5]$	11.4	3.3	8.1	1.5 (Re)	-1.0	[40]
$[CpFe(CO)_2(C_3H_6OSiMe_3)]$	-2.5			3.5 (O)	1.0	*a*
$[CpFe(CO)_2(C_3H_6OCOCH_3)]$	-3.7			3.5 (O)	1.0	*a*
$[CpFe(CO)_2(C_3H_6OCPh_3)]$	-1.6			3.5 (O)	1.0	*a*

a: data were reported in this study *b*: data were obtained from authentic samples
chemical shifts are in ppm

It is noticed that most of the propyl iron complexes are shifted toward high frequency, except for the bromo and hydroxypropyl iron complexes. The changes of δ values are correlated to the nominal electronegativities [41] of the heteroatoms on functional groups, as shown in Table 2.5.

It is found that the high frequency shift only occurs when the electronegativity of the hetroatom on the functional group was lower than the electronegativity of carbon, whereas low frequency shift occurred when the electronegativity of heteroatom on the functional group was higher than the electronegativity of carbon. Thus, in the cases of the bromopropyl and hydroxypropyl complexes, the heteroatoms (Br and O) are more electronegative than carbon; therefore low frequency shifts were observed. Whereas, in the cases of iodopropyl, propyl and propylene bridged bimetallic complexes, the heteroatoms (I, H and transition metals) are less electronegative than carbon, thus high frequency shifts were detected.

We believe that this correlation is due to a remote interaction between the metal and the heteroatom of the functional group, in which the metal carbon bonds are polarized by the heteroatoms, as shown in Figure 2.2. Therefore, if the heteroatoms were more electronegative than carbon, a partial negative charge would be generated on the heteroatom. The iron carbon bond would thus be polarized to yield partial negative charge on the α-carbon, as shown in Figure (2b), and this extra electron density could cause the low frequency shift of α-carbon in ^{13}C NMR. In contrast, if the heteroatom were less electronegative than carbon, a partial positive charge would be generated on the α-carbon through a similar interaction, as shown in Figure (2a), thus a high frequency shift of the α-carbon was observed.

Also, from Table 2.5, we found that the substituents on the functional group could affect the δ value of α-CH_2, as shown in the examples of $[CpFe(CO)_2(C_3H_6OSiMe_3)]$, $[CpFe(CO)_2(C_3H_6OCOCH_3)]$, $[CpFe(CO)_2(C_3H_6OCPh_3)]$ and **(15)**. These results indicate that an electron withdrawing group, like CH_3CO, increases the remote interaction, and causes a further shift toward low frequency. Whereas, the electron donating group, like CPh_3, decreases the remote interaction, and causes a shift toward high frequency compared to the δ value of **(15)**.

2.7 MASS SPECTROMETRY

The molecular ions in the low resolution electron impact mass spectra for **(14)** - **(21)** are given in Table 2.2. They showed either a parent ion peak, or in one case, an ion corresponding to $(P\text{-}CO)^+$.

The fragmentations of **(14)** - **(21)** are similar to their haloalkyl analogues, $[L_mM\{(CH_2)_nX\}]$ (where L_mM = $CpFe(CO)_2$, $Cp^*Fe(CO)_2$, $CpRu(CO)_2$). Fragmentation pathways for haloalkyl metal complexes have been proposed [36], however in addition to the previously proposed fragmentation, an unusual fragmentation occurred in the complex **(14)**. The mass spectrum of **(14)** showed a set of peaks which correspond to P^+-16, P^+-CO-16, P^+-2CO-17. We believe that this fragmentation is due to the formation of a molecular ion $[CpFe(CO)_2C_2H_5]^+$, by losing one oxygen atom in the fragmentation process, which was then followed by the same fragmentation process as the alkyl iron complexes of the type $[CpFe(CO)_2R]$.

The fragmentation mechanism of **(14)** is summarized in Scheme 2.10. Paths I and II are common in all functionalized alkyl iron complexes and the length of alkyl chain seems to have no effect on the fragmentation mechanism. However path III can only

be observed in complex **(14)**. To our knowledge, path III has never been observed before, and this unusual fragmentation may have significance to the properties of **(14)**. Although in the cases of organic alcohols, the P^+-H_2O and P^+-CH_2OH are the most important fragments. However, we observed no such fragments in the mass spectra of **(14)** - **(21)**. Presumably this is due to the metal centre in complexes **(14)** - **(21)** being more susceptible to the electron impact, and the positive charge is essentially localized at the metal centre, and thereafter the fragmentation was observed to take place at the metal centre.

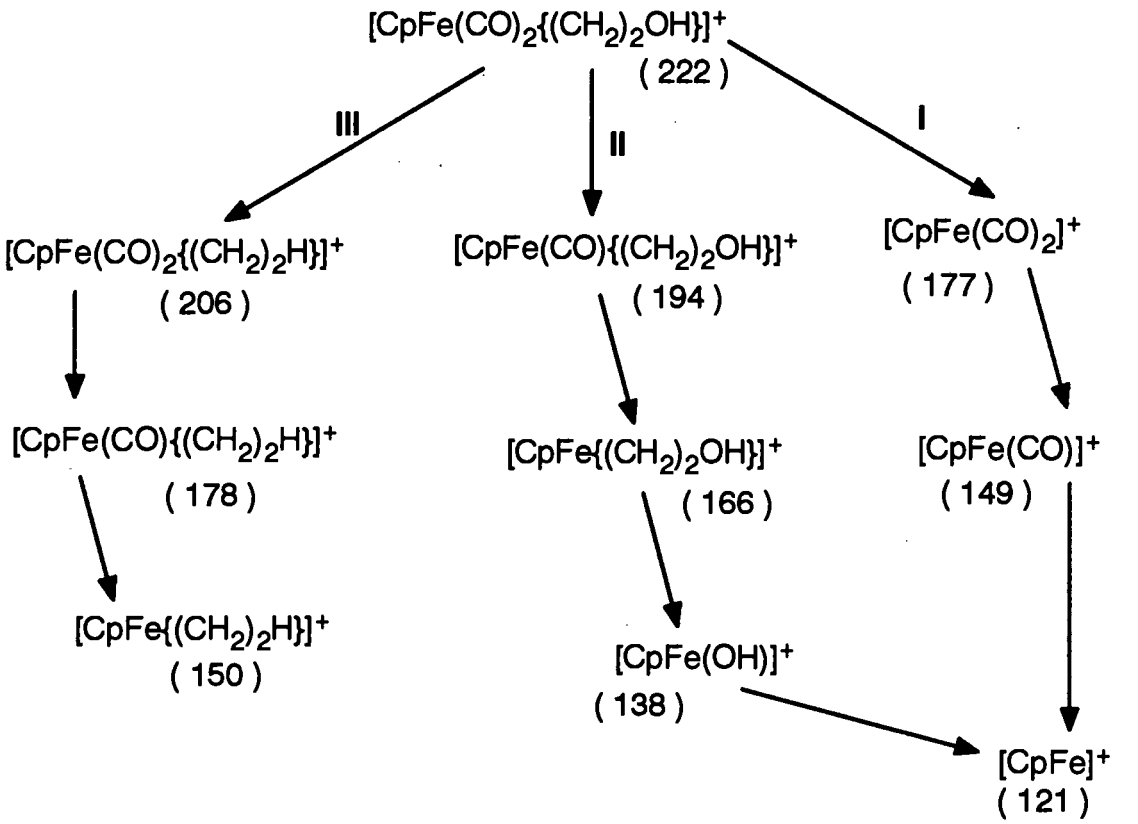

Scheme 2.10

2.8 REFERENCES

1. G. Henrici-Olivé and S. Olivé, *Angew. Chem. Int. Ed. Engl.*, **1976**, *15*, 136.
2. C. Masters, *Adv. Organomet. Chem.*, **1979**, *17*, 61.
3. E. L. Muetterties and J. Stein, *Chem. Rev.*, **1979**, *79*, 479.
4. C. K. Rofer-DePoorter, *Chem. Rev.*, **1981**, *81*, 447.
5. W. A. Herrmann, *Angew. Chem. Int. Ed. Engl.*, **1982**, *21*, 117.
6. T. Blackmore, M. I. Bruce, P. J. Davidson, M. Z. Iqbal and F. G. A. Stone, *J. Chem. Soc. (A)*, **1970**, 3153.
7. J. A. Roth and M. Orchin, *J. Organomet. Chem.*, **1979**, *172*, C27.
8. G. D. Vaughn and J. A. Gladysz, *J. Am. Chem. Soc.*, **1981**, *103*, 5608.
9. B. B. Wayland, B. A. Woods and V. M. Minda, *J. Chem. Soc. Chem. Commun.*, **1982**, 634.
10. G. R. Clark, C. E. L. Headford, K. Marsden and W. R. Roper, *J. Organomet. Chem.*, **1982**, *231*, 335.
11. H. Berke, G. Huttner, G. Weiler and L. Zsolnai, *J. Organomet. Chem.*, **1981**, *219*, 353.
12. W. Schmidt, J. H. Swinehart and H. Taube, *J. Am. Chem. Soc.*, **1971**, *93*, 1117.
13. A. Bakač and J. H. Espenson, *J. Am. Chem. Soc.*, **1981**, *103*, 2721.
14. H. Elroi and D. Meyerstein, *J. Am. Chem. Soc.*, **1978**, *100*, 5540.
15. J. C. Selover, G. D. Vaughn, C. E. Strouse and J. A. Gladysz, *J. Am. Chem. Soc.*, **1986**, *108*, 1455.
16. C. P. Casey, M. A. Andrews, D. R. McAlister and J. E. Rinz, *J. Am. Chem. Soc.*, **1980**, *102*, 1927.
17. J. R. Sweet and W. A. G. Graham, *J. Am. Chem. Soc.*, **1982**, *104*, 2811.

18. D. L. Thorn and T. H. Tulip, *Organometallics*, **1982**, *1*, 1580.

19. C. Lapinte, D. Catheline and D. Astruc, *Organometallics*, **1988**, *7*, 1683.

20. G. O. Nelson and C. E. Sumner, *Organometallics*, **1986**, *5*, 1983.

21. C. J. May and W. A. G. Graham, *J. Organomet. Chem.*, **1982**, *234*, C49.

22. Y. C. Lin, D. Milstein and S. S. Wreford, *Organometallics*, **1983**, *2*, 1461.

23. P. M. Henry, *Adv. Organomet. Chem.*, **1975**, *13*, 363.

24. J. Halpern and R. A. Jewsbury, *J. Organomet. Chem.*, **1979**, *181*, 223.

25. G. A. Luinstra, J. A. Labinger and J. E. Bercaw, *J. Am. Chem. Soc.*, **1993**, *115*, 3004.

26. K. A. Hofmann and J. Sand, *Chem. Ber.*, **1900**, *33*, 1340.

27. R. T. Morrison and R. N. Boyd, *Organic Chemistry*, 4th Ed., pp 468, Allyn and Bacon, Boston, **1983**.

28. H. Cohen, A. Feldman, R. Ish-Shalom and D. Meyerstein, *J. Am. Chem. Soc.*, **1991**, *113*, 5292.

29. G. N. Schrauzer and R. J. Windgassen, *J. Am. Chem. Soc.*, **1967**, *89*, 143.

30. W. P. Giering, M. Rosenblum and J. Tancrede, *J. Am. Chem. Soc.*, **1972**, *94*, 7170.

31. S. G. Davies, I. M. Dordor, J. C. Walker and P. Warner, *Tetrahedron Letters*, **1984**, *25*, 2709.

32. D. H. Gibson, J. O. Franco, M. T. Harris and T.-S. Ong, *Organometallics*, **1992**, *11*, 1993.

33. W. H. Knoth, *Inorg. Chem.*, **1975**, *14*, 1566.

34. J. D. Basil, A. A. Aradi, N. K. Bhattacharyya, N. P. Rath, C. Eigenbrot and T. P. Fehlner, *Inorg. Chem.*, **1990**, *29*, 1260.

35. J. R. Moss and L. G. Scott, *J. Organomet. Chem.*, **1985**, *282*, 255.

36. H. B. Friedrich, P. A. Makhesha, J. R. Moss and B. K. Williamson, *J. Organomet. Chem.*, **1990**, *384*, 325.

37. M. D. Joesten and L. J. Schaad, *Hydrogen Bonding*, Marcel Dekker, **1974**.

38. L. Pope, P. Sommerville, M. Laing, K. J. Hindson and J. R. Moss, *J. Organomet. Chem.*, **1976**, *112*, 309.

39. H. B. Friedrich, PhD Thesis, University of Cape Town, **1990**.

40. H. B. Friedrich, J. R. Moss and B. K. Williamson, *J. Organomet. Chem.*, **1990**, *394*, 313.

41. K. F. Purcell and J. C. Kotz, *Inorganic Chemistry*, pp 59, Philadelphia, Holt-Saunder, **1977**.

CHAPTER 3 A STUDY ON THE CHEMICAL REACTIVITY, ELECTROCHEMICAL BEHAVIOUR AND THERMAL PROPERTIES OF $[CpFe(CO)_2\{(CH_2)_3OH\}]$

3.1 INTRODUCTION

As we stated in Chapter 2, hydroxyalkyl metal complexes have been known since 1967 and complexes of this type have often been proposed as intermediates or model complexes for catalytic reactions. Scheme 3.1 shows the involvement of α-hydroxyalkyl metal complexes in various catalytic reactions.

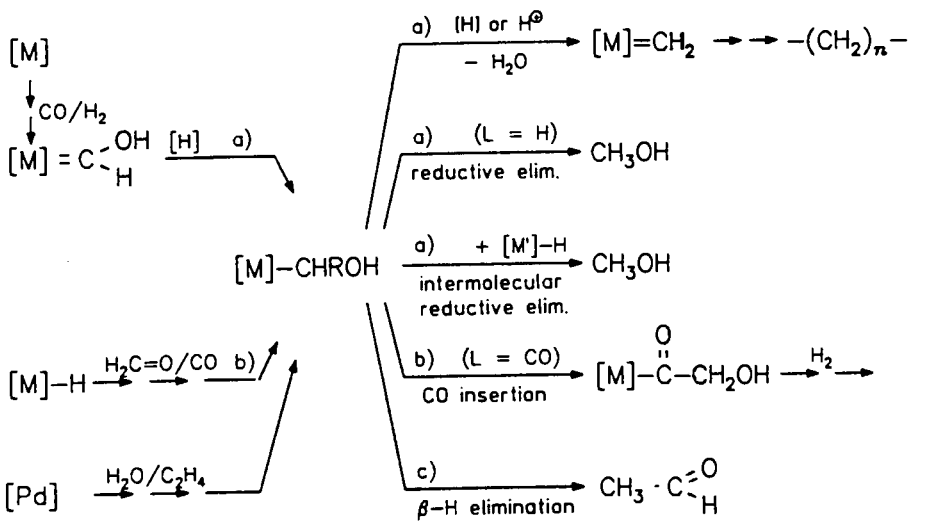

Scheme 3.1 α-Hydroxyalkyl metal complexes in catalytic reactions.
a) CO hydrogenation b) Hydroformylation reaction c) Wacker process

As a result of this, many hydroxymethyl complexes have been synthesized and studied (see Section 2.1.1). Although β-hydroxyethyl metal complexes are known (see Section 2.1.2) and also proposed as intermediates in catalytic processes, such as the Wacker process (Scheme 2.5), there have been very few studies on β-hydroxyethyl and ω-hydroxyalkyl metal complexes.

In this Chapter, we report various reactions of $[CpFe(CO)_2\{(CH_2)_3OH\}]$ **(1)** (Figure 3.1).

These reactions are expected to occur either at the metal centre or at the hydroxy group .

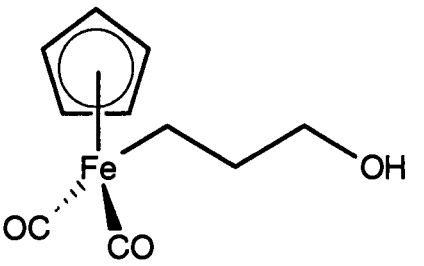

Figure 3.1 A ω-hydroxypropyl iron complex

Previously Davies *et al.* have reported a carbonyl insertion reaction for the β-hydroxyethyl iron complex, $[CpFe(CO)_2\{(CH_2)_2OH\}]$ **(5)** to give an acyl iron complex, as shown in Equation 3.1 [1].

$$[CpFe(CO)_2\{(CH_2)_2OH\}] \xrightarrow{PPh_3} [CpFe(CO)(PPh_3)\{CO(CH_2)_2OH\}]$$

Equation 3.1

Also, as stated in Chapter 1, the related complex $[CpFe(CO)_2\{(CH_2)_3Br\}]$ is known to be a precursor for cyclopropane and to form cyclic carbene species by a carbonyl insertion reaction, as shown in Scheme 3.2.

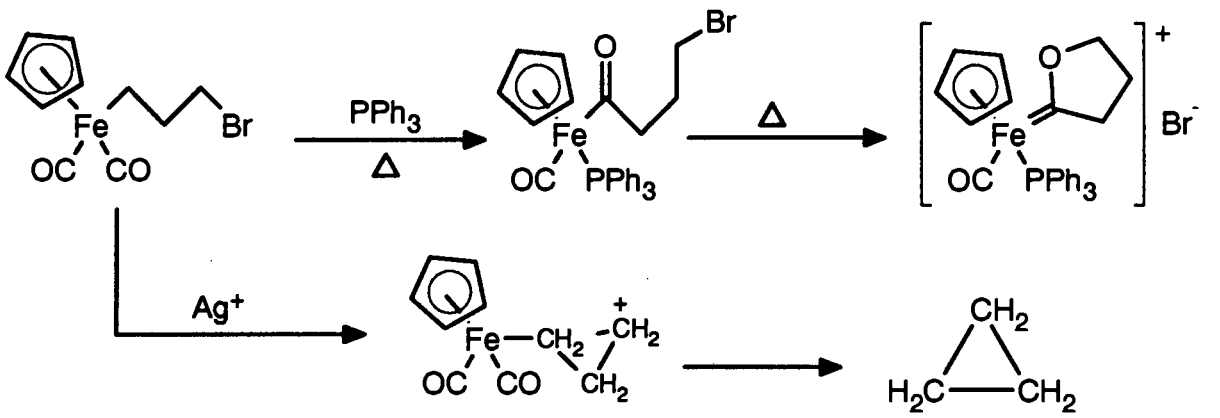

Scheme 3.2

We are particularly interested in the selectivity of the reactions studied, and also a comparison of the reactivity with that of related complexes. Cyclic voltammetry and differential scanning calorimetry were also employed to investigate the electrochemical and thermal properties of **(1)**.

3.2 THE CHEMICAL REACTIVITY OF $[CpFe(CO)_2\{(CH_2)_3OH\}]$ (1)

3.2.1 Reactions with silyl chlorides

Complex **(1)** reacts with silyl chlorides under basic conditions to give the corresponding silylether derivatives, complexes **(2)** - **(4)**. The reactions are shown in Equation 3.2.

$$[CpFe(CO)_2\{(CH_2)_3OH\}] + R_3SiCl \xrightarrow{\text{Base}} [CpFe(CO)_2\{(CH_2)_3OSiR_3\}]$$

(1)

$R_3 = Me_3$ **(2)**

$R_3 = t\text{-}BuMe_2$ **(3)**

$R_3 = t\text{-}BuPh_2$ **(4)**

Equation 3.2

Complex **(2)** was obtained as a yellow oil in good yield (83 %), whereas **(3)** and **(4)** were obtained as yellow crystalline solids (mp 47 and 73 °C, respectively) in moderate to good yields (79 and 39 %, respectively). The reaction conditions used in this study are very similar to those reported for the conversion of primary alcohols to their silylether derivatives [2]. However, the yields of **(2)** - **(4)** are lower than those reported for silylethers of primary alcohols.

The new complexes **(2)** - **(4)** were fully characterized by standard spectroscopic and analytical methods, and the data are given in the experimental section. The results

obtained from IR spectroscopy showed that there is no change in the position of the carbonyl bands between **(1)** and **(2)** - **(4)**. Also, the resonance of the CH_2O group in the ^1H NMR spectrum showed no significant change between **(1)** and **(2)** - **(4)**. Nevertheless, the identification of the products **(2)** - **(4)** can easily be made by the integration of resonances in the ^1H NMR spectra. The observed molecular ion peaks in the mass spectra and the satisfactory microanalysis results give further confirmation for **(2)** - **(4)**.

In an attempt to prepare a silylether derivative of the β-hydroxyethyl iron complex **(5)** in basic conditions, we obtained only the cationic iron complex, $[CpFe(CO)_2(\eta^2$-ethylene$)]^+$; no anticipated silylether complex was observed. This could be due to the significant contribution of the cationic resonance form in **(5)**, which reacts with Me_3SiCl to give Me_3SiOH and $[CpFe(CO)_2(\eta^2$-ethylene$)]^+$, as shown in Scheme 3.3.

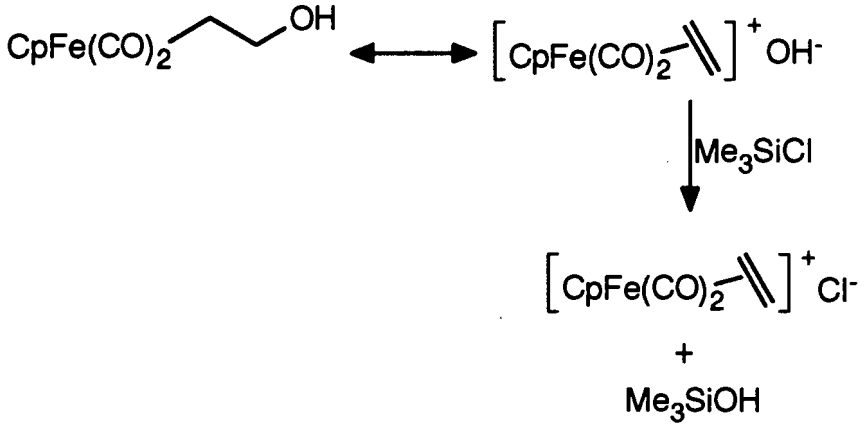

Scheme 3.3

The contribution of the cationic resonance form to the total structure of **(5)** was estimated by IR spectroscopy (see Section 2.4) and the reaction shown here further demonstrates this effect on the chemical reactivity of **(5)**.

3.2.2 Reaction with PPh_3/CBr_4

The complex **(1)** was reacted with PPh_3/CBr_4 in a minimum amount of THF solution to give the known complex $[CpFe(CO)_2\{(CH_2)_3Br\}]$ **(6)**, as shown in Equation 3.3.

$$[CpFe(CO)_2\{(CH_2)_3OH]\xrightarrow{PPh_3/CBr_4}[CpFe(CO)_2\{(CH_2)_3Br]$$
(6)

Equation 3.3

The yield of this reaction is moderate (42 %). $[CpFe(CO)_2\{(CH_2)_3Br\}]$ was identified by comparison of its ^1H NMR spectrum with that of an authentic sample. It is known that PPh_3 can react with **(1)** to give a carbonyl insertion product (see Section 3.2.5); however, under the conditions used here, we observed no carbonyl insertion product in this reaction. This reaction is one of the model reactions for building up organometallic dendrimers (see Section 4.3). The remarkable selectivity of this reaction is very important for the construction of organometallic dendrimers.

3.2.3 Reaction with trityl salt

Complex **(1)** was reacted with the trityl salt (CPh_3PF_6) to give a dark green solution, which suggested that a 17 e^- iron complex was formed in the reaction [3]. The IR spectrum of the resulting solution showed that no η^2-olefin iron complex was formed in the solution. This reaction is very similar to that of $[CpFe(CO)_2\{(CH_2)_3Br\}]$ - both functionalized (-Br and -OH) propyl iron complexes underwent an oxidation reaction when treated with the trityl salt.

However, when **(1)** was reacted with trityl salt in the presence of pyridine, a white

precipitate formed in the solution immediately. After filtration, the resulting yellow solution was purified by column chromatography to give the new complex $[CpFe(CO)_2\{(CH_2)_3OCPh_3\}]$ **(7)** in *ca.* 30% yield, as shown in Equation 3.4. A higher yield of **(7)** (60%) was achieved by reacting (1) with Ph_3CCl in the presence of pyridine.

$$[CpFe(CO)_2\{(CH_2)_3OH\}] + CPh_3PF_6 \xrightarrow{\text{pyridine}} [CpFe(CO)_2\{(CH_2)_3OCPh_3\}]$$
(7)

Equation 3.4

Complex **(7)** was obtained as a yellow crystalline solid (mp 116 °C) and was fully characterized by standard spectroscopic and analytical methods. The characterization data are given in the experimental section. The ^1H NMR spectrum of **(7)** showed a characteristic triplet at δ 3.02 ppm, which was assigned to the CH_2O protons. The mass spectrum of **(7)** only showed a daughter peak at 422 mass units, corresponding to $[P\text{-}2CO]^+$. Nevertheless, microanalysis results confirmed the formula of **(7)**.
This reaction is interesting since we have demonstrated that under various conditions the reaction can be selectively directed towards either the metal centre or the hydroxy group of **(1)**.

3.2.4 Reactions with 4-nonyloxybenzoyl chloride

Complex **(1)** reacts readily with 4-nonyloxybenzoyl chloride to give a benzoylester derivative **(8)** in reasonable yield (40%). The reaction is shown in Equation 3.5.

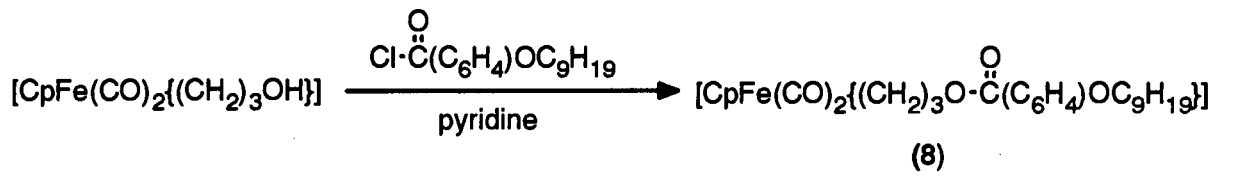

Equation 3.5

This reaction was carried out in the presence of pyridine and monitored by TLC. The new complex **(8)** was characterized by standard spectroscopic and analytical methods. The data are given in the experimental section. The IR spectrum of **(8)** showed two strong bands at 2003 and 1943 cm^{-1} for the terminal CO groups, while the benzoyl CO gave a peak at 1700 cm^{-1}. In the ^1H NMR spectrum, the CH_2O protons of **(8)** appeared as a triplet at about δ 4.2 ppm, which confirmed the formation of **(8)**. The mass spectrum of **(8)** also showed a molecular ion peak at m/z 182. Satisfactory elemental analysis results further confirmed the formula of **(8)**.

4-Nonyloxybenzoic acid is known to be a liquid crystalline compound. It was suspected that complexes such as **(8)** may show liquid crystalline properties. However a DSC trace of **(8)** gives only one peak at 39 °C, which corresponded to the melting of the sample. No mesogenic phase transition could be observed in **(8)**.

3.2.5 Reaction with PPh_3

Complex **(1)** was reacted with PPh_3 in refluxing benzene solution for 5 hours to give the complex $[CpFe(CO)(PPh_3)\{(CO)(CH_2)_3OH\}]$ **(11)** in 37 % yield, as shown in Equation 3.6.

$$[CpFe(CO)_2\{(CH_2)_3OH\}] + PPh_3 \xrightarrow{\Delta} [CpFe(CO)(PPh_3)\{CO(CH_2)_3OH\}]$$
(9)

Equation 3.6

This reaction went in a similar fashion to the reaction of $[CpFe(CO)_2\{(CH_2)_6Br\}]$ with PPh_3 (Section 1.2.9). Although, as shown in Scheme 3.2, $[CpFe(CO)_2\{(CH_2)_3Br\}]$ reacts with PPh_3 to give cyclic carbene species, no such complexes can be found in the reaction of the hydroxypropyl complexes. This could be due to the poor leaving ability of hydroxy group, which prevents the cyclization of hydrocarbon chain.

As shown in Equation 2.1, the β-hydroxyethyl iron complex **(5)** also gives an acyl complex on reaction with PPh_3, which may reflect the fact that the hydrocarbon chain length has no effect on the course of reaction in the ω-hydroxyalkyl complexes.

The new complex $[CpFe(CO)(PPh_3)\{(CO)(CH_2)_3OH\}]$ exists as a mixture of optical isomers but no attempt was made to separate them in this study. Complex **(9)** was characterized by IR, ^1H, and ^{13}C NMR spectroscopy and microanalysis and the data are given in the experimental section. The IR spectrum of **(9)** showed two υ(CO) bands at 1920 and 1614 cm^{-1} for the terminal and acyl carbonyls respectively. The prochiral α-CH_2 of **(9)** gives two resonances at δ 2.52 and 2.85 ppm in the ^1H NMR spectrum.

3.3 THE ELECTROCHEMICAL BEHAVIOUR OF $[CpFe(CO)_2\{(CH_2)_3OH\}]$ (1)

The electrochemical behaviour of **(1)** was studied by cyclic voltammetry at room temperature in an acetonitrile solution.

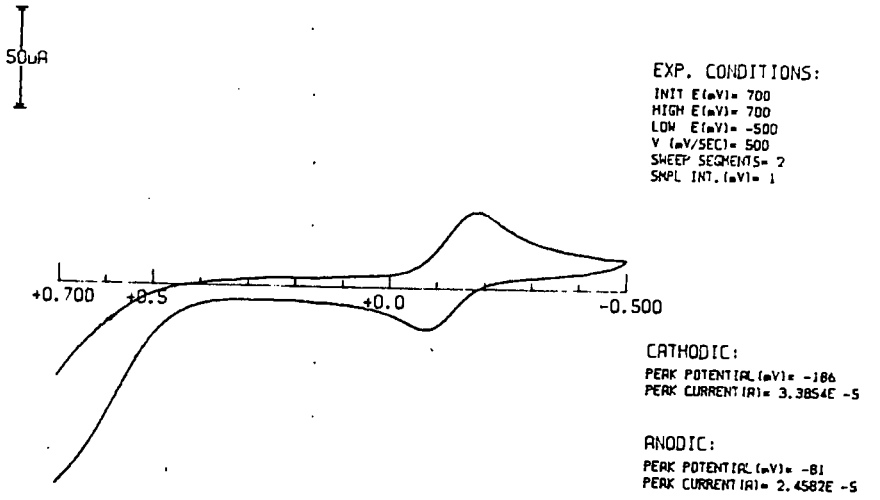

Figure 3.2 A cyclic voltammogram of $[CpFe(CO)_2\{(CH_2)_3OH\}]$

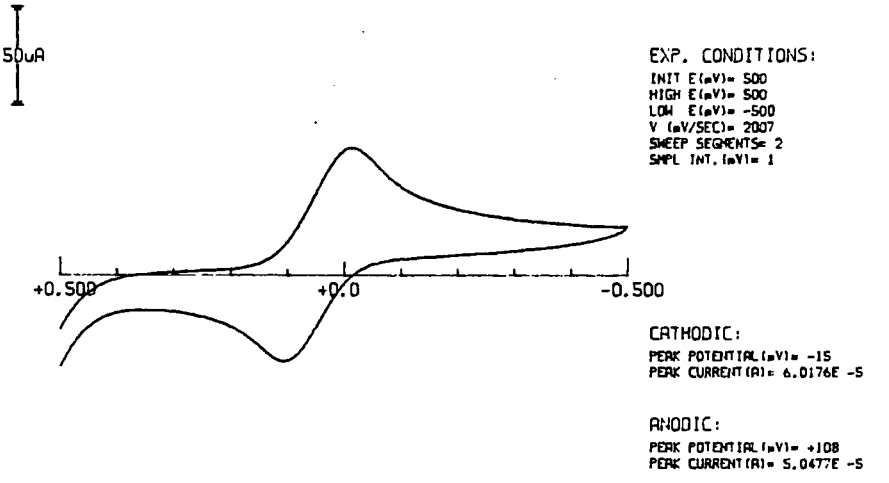

Figure 3.3 A cyclic voltammogram of mixture of $[CpFe(CO)_2\{(CH_2)_3OH]$ and PPh_3

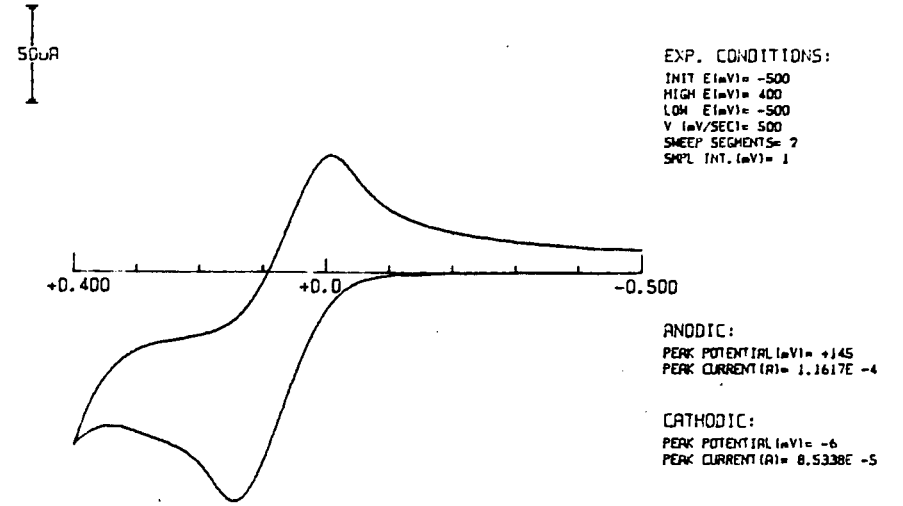

Figure 3.4 A cyclic voltammogram of $[CpFe(CO)(PPh_3)\{C{=}O(CH_2)_3OH\}]$

The cyclic voltammogram of **(1)**, as shown in Figure 3.2 gives a very similar pattern to that shown by $[CpFe(CO)_2\{(CH_2)_6Br\}]$. A quasi-reversible redox couple was found at +0.05 V, after oxidation of **(1)** at +0.5 V. We can assign this quasi-reversible couple to the formation of $[CpFe(CO)(CH_3CN)\{CO(CH_2)_3OH\}]$ by a similar mechanism to that shown in Section 1.3.

The cyclic voltammograms of **(1)** with added PPh_3 and of pure $[CpFe(CO)(PPh_3)\{CO(CH_2)_3OH\}]$ are given in Figures 3.3 and 3.4 respectively. The results obtained here consolidate our previous conclusions that the electrochemical behaviour and redox potentials of complexes $[CpFe(CO)_2\{(CH_2)_nX\}]$ are affected neither by the hydrocarbon chain length nor the nature of the ω-functional groups.

3.4 THE THERMAL PROPERTIES OF $[CpFe(CO)_2\{(CH_2)_3OH\}]$ (1)

The DSC trace of **(1)** recorded over the range of 30 - 400 °C under nitrogen is shown in Figure 3.5.

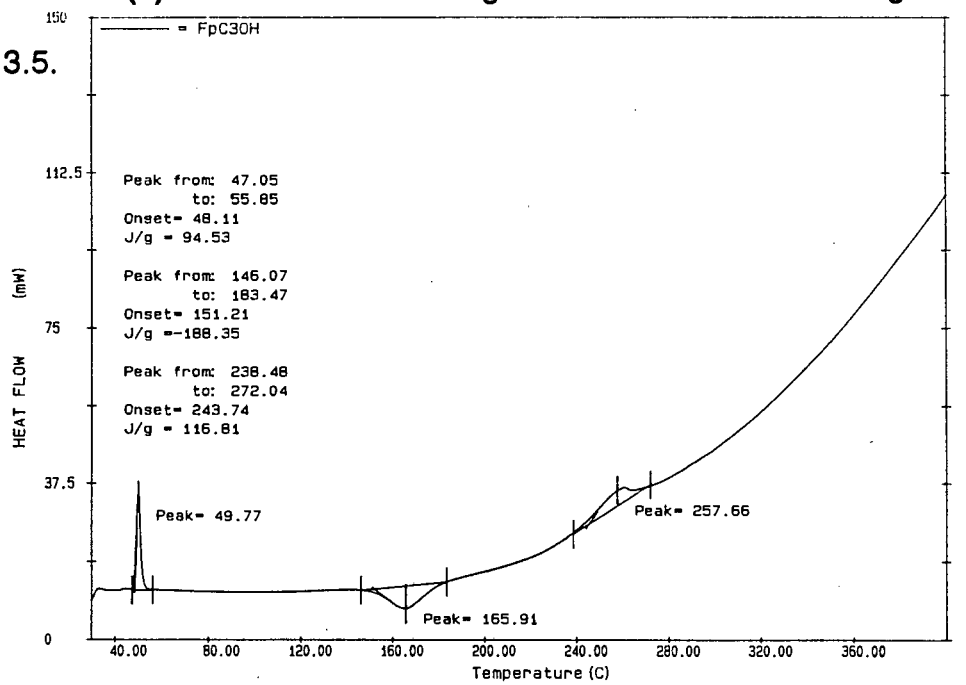

Figure 3.5 A DSC trace of $[CpFe(CO)_2\{(CH_2)_3OH\}]$

The trace shows two endothermic peaks at 50 °C and 258 °C, with an exothermic peak at 178 °C. The first endothermic peak was assigned to the melting of the crystalline sample and compared well with the melting point determined by the hot-stage microscope. The broad exothermic peak in the range of 150 - 180 °C was assigned to the decomposition of **(1)**. As we have shown in the Section 1.4, this temperature range is the normal decomposition temperature for this type of iron complex. The broad endothermic peak at 258 °C is assigned to the decomposition product, ferrocene. On comparing the DSC traces of **(1)** and $[CpFe(CO)_2\{(CH_2)_6Br\}]$, we found that both complexes showed very similar thermal behaviour. The similar decomposition temperatures for **(1)** and $[CpFe(CO)_2\{(CH_2)_6Br\}]$ indicate that the length of the hydrocarbon chain and the nature of the ω-functional groups have very little effect on the decomposition temperature. Also, since the same decomposition product was obtained for both **(1)** and $[CpFe(CO)_2\{(CH_2)_6Br\}]$, this may imply that both complexes have undergone a similar thermal decomposition mechanism.

3.5 CONCLUSION

In this chapter, again we have demonstrated that it is possible to direct reactions selectively in **(1)**. The various reactions mentioned in this chapter and their products are summarized in Table 3.1.

Reactants	Products
Me_3SiCl	$[CpFe(CO)_2\{(CH_2)_3OSiMe_3\}]$ **(2)**
t-$BuMe_2SiCl$	$[CpFe(CO)_2\{(CH_2)_3OSiMe_2t\text{-}Bu\}]$ **(3)**
t-$BuPh_2SiCl$	$[CpFe(CO)_2\{(CH_2)_3OSiPh_2t\text{-}Bu\}]$ **(4)**
PPh_3/CBr_4	$[CpFe(CO)_2\{(CH_2)_3Br\}]$ **(6)**
CPh_3PF_6	$[CpFe(CO)_2\{(CH_2)_3OCPh_3\}]$ **(7)**
4-Nonyloxybenzoyl chloride	$[CpFe(CO)_2\{(CH_2)_3O_2C(C_6H_4)OC_9H_{19}\}]$ **(8)**
PPh_3	$[CpFe(CO)(PPh_3)\{CO(CH_2)_3OH\}]$ **(9)**

Table 3.1 Summary of reactions of **(1)** described in Chapter 3

From the results obtained here, we can draw the following conclusions:

1) the reactions that occurred at the hydroxy group are very similar to those that occur in primary alcohols, but with lower yields. This could be due to the metal functional group which decreased the thermal stability of products.

2) in comparison to the results with $[CpFe(CO)_2\{(CH_2)_3Br\}]$, the reaction of **(1)** with PPh_3 gives no cyclic carbene species, which indicates that in this case the ω-functional group does have significant effect on this type of reaction. However, reaction of **(1)** with trityl salt suggests that the ω-functional group has no effect on the chemical reactivity of complexes $[CpFe(CO)_2\{(CH_2)_3X\}]$.

3) reaction of **(1)** with trityl salt can either occur at the metal centre or at the hydroxy

end, depending on the reaction conditions. This demonstrates that highly selective reactions (*ie.* chemoselective) can be achieved with **(1)**.

4) cyclic voltammetry and differential scanning calorimetry results for **(1)** suggest that the metal ligand system ($CpFe(CO)_2$) plays a crucial role in the thermal and electrochemical behaviour of **(1)**. In the comparison of the results of **(1)** and $[CpFe(CO)_2\{(CH_2)_6Br\}]$, we can further confirm that the ω-functional groups and the length of the alkyl chain have very little effect on the thermal and electrochemical properties of complexes of the type $[CpFe(CO)_2\{(CH_2)_nX\}]$.

3.6 REFERENCES

1. S. G. Davies, I. M. Dordor, J. C. Wacker and P. Warner, *Tetrahedron Letters*, **1984**, *25*, 2709.
2. T. W. Greene, *Protective Groups in Organic Synthesis*, Wiley, New York, **1981**.
3. R. H. Magnuson, S. Zulu, W.M. T'sai and W. P. Giering, *J. Am. Chem. Soc.*, **1980**, *102*, 6887.

CHAPTER 4 SYNTHESIS AND CHARACTERIZATION OF ORGANOTRANSITION METAL DENDRIMERS

4.1 INTRODUCTION

"Modern chemistry, like modern architecture, deals with structures whose design is constrained by natural forces, as well as depending on their eventual use." [1] Particularly in the history of polymer science, the development of controlled polymerization methodology has enabled polymers to be synthesized in a fashion that exhibit specific properties such as: defined molecular weight, narrow molecular weight distribution, pendant and end functional group, and main chain stereoregularity [2]. However, in terms of molecular topology, the traditional polymers are linear in shape and exist as a random coil in solution.

Recently, there has been a growing interest in synthesizing highly branched polymers with well-defined three dimensional structures. The shapes of molecules, which are carefully controlled by a series of elaborate synthetic strategies, can be either comb-like, star-like, or even tree-like, as shown in Figure 4.1

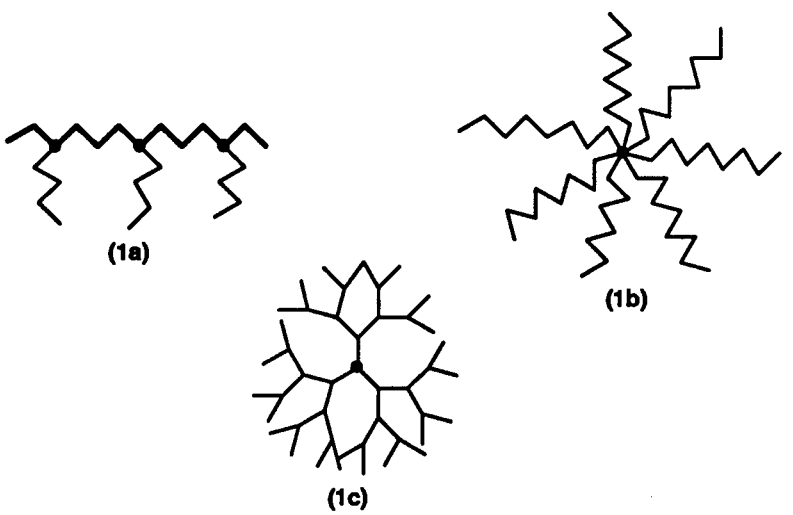

Figure 4.1 Examples of some types of highly branched polymers

The comb-like polymers (1a) have linear side chains (normally short) grown from various points along the main linear polymer chain (normally long). Whereas, in the case of star-like polymers (1b), several linear polymer chains grow from a central molecule or atom, and the number of polymer chains remains constant during the chain propagation. The tree-like polymers (1c) are similar to the star-like polymers in the chain initiation, however during the chain propagation, the polymer chain of the tree-like polymer further branches out. Thus, depending on the multiplicities of the repeating unit, the number of polymer chains can grow exponentially during the chain propagation.

4.1.1 THE STRUCTURAL FEATURES OF DENDRIMERS

The tree-like polymers are also known in various names, such as dendrimer (*dendron*: Greek, tree), arborol (*arbor*: Latin, tree), cascade molecules, or starburst polymers, and it is this type of molecule that has attracted a great deal of attention in recent years [3 - 8]. Several review articles on dendrimers have been published recently [2, 9 - 16]. The reasons for interest in dendrimers is that their molecular architecture is so different from the traditional linear polymers. Perhaps the most distinct feature of dendrimers is their rigid highly branched structure, and the huge numbers of chain ends (normally hundreds) that lie exclusively on the surface of the molecules. Therefore, one can expect that the functional groups on the chain ends would play an important role in the physical properties of these polymers, such as solubilities in organic solvents, or the glass transition temperature. Also, because most of the dendrimers have been prepared by controlled stepwise methods, an ideally branched dendrimer would have a specific molecular weight, *ie.* they are monodispersed.

Computer assisted molecular models have been used extensively to investigate the shapes of dendrimers, since these dendrimers are amorphous, and are not available for X-ray crystallographic analysis. From molecular models, it is found that the shapes of dendrimers are very well defined, but change dramatically during chain propagation. For example, a series of polyamidoamine dendrimers (Figure 4.2) have been studied by a computer model program [17]. The results show that the shapes of these dendrimers are star-like up to the third generation and that the dendrimers after the fifth generation are more spherical, which corresponds to a closed, densely packed surface structure.

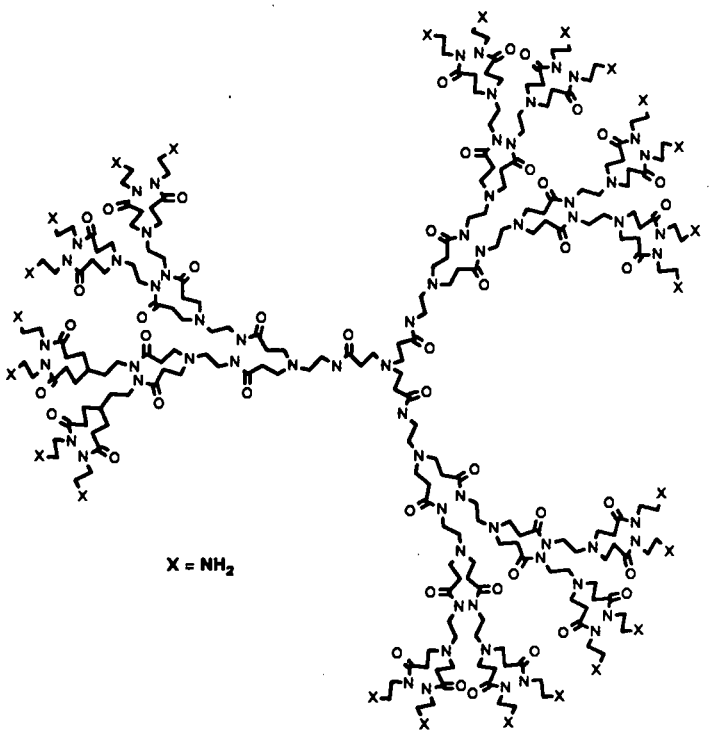

Figure 4.2 A third generation polyamidoamine dendrimer

Ottaviani *et al.* have reported a study on the electron paramagnetic resonance spectroscopy (EPR) of copper complexes in a series of polyamidoamine dendrimers. The line shapes of copper complexes in the EPR spectra show significant differences between earlier and later generation of dendrimers [18]. The results compare well with

those reported by Tomalia *et al.*, which were obtained from a fluororescent probe method [19, 20]. They are consistent with the change of dendrimer shapes, and support the results obtained from computer assisted molecular modelling studies. Furthermore the density of polyamidoamine dendrimers has been found to pass through a minimum on increasing generation number [9], whereas the intrinsic viscosity of polybenzylphenylether dendrimers has gone through a maximum as the generation number increases [21]. All these results suggest that there is a transition of dendritic structure during the polymer chain propagation. It is generally believed that this dramatic change in dendrimer shape is due to the dense packing of side chains on the periphery of the dendrimers.

Logically, one might think that the chain propagation process in an ideally branched dendrimer has no limits. However, theoretical models have shown that there will be a limit, called the starburst limit generation, beyond which the polymer branching can no longer take place in an ideal fashion [22]. This is because the theoretical maximum radius of dendrimers grows in a linear fashion with the generation, whereas the number of chain ends increases exponentially. Indeed, it has been shown that an ideally branched polyethylenimine dendrimer (Figure 4.3) can only grow up to the fourth generation dendrimer, with 48 terminal groups, beyond which the

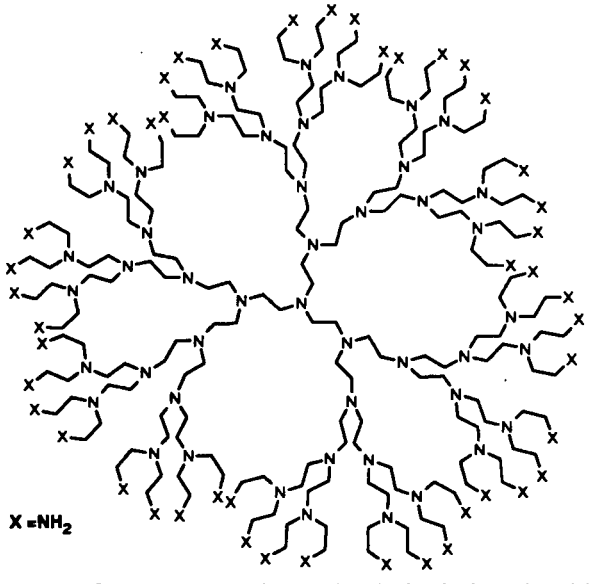

Fig. 4.3 A fourth generation polyethylenimine dendrimer

defect level becomes severe and no ideally branched fifth generation dendrimer can be isolated. However, an ideally branched polyamidoamine dendrimer (Figure 4.2) was reported up to the ninth generation with 1,536 terminal groups [9]. This indicates that the starburst limit generation can be effectively controlled by the structure of the molecules used as building blocks. De Gennes *et al.* have derived a simple equation to correlate the starburst limit generation (m) with a structural factor (P) of the repeating molecule, as shown in the following equation [22]:

$$m \approx 2.88 (\ln P + 1.5)$$

4.1.2 GLASS TRANSITION TEMPERATURE OF DENDRIMERS

The glass transition temperature (T_g) is the temperature at which an amorphous material undergoes the transformation from a glassy state to a rubbery or flexible thermoplastic state. This transition is one of the most important characteristics of a polymeric material, due to the fact that the practical usefulness as well as polymeric properties depend very much on the glass transition temperature. For example, the heat capacity and thermal expansion coefficient change dramatically during the glass transition state. Also, the mechanical stiffness of amorphous polymers gives a sharp increase when its temperature is below T_g.

Basically, the T_g value is dependent on the chemical structure of the amorphous material. Fréchet *et al.* have reported a comprehensive study on the glass transition temperature of some dendritic polymers [23]. It is found that the T_g value is related to the molecular weight, to the chain-end functional groups, and to the chemical composition of the dendrimers. In the following account, these factors will be

discussed individually.

Effect of molecular weight The T_g value of a dendrimer is found to increase as the molecular weight of the dendrimer increases, which is universal for all polymeric materials. However, the dependency of the glass transition temperature on the molecular weight shows differences between traditional linear polymers and dendritic polymers. This is because the number of chain-end group in a dendrimer is dependent on the molecular weight, whereas in the case of a linear polymer the number of chain-end groups is a constant, *ie* two. The correlation of glass transition temperature and the dendrimer's molecular weight, derived from the chain-end free volume theory, can be expressed as an equation of the form:

$$T_g = T_{g\infty} - (\rho N\theta / \alpha) (n_e / M)$$

This equation can be simplified to

$$T_g = T_{g\infty} - K (n_e / M) \qquad \text{(Equation 4.1)}$$

n_e : the number of chain ends
M : molecular weight

in which

$$K = \rho N\theta / \alpha \qquad \text{(Equation 4.2)}$$

ρ : the density of dendrimer
N : Avogadro's number
θ : the free volume per chain end
α : free volume expansion coefficient

The $T_{g\infty}$ is a theoretical value of T_g extrapolated to infinite molecular weight, which is a constant for a specific family of dendrimers. Since in the cases of dendritic polymers both the n_e and M increase exponentially, the n_e/M value should reach a

constant, as M approaches infinity in a perfectly branched dendrimer. This is in contrast to the traditional linear polymers in which the n_e remains constant as M increases. Thus n_e/M would approach zero as M approaches infinity, and $T_{g\infty}$ can be obtained as the Y intercept from the plot of T_g *vs.* 1/M. Therefore, for dendritic polymers, a new constant $(n_e/M)_\infty$ needs to be included in the equation to give

$$T_g = T_{g\infty} - K [n_e / M - (n_e / M)_\infty] \qquad \text{(Equation 4.3)}$$

The value of $(n_e/M)_\infty$ can be obtained from linear regression. From Equation 4.3, the $T_{g\infty}$ value of dendritic polymers will be the Y intercept from the plot of T_g *vs.* $[n_e/M - (n_e/M)_\infty]$. Also, the plot of T_g *vs.* $[n_e/M - (n_e/M)_\infty]$ correlates well with dendrimers of the similar type whose branched structure is impaired. Thus an average molecular weight of a dendrimer may be estimated alternatively from its T_g value.

Another interesting aspect of T_g for polymers is its "levelling-off" with increasing molecular weight. This is universal for all polymeric materials. Although in the cases of linear polymers, this effect is believed to be due to the entanglement of the polymer chains. However, this is not the case for dendritic polymers, since the polymer chain length of dendrimers is fairly short, when compared to linear polymers. Thus, it was proposed that the "levelling-off" effect of T_g in dendritic polymers may be due to the transition of macromolecular shape of dendrimers from a loose, flexible structure to a densely-packed globular structure [23].

Effect of the chain-end functional groups It has been observed that the chain-end functional groups have significant effects on the T_g and K value of dendrimers. The T_g value is found to depend on the polarity of chain-end functional groups. Whereas

the K value is dependent on the size of functional groups. For example, the T_g values for a series of fourth generation polybenzylphenylether dendritic wedges (Figure 4.4) were found to increase from 312 to 325 to 349 K, as the polarity of chain-end functional group increased from H to Br to CN. Also the K values were observed to increase from 13600 to 16800 to 20800 when the size of functional group is increased from H to CN to Br.

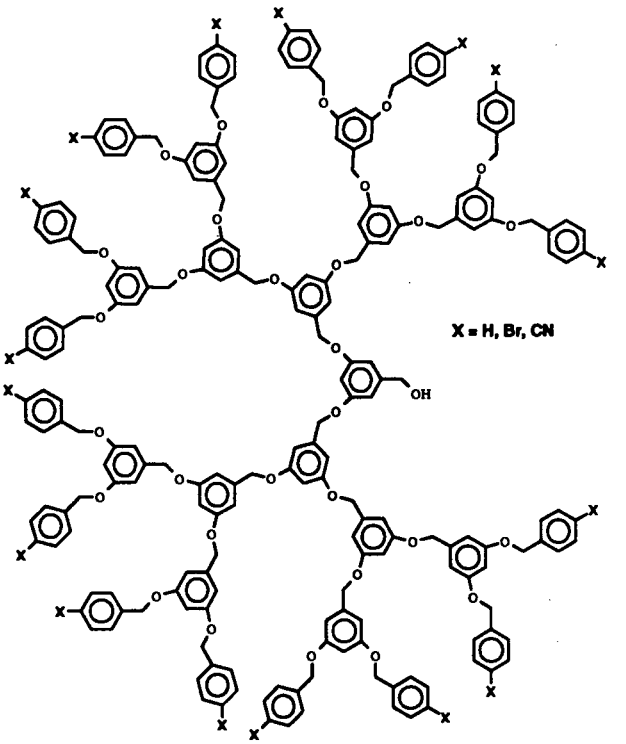

Fig. 4.4 A fourth generation polybenzylphenylether dendritic wedge

Effect of chemical structure and composition The chemical structure of a dendrimer has a significant effect on the T_g and K values. For example, the T_g value of the third generation polyphenylbenzoate dendrimer (399 K) is significantly higher than that of the third generation polybenzylphenylether dendrimer (312 K), although both of them have very similar molecular weights and the steric bulkiness of both monomers are also similar (Figures 4.5, 4.6).

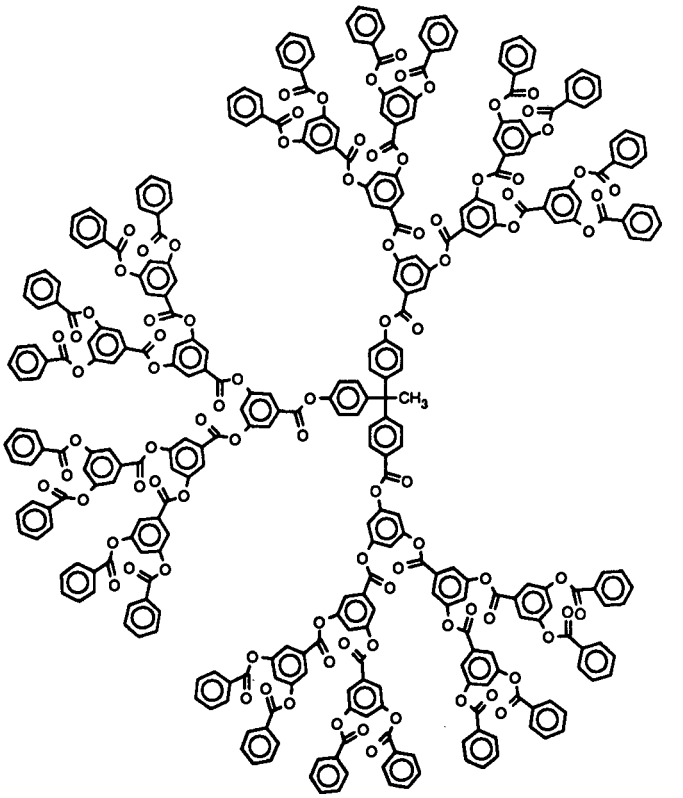

Fig. 4.5 A third generation polyphenylbenzoate dendrimer

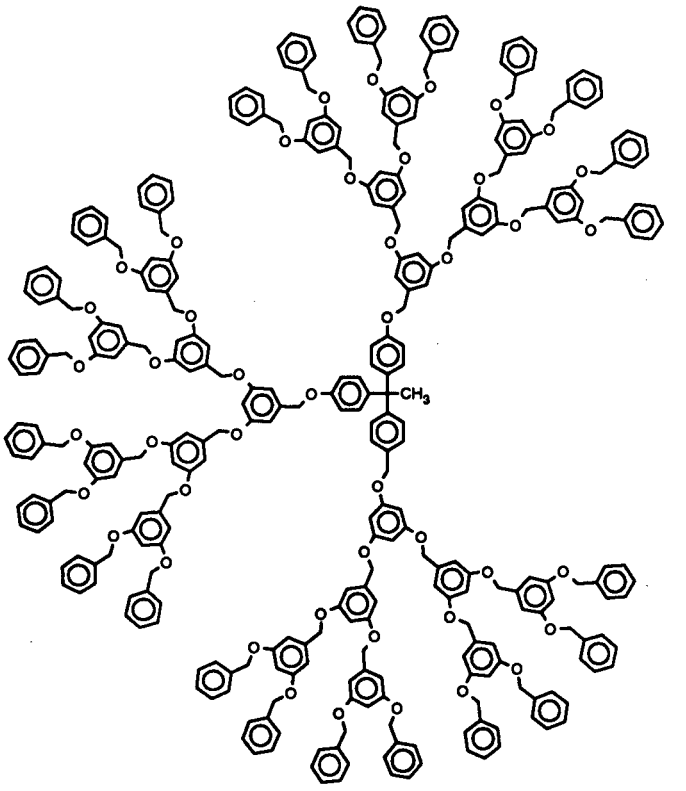

Fig. 4.6 A third generation polybenzylphenylether dendrimer

The difference in T_g is due to the fact that the ester linkages in the polyphenylbenzoate dendrimers are much more rigid than the ether linkages in the polybenzylphenylether dendrimers. Thus a higher T_g is expected in the polyphenylbenzoate dendrimers. It has also been reported that the T_g value of a copolymer is dependent on the composition of the individual components. For example, the T_g value for a dendritic copolymer of polyphenylbenzoate and polybenzylphenylether can be correlated to the T_g value of the individual components by an equation of the form:

$$\ln T_g = m_1 \ln T_{g1} + m_2 \ln T_{g2} \qquad \text{(Equation 4.4)}$$

In some cases, the dendritic copolymers may show more than one T_g value, which is entirely dependent on the compatibility of its components. This effect can also be seen in linear polymers.

4.1.3 SYNTHETIC STRATEGIES FOR THE IDEALLY BRANCHED DENDRIMERS

The beauty of a perfectly branched dendrimer, in the aspect of molecular topology, derives from its symmetrically branched structure; this will require a very carefully controlled synthetic strategy. Normally dendrimers are synthesized in a stepwise manner, in which chain propagation is controlled by repeated coupling and activation reactions. The direction of chain propagation can be either outward (divergent approach) or inward (convergent approach).

Divergent approach This approach was first developed by Tomalia in 1986 [24], and originated from the idea of cascade-like synthesis of noncyclic, branched polyamines

[25]. In the divergent approach, the chain propagation of the dendrimer initiates from a core molecule, followed by repeated coupling and activation reactions. The most important characteristic of the divergent approach is that the number of reacting sites on the dendrimer increases exponentially as the chains propagate, and so must the reactants required in the subsequent reactions. For example, the polypropyleneimine dendrimer (Figure 4.7) was constructed from the core molecule, NH_3 [26].

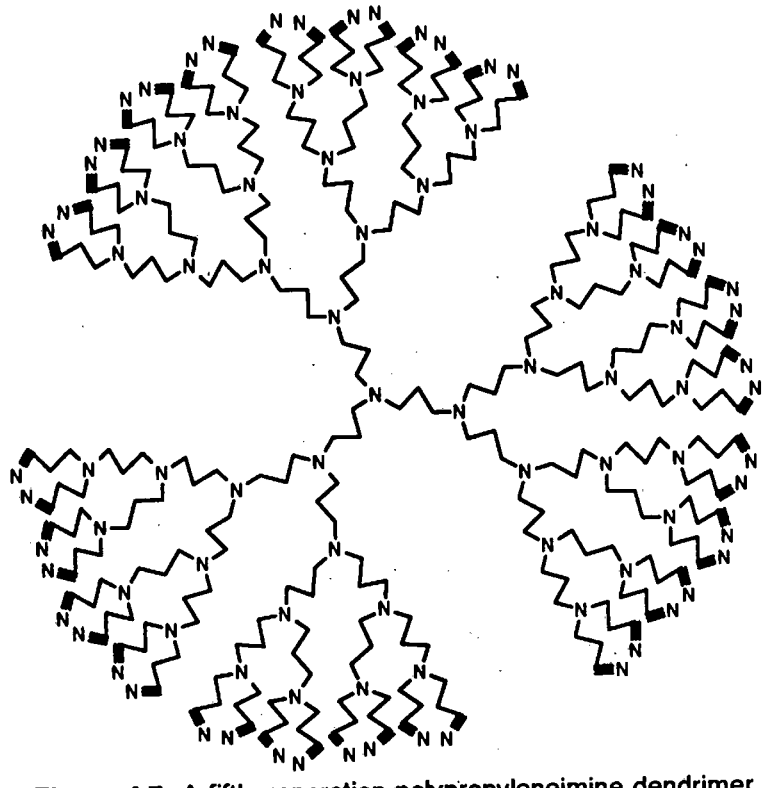

Figure 4.7 A fifth generation polypropyleneimine dendrimer

The chain propagation reactions were followed by Michael addition reactions with three molar equivalents of acrylonitrile. Catalytic hydrogenation reaction of **(1)** by Raney nickel under hydrogen gave the first generation dendrimer **(2)**. The same reactions were then repeated but with six molar equivalents of acrylonitrile to give the second generation dendrimer **(3)**, as shown in Scheme 4.1.

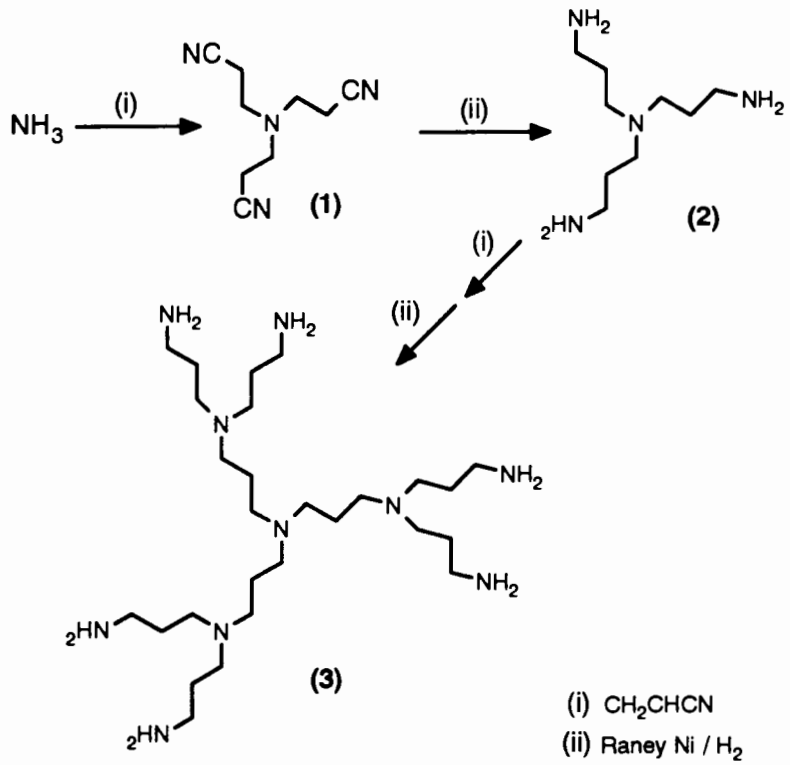

Scheme 4.1

Therefore, one can expect that, in the later generation dendrimers, a large excess of reactant will normally be required to achieve an ideally branched dendrimer. This may cause serious problems in purification of the anticipated products. Another difficulty which one may experience in this approach is the characterization of products. It will become almost impossible to detect the defects in the dendrimers from spectroscopic methods, once the dendrimers grow larger. Thus, it is very important that the reactions chosen for constructing the dendrimers must go in high yields and the side reactions must be minimized and be controllable. Despite all these inconveniences, Tomalia has prepared a series of ideally branched polyamidoamine dendrimers (Figure 4.2) by this approach up to the ninth generation [9]. This dendrimer has 1,536 chain ends with a nominal molecular weight of 349,883. Also, it has recently been reported that kilogram quantities of a ideally branched polypropyleneimine dendrimer

are accessible by this approach [27].

Convergent approach The convergent approach to an ideally branched dendrimer was first announced by Hawker and Fréchet in 1990 [28, 29]. The basic idea of this synthetic strategy is shown in Scheme 4.2.

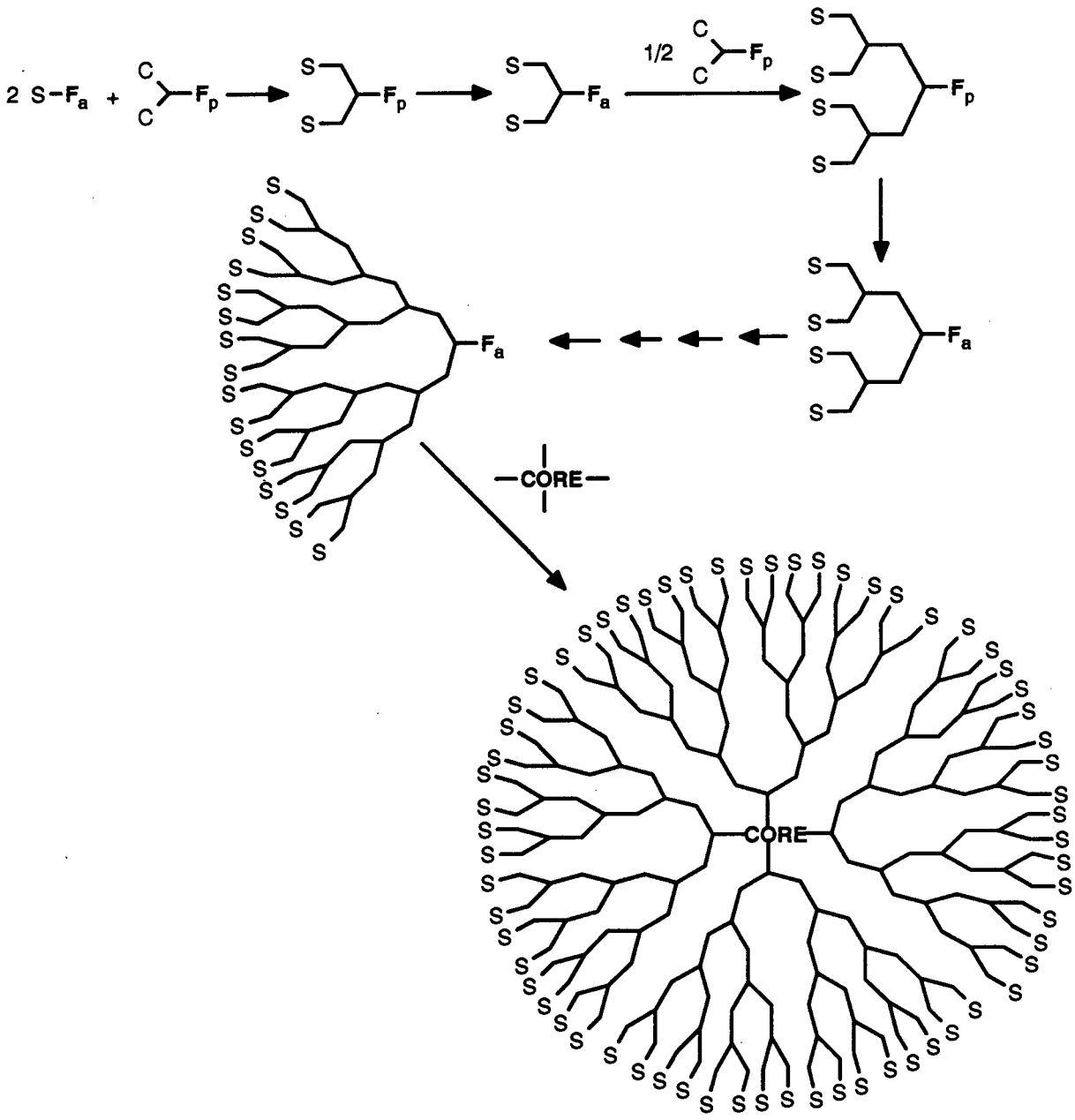

Scheme 4.2

In contrast to the divergent approach, the convergent approach initiates the chain

propagation from what will eventually become the periphery functional group. The dendritic wedges were then grown inward with repeated coupling and activation reactions. Afterwards, the dendritic wedges, with an activated functional group at the focal point were coupled to the core molecule.

The main feature of the convergent approach is that the stoichiometry of the reactions are under control. This suggests that there is no need of exhaustive reaction conditions and large excesses of reactants; this is of significant help in purification of the products. Also, the efficiency of reactions can easily be monitored by spectroscopic methods at each individual stage, thus preventing the occurrence of defects in the dendrimers. Perhaps, the greatest advantage of the convergent approach is that dendritic copolymers, either segment-blocked or layer-blocked, can be easily prepared by this approach. This would offer more controllable factors on implementation of dendrimer architecture. Hawker and Fréchet have reported various copolymers prepared by this approach [30 - 32] (see examples, Figures 4.8 and 4.9).

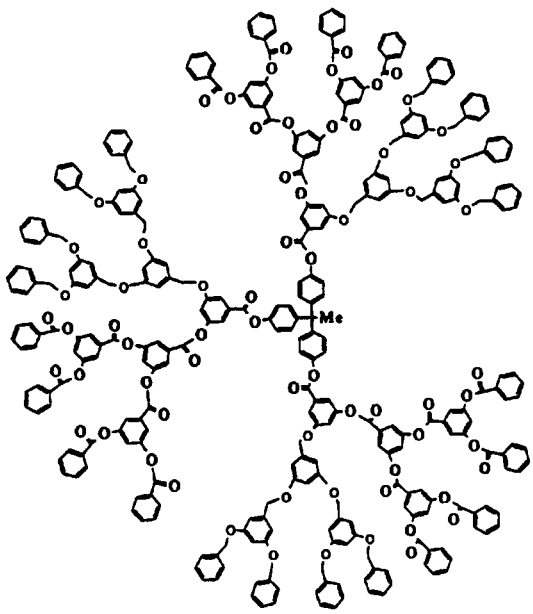

Figure 4.8 A segment block copolymer

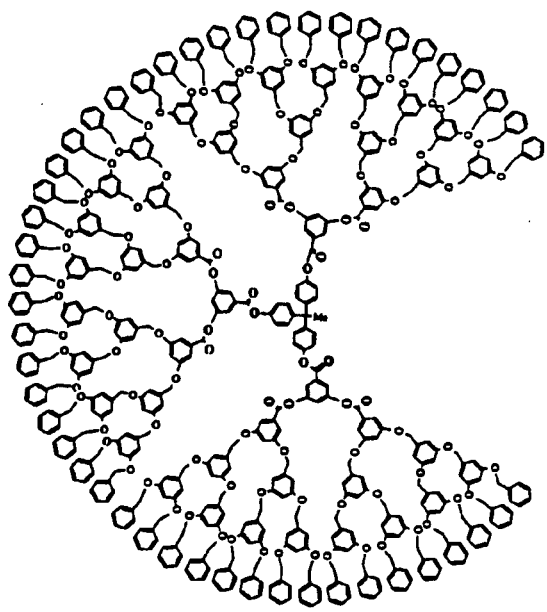

Figure 4.9 A layer block copolymer

A comparison between the divergent approach and the convergent approach is briefly summarized in Table 4.1.

Table 4.1 A comparison of the divergent approach and the convergent approach

	Advantage	Disadvantage
Divergent Approach	1. suitable for high molecular weight dendrimers (>100,000) 2. less reaction sequences involved 3. large quantity production is accessible	1. large excess of reactant required 2. less control on the molecular architecture
Convergent Approach	1. block copolymers are accessible 2. reaction stoichiometry is under control	1. molecular weight of dendrimer is limited (<100,000) 2. more elaborate reaction sequences involved

4.1.4 INORGANIC DENDRIMERS

Research on dendritic polymers has expanded dramatically in recent years. However, the majority of known dendrimers are organic in nature. Nevertheless dendritic polymers which include transition metals or main-group elements are also known. In this section, we intend to provide a brief summary of known inorganic dendrimers. The first known inorganic dendrimer was reported by Bochkarev *et al.* in 1988 [33]. These dendritic polymers were prepared *via* a "one-pot" non-controlled method by the anionic polymerization of $HM(C_6F_5)_3$ (where M = Ge, Si, Sn). It was hypothesized that this polymerization reaction initiates from a deprotonation reaction to give metal anions which undergo nucleophilic substitution reactions with fluoride at the *para* position. The structure of complexes is shown in the Figure 4.10.

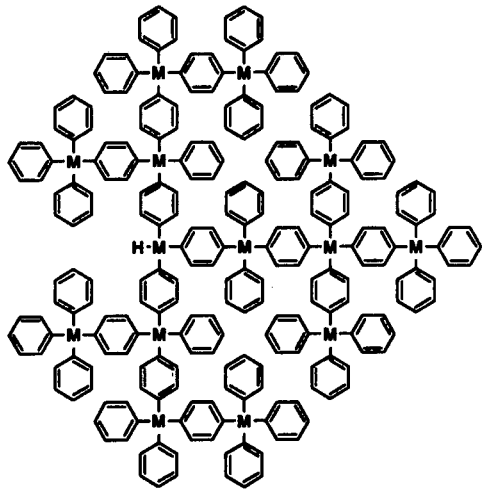

Figure 4.10 A dendrimer containing main group elements
The fluorine atoms are omitted for clarity

It is interesting that, in the case of germanium, a self-limiting molecular weight was obtained in the range of 100,000 - 170,000. Although the reaction went in a non-controlled fashion, this is the first example of a self-limiting polymerization reaction in dendritic polymers.

The first Werner-type of ruthenium containing dendrimer was reported by Balzani *et al.* in 1992 [34]. The synthetic strategy, shown in Scheme 4.3, is very similar to the divergent approach with slight modification. The construction of the complexes starts from the core molecule, $[Ru(2,3\text{-depp})_3]^{2+}$ **(4)** which contains three active sites on the molecule. After reacting with three equivalents of the dendritic building block, $[Ru(2,3\text{-Medpp})_2Cl_2]^{2+}$ **(5)**, a four-ruthenium-metal complex, which is the first generation dendrimer **(6)**, is formed. This complex is then deprotected to give complex **(7)** with six active sites on the periphery of complex. At this stage, the complex can either further react with six equivalents of the dendritic building block **(5)** to give a decanuclear (10 metal atom) complex, or react with a trinuclear ruthenium complex

(8) to give the docosanuclear (22 metal atom) ruthenium complex (9).

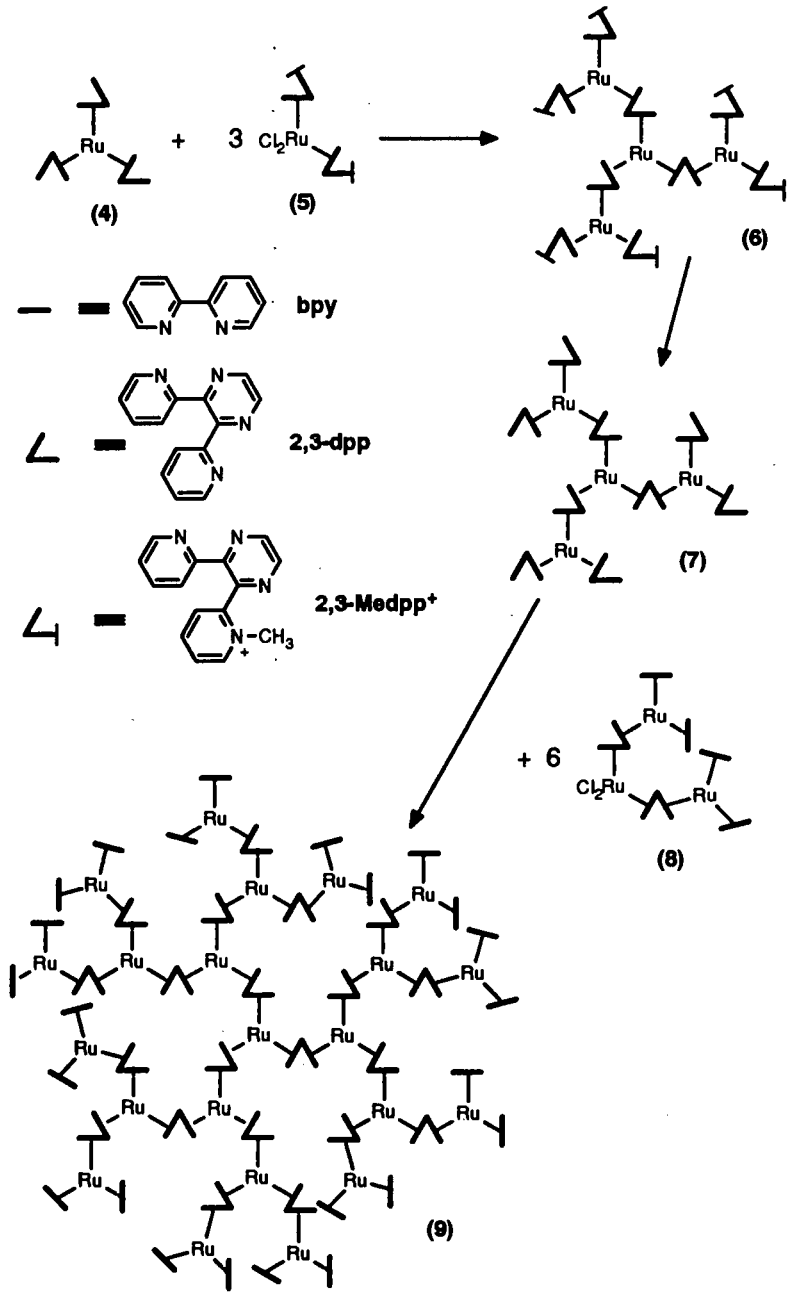

Scheme 4.3

The docosanuclear ruthenium complex (9) in Scheme 4.3 was reported as the largest Werner-type metal complex ever prepared, with molecular weight of 10,890, and an estimated size of about 5 nm. Also, the complex (9) shows very interesting photochemical and electrochemical properties. It was proposed that this type of

dendrimer may be useful in solar energy conversion devices, or may be good candidates for multi electron-transfer catalysts.

Newkome *et al.* have reported a series of dendrimers containing a ruthenium terpyridine complex [35] and also a carborane [36] in a dendritic micellane (a unimolecular micelle) framework. Basically the dendritic structure was constructed first with functional groups located at specific sites of the dendritic structure. Afterwards, the metal groups are brought into the dendrimer, and the micelle property of the dendrimer was achieved in the subsequent reactions. For example, the synthetic strategy of the ruthenium coordination dendrimers are shown in Scheme 4.4. In this case, the core molecule **(10)** with four carboxylic acid functional groups was first converted to acid chloride **(11)**, followed by reaction with four equivalents of the tri-terpyridine compound to give compound **(12)** with twelve terpyridine functional groups. Compound **(12)** was then reacted further with twelve equivalents of ruthenium complex, to give complex **(13)**.

Astruc *et al.* have also reported a series of dendrimers with $[CpFe(C_6R_6)]^+$ units either on the periphery or at the centre of the dendrimers [37]. The synthetic strategy, they adopted, is a divergent approach, as shown in Scheme 4.5. The compound $[CpFeC_6H_3Me_3]^+PF_6^-$ **(14)** was reacted with nine equivalents of allyl bromide to give complex **(15)**. After demetallation and hydroboration reactions, the resulting compound **(17)** was treated with nine equivalents of $[CpFe(C_6H_4FCH_3)]^+PF_6^-$ to give complex **(18)**.

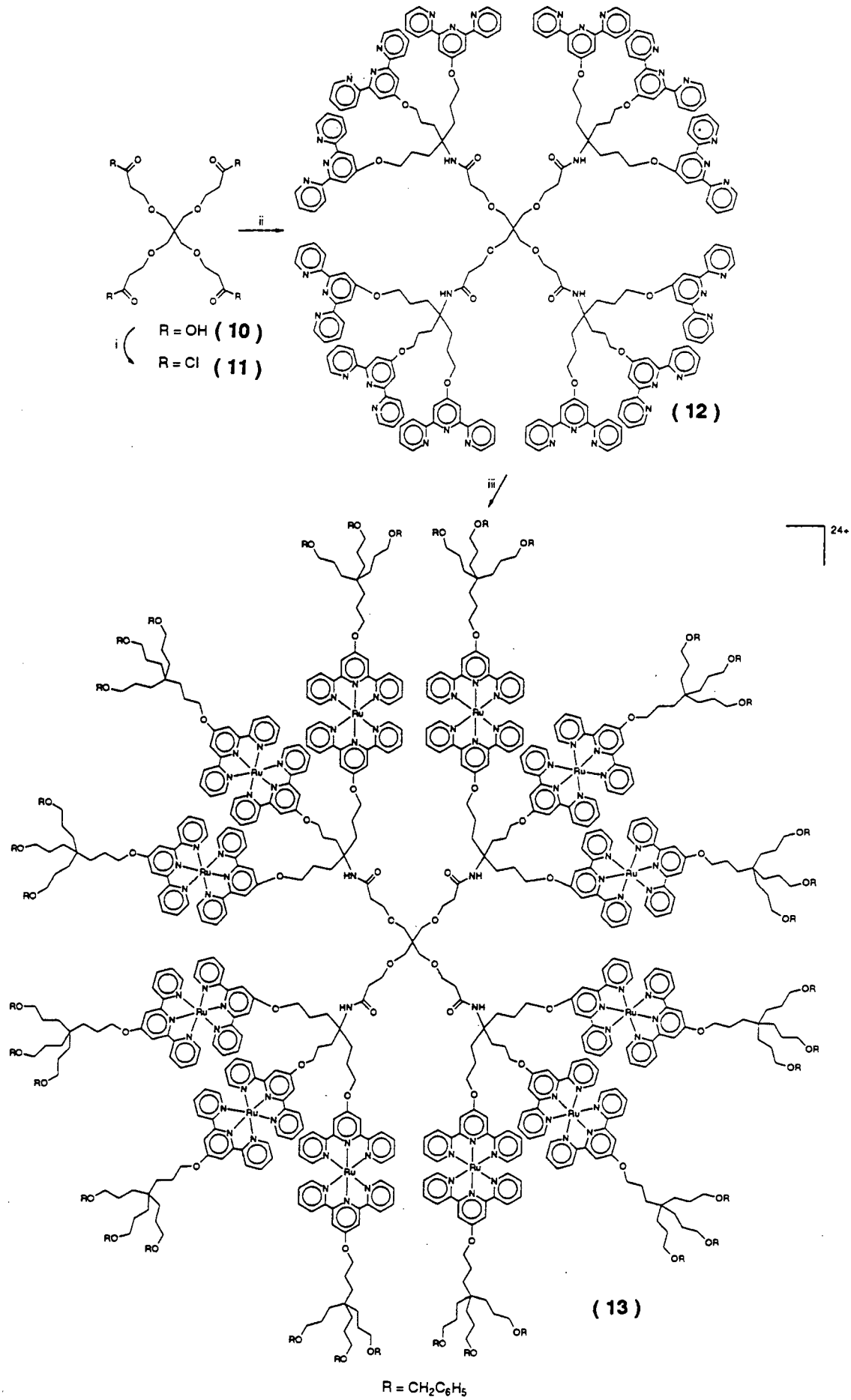

Scheme 4.4

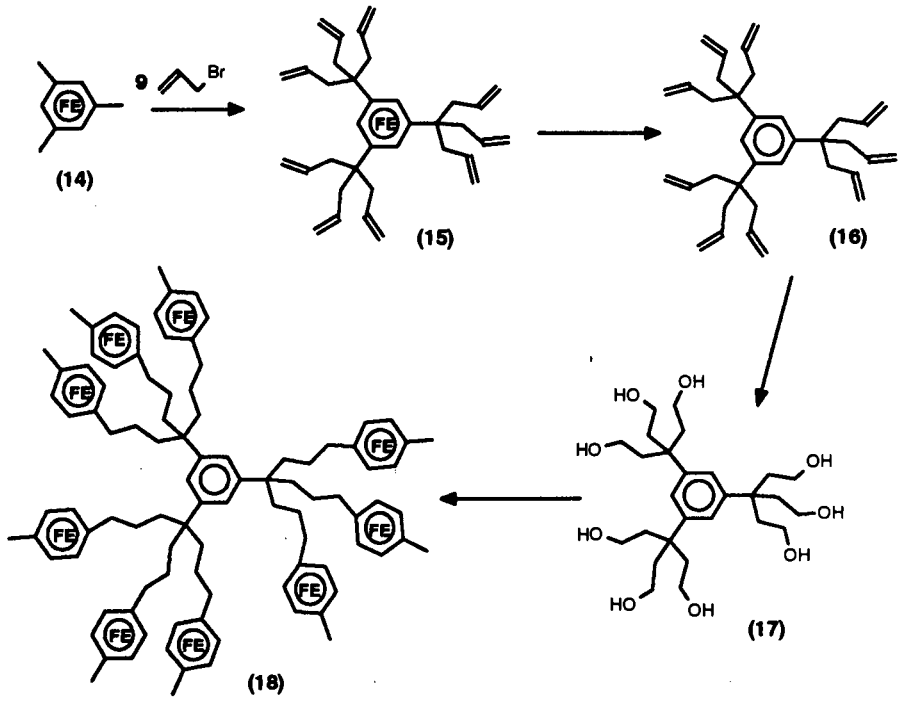

FE = $(CpFe^{II})^+ PF_6^-$

Scheme 4.5

Complex **(18)** which has nine methyl groups on periphery may potentially react further with twenty seven equivalents of allyl bromide to give the second generation dendrimer, although this has not yet been demonstrated. In a cyclic voltammetry experiment, complex **(18)** displays only one reversible couple, corresponding to nine electrons. This is rather unusual since the redox active sites are far apart in the complex, and some of them are even far away from the electrode surface.

Recently van der Made [38] and Roovers [39] independently reported a series of carbosilane dendrimers. Both research groups adopted the divergent approach, but with different synthetic methodologies. For example, Scheme 4.6 shows the synthetic strategy for the carbosilane dendrimers reported by van der Made. The carbosilane dendrimers are constructed from the core molecule, $SiCl_4$ which was reacted with four equivalents of allylmagnesium bromide to give the silane compound **(19)**.

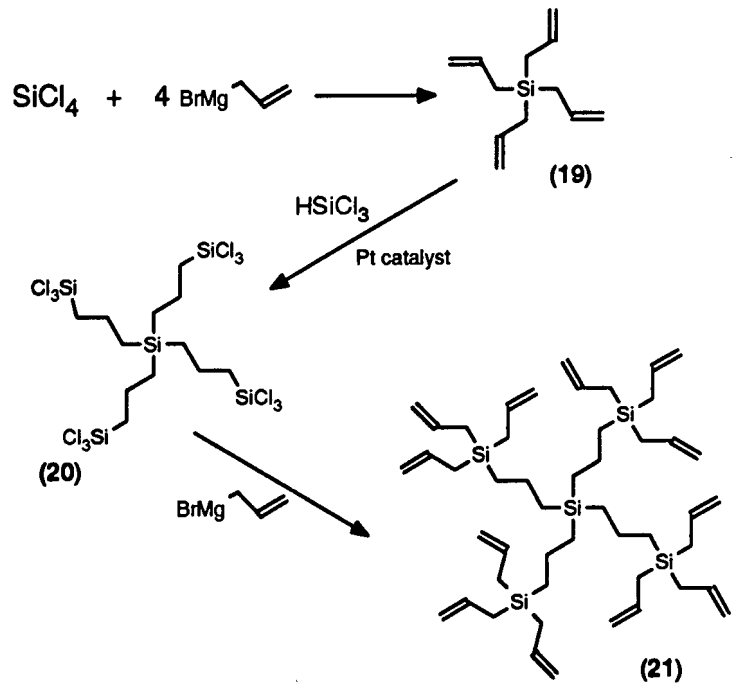

Scheme 4.6

Compound **(19)** with four allyl chains then underwent a hydrosilation reaction with four equivalents of $HSiCl_3$ to give compound **(20)**. Now compound **(20)** has twelve SiCl functional groups available for reaction with allylmagnesium bromide, and the second generation dendrimer **(21)** can be obtained. The same reaction sequences are repeated to give higher generation carbosilane dendrimers.

Van der Made has reported a carbosilane dendrimer up to the sixth generation with 972 end groups, and a nominal molecular weight of 73,912. Roovers has reported that the carbosilane dendrimers have very low T_g (*ca.* -20 °C). This could be due to the fact that the Si-C bond has considerable torsional mobility, and thus lowers the T_g value.

Engel and Rengan have reported a series of phosphonium salt dendrimers [40]. These dendrimers were prepared by the divergent approach, as shown in Scheme 4.7.

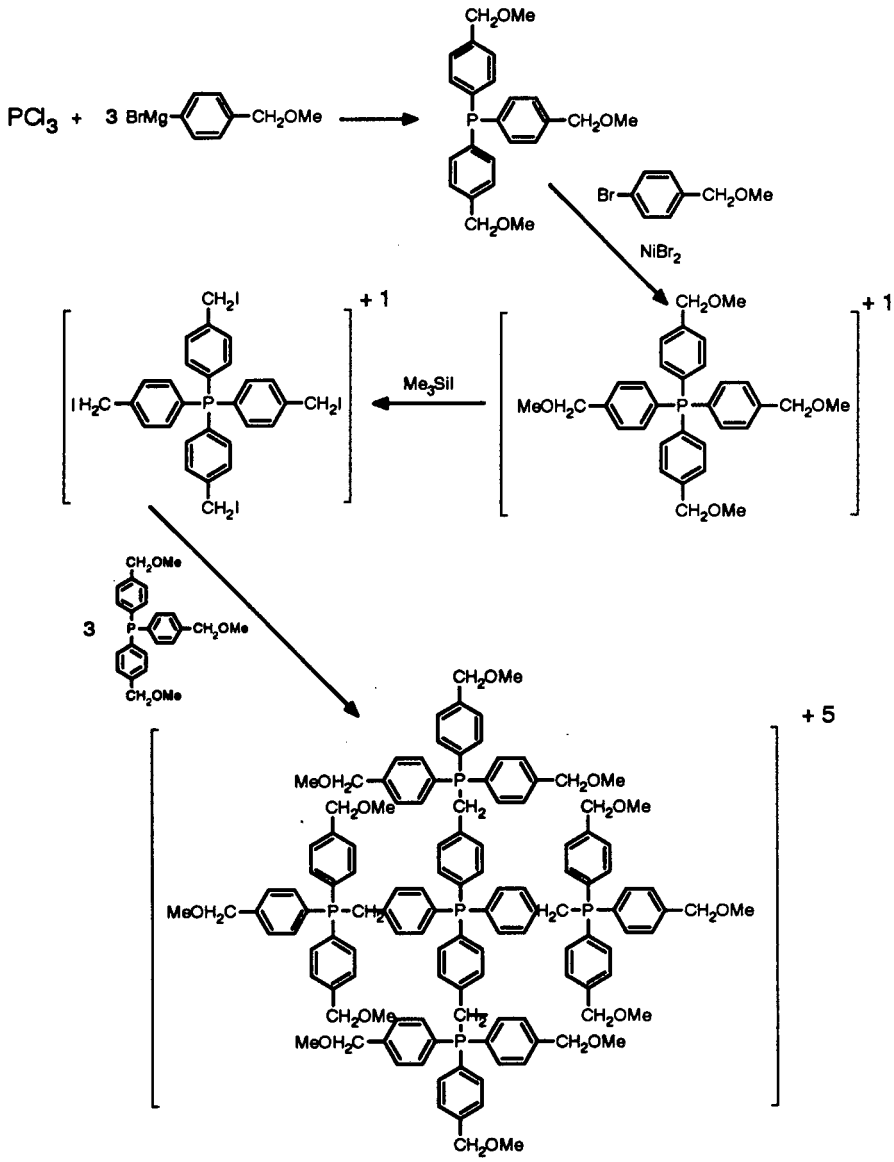

Scheme 4.7

The authors reported that the solubility of these dendrimers decreased as the molecular weight increased. However, the readily soluble phosphonium dendrimers, in polar protic solvents, doesn't change significantly. All these phosphonium dendrimers are hygroscopic.

Fréchet [41, 42] and Inoue [43] have reported a series of polybenzylphenylether dendrimers which contain fullerene or porphyrin core molecules. The

polybenzylphenylether dendritic wedges are prepared by the convergent approach, with benzyl or methyl functional groups on the periphery. The structures are shown in the Figures 4.11, 4.12.

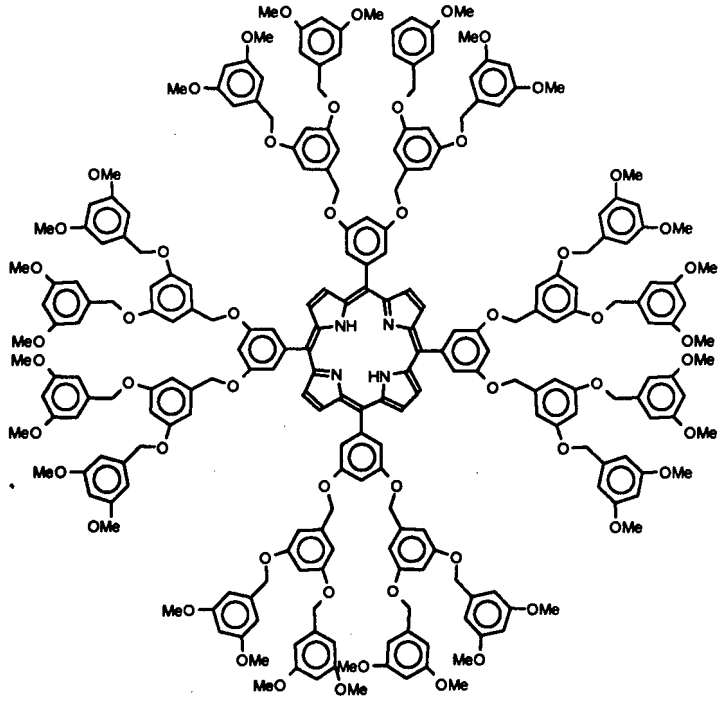

Figure 4.11 A porphyrin centred polybenzylphenylether dendrimer

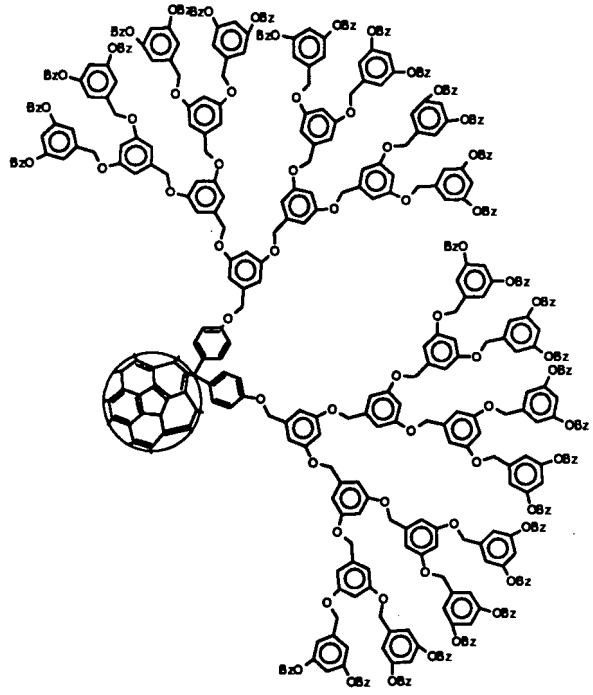

Figure 4.12 A fullerene centred polybenzylphenylether dendrimer

The fullerene centred polybenzylphenylether dendrimer has been reported to dramatically increase the solubility of the fullerene in organic solvents, while the globular structure of the fullerene derivatives is still maintained. The fourth generation porphyrin centred polybenzylphenylether dendrimer was further reacted with $Zn(CH_3CO_2)_2$. Fluorescence spectroscopy of the resulting Zn complex suggested that the dendritic structure acted as a filter or served for UV quencher molecules.

In 1992, Shinkai *et al.* reported a second generation dendrimer, containing nine diaza-18-crown-6 units [44]. The structure of compound is shown in Figure 4.13.

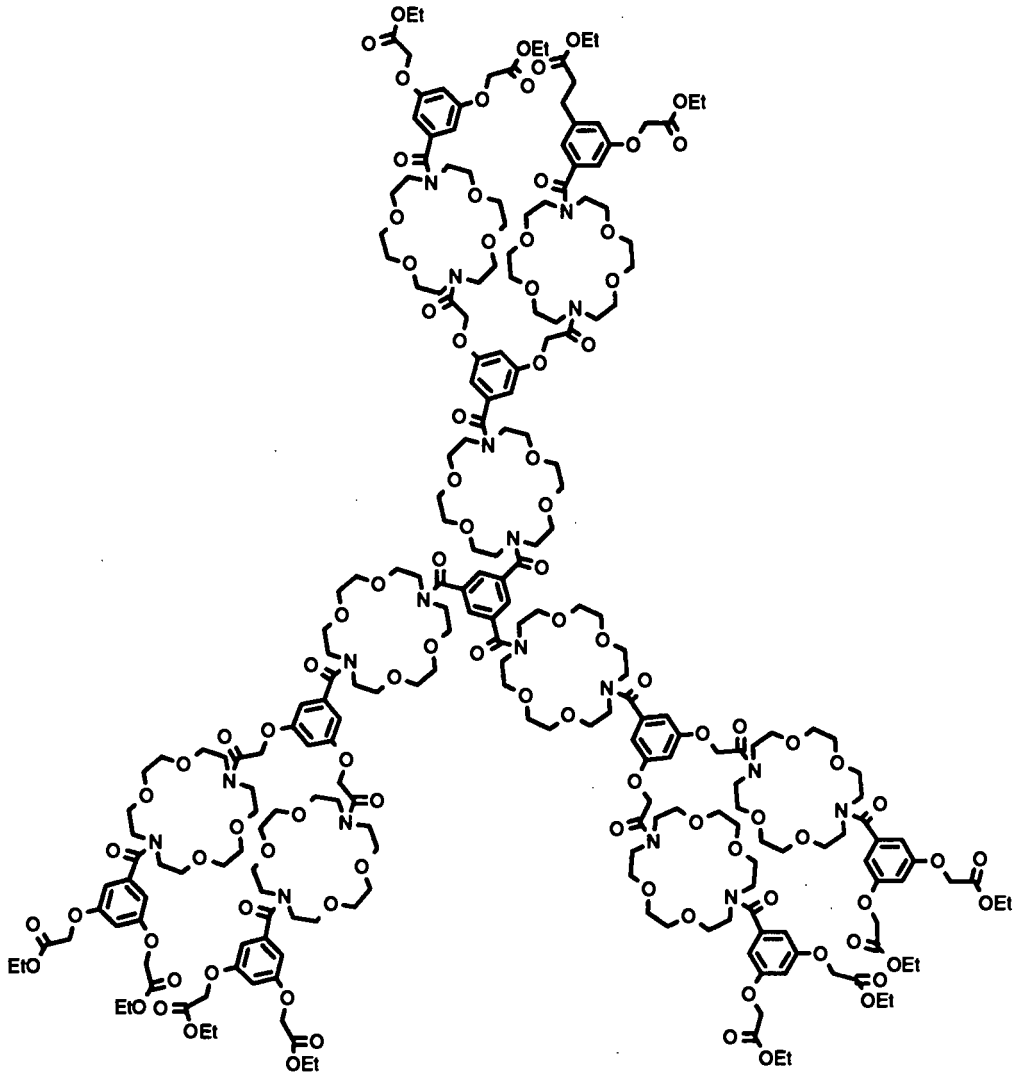

Figure 4.13 A crown ether containing dendrimer

This dendrimer was successfully synthesized via a convergent approach, after failing with the divergent approach. The crown ether in the dendritic structure, as the authors suggested "should act as a nest for metal ions to perch"! However the binding ability of this crown ether dendrimer toward metal ions has not yet been demonstrated.

More recently, Puddephatt and Achar have reported a series of Pt containing organometallic dendrimers [45]. This series of dendrimers are prepared by the convergent approach. A dendritic wedge containing 14 Pt metal atoms, as shown in Figure 4.14, has been synthesized and has reached the starburst limit generation.

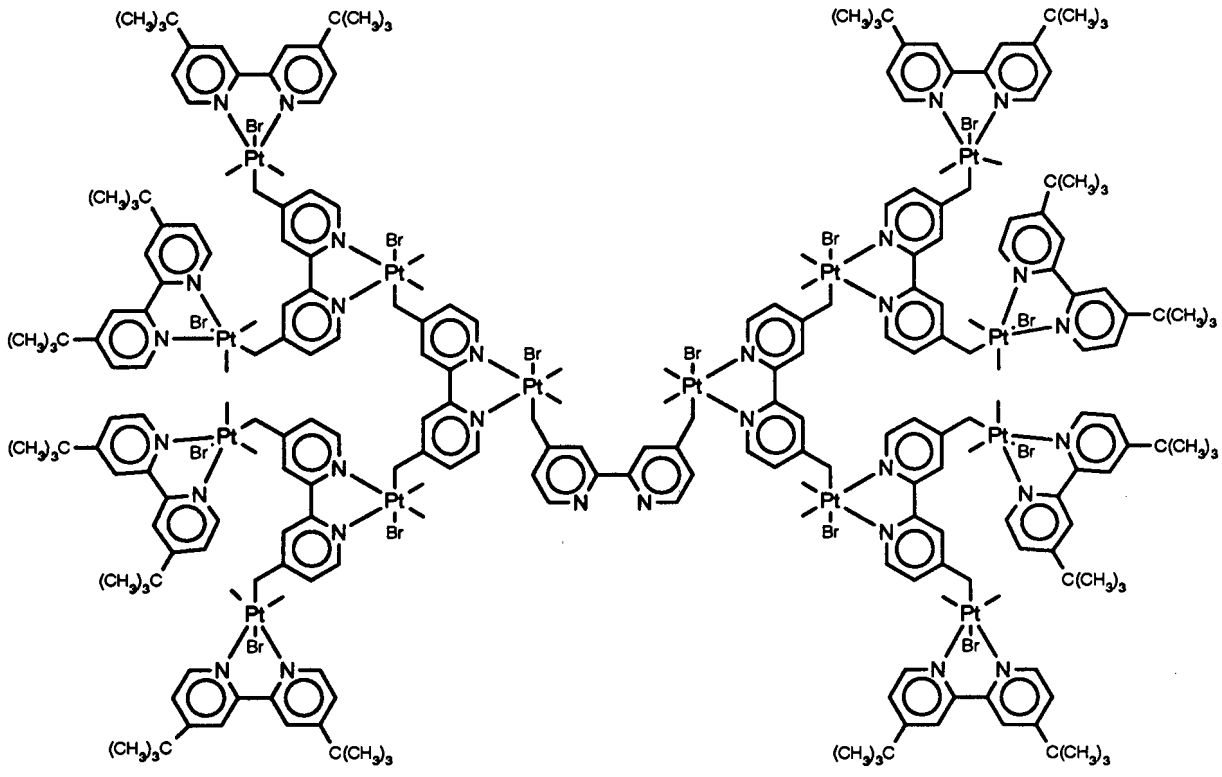

Figure 4.14 An organometallic dendritic wedge containing 14 Pt metal atoms

4.2 A CONCISE NOTATION FOR THE DENDRIMERS PREPARED IN THIS STUDY

For clarity of presentation, the following concise notation for the dendrimers prepared in this study will be used throughout this chapter. This notation is generally in the form:

$$Mn_1Gn_2X$$

where

M: is the organometallic functional group on the periphery of the dendrimer, and Rp = $CpRu(CO)_2$, Fp = $CpFe(CO)_2$.

n_1: a number refers to the length of the polymethylene chain, thus the $(CH_2)_3$ group is symbolized by 3.

G: a character stands for "generation".

n_2: the generation number of the dendrimer

X: the functional group at the focal point of the dendrimer. For examples; OH stands for hydroxy group, Br stands for bromo group and C stands for three dendritic wedges attached to a CORE molecule.

For example, Rp3**G**2OH stands for the second generation dendritic wedge with benzyl alcohol functional group at the focal point, while four organometallic functional groups ($CpRu(CO)_2(CH_2)_3$) are attached to the polymer chain ends at the periphery of the molecule. The chemical structure of Rp3**G**2OH is shown in Scheme 4.9.

4.3 SYNTHESIS OF NEW ORGANOTRANSITION METAL DENDRIMERS

In this Chapter, we have synthesized a series of new organotransition metal dendrimers. Prior to this study, no organotransition metal dendrimers containing metal carbon σ bonds had been reported. The dendrimers, prepared in this study are based on 3,5-dihydroxybenzyl alcohol as the monomer unit, and the organometallic functional groups are attached exclusively at the periphery of the dendrimers.

The synthetic strategy, adopted here is the convergent approach, as developed by Hawker and Fréchet. The preparation of these new organometallic dendrimers starts from the haloalkyl metal complexes **(22)** and **(23)**, which will eventually become the chain-end functional groups. As we have demonstrated in Chapter 1, the reactions of bromoalkyl metal complexes can be exclusively directed to the halo functional groups, while the metal and its associated ligands remain intact.

Thus two molar equivalents of complex **(22)** or **(23)** were reacted with one molar equivalent of 3,5-dihydroxybenzyl alcohol in the presence of potassium carbonate and 18-crown-6 in refluxing acetone for two days. The reaction was monitored by TLC, eluting with a 70% CH_2Cl_2/hexane solution.

The resulting complexes **(24)** and **(25)**, as shown in Scheme 4.8, were purified by column chromatography and recrystallization to give reasonable yields of 40% and 70% respectively. The relatively low yield of **(24)**, compared with **(25)**, may be due to the low thermal stability of iron complexes of this type, as we have discussed in Chapter 1. To our experience, vigorous stirring throughout the reaction is essential in order to ensure high conversion. Also, in the case of complex **(24)**, we found that light protection is necessary to optimize the yield of the product.

Complexes **(24)** and **(25)** (*ie* Fp3**G**1OH and Rp3**G**1OH, respectively) are the first generation benzyl alcohol complexes and were characterized by standard spectroscopic methods. Complex **(24)** is obtained as a yellow oil and **(25)** is a colourless crystalline solid (mp 95 °C). Both complexes are relatively air and thermally stable. Complexes **(24)** and **(25)** were converted to their corresponding benzyl bromide complexes **(26)** and **(27)** in high yields (70 and 90%, respectively) by treatment with PPh_3/CBr_4 in a minimum volume of THF (Scheme 4.8).

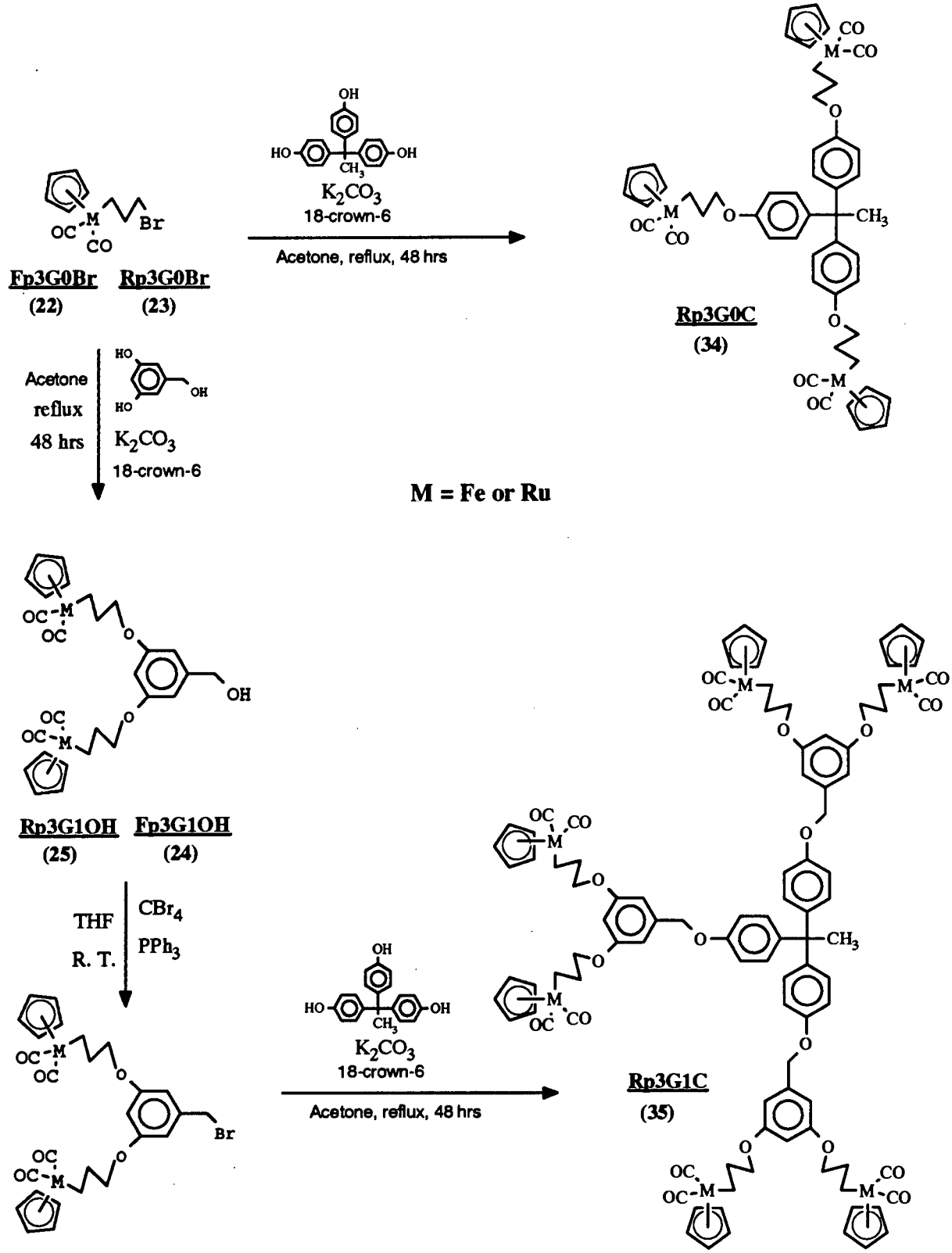
Fp3G0Br (22)
Rp3G0Br (23)
K2CO3
18-crown-6
Acetone, reflux, 48 hrs
Rp3G0C (34)
Acetone
reflux
48 hrs
K2CO3
18-crown-6
M = Fe or Ru
Rp3G1OH (25)
Fp3G1OH (24)
THF
R. T.
CBr4
PPh3
Fp3G1Br (26)
Rp3G1Br (27)
K2CO3
18-crown-6
Acetone, reflux, 48 hrs
Rp3G1C (35)

Scheme 4.8

This reaction is generally complete within 20 minutes and was monitored by TLC eluting with a 30% CH_2Cl_2/hexane solution. Analytically pure **(26)** and **(27)** were obtained after column chromatography and recrystallization.

It was found that a large excess of PPh_3/CBr_4 is usually needed in order to achieve complete conversion in the reaction, especially in the cases of the higher generation benzyl alcohol complexes. Also, in our experience, the volume of THF solvent used in the reaction has a significant effect on the yields of products as does the quantity of PPh_3/CBr_4 needed for the reaction.

Complex **(26)**, which was obtained as a yellow oil, is relatively unstable and shows significant decomposition even under nitrogen at room temperature. Several attempts have been made to react **(26)** with either 3,5-dihydroxybenzyl alcohol or 1,1,1-tris(4'-hydroxyphenyl)ethane (we refer to this as the CORE molecule) in refluxing acetone. None of the anticipated products were observed from TLC, only decomposition products.

Nevertheless, complex **(27)** obtained as a colourless crystalline solid (mp 110 °C) is stable at room temperature. The reaction of two equivalents of **(27)** with one equivalent of 3,5-dihydroxybenzyl alcohol gives the anticipated second generation benzyl alcohol complex **(28)** as a white glassy solid in 70 % of yield. Similarly, the second generation benzyl alcohol complex **(28)** was converted to the analogous benzyl bromide complex **(29)** by reacting with PPh_3/CBr_4. These reactions are summarized in scheme 4.9.

Up to this point, we experienced a few difficulties in purification of these new polymeric compounds. This is due to the fact that these organometallic dendrimers are highly soluble in common organic solvents, except hexane and methanol.

Rp3G1Br (27)

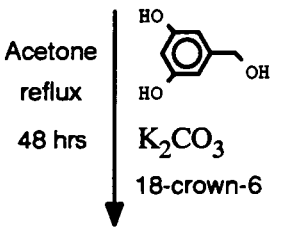

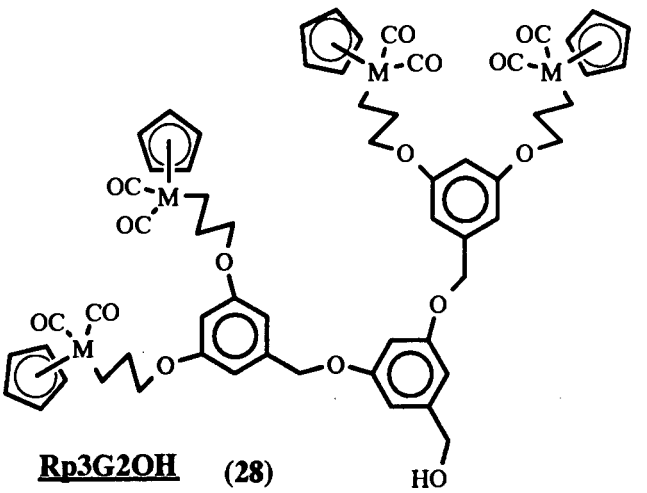

Rp3G2OH (28)

M = Ru

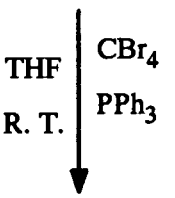

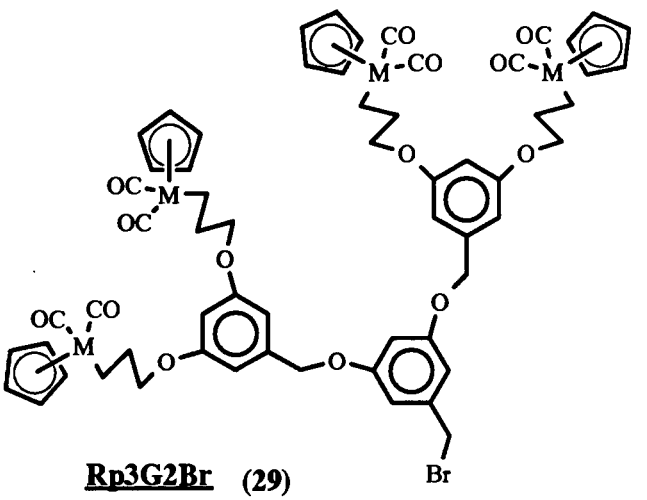

Rp3G2Br (29)

Scheme 4.9

Thus in the recrystallization process, these dendritic polymers generally separate out as oils rather than solids, and the resulting glassy solid can only be obtained after drying under high vacuum. We find that, in some cases, several recrystallizations (after column chromatography) may be needed in order to obtain products that are sufficiently pure for the subsequent reactions.

The third and fourth generation dendritic wedges *viz.* **(30)** - **(33)** are prepared in a similar fashion to their earlier generation analogues. Scheme 4.11 shows the reaction sequences for the third generation dendritic wedges **(30)** and **(31)**. It was found that the yields of reactions decrease slightly as the size of the dendrimers grow. This may be due to the increasing steric congestion around the focal points of the dendritic wedges, which reduces the reactivity of functional groups at the focal point. In this study, we have prepared organometallic dendritic wedges up to the fourth generation, **(32)** and **(33)**, containing 16 ruthenium atoms, with nominal molecular weights of about 6,000 (Figure 4.14).

In the convergent approach, the dendritic wedges, containing benzyl bromide functional groups can be reacted with a polyfunctional CORE molecule. In this study, the chosen trifunctional CORE molecule is 1,1,1-tris(4'-hydroxyphenyl)ethane. The reaction is similar to the one used in building the dendritic wedges (Rp3**G**xOH). Thus in a typical reaction, three molar equivalents of the dendritic wedge (Rp3**G**xBr) are reacted with one molar equivalent of the CORE molecule in the presence of potassium carbonate and 18-crown-6 in the refluxing acetone for 48 hours. The reactions are shown in Schemes 4.8 and 4.10. The resulting products, **(34)** - **(38)**, were purified by column chromatography and recrystallization.

Rp3G2Br (29)

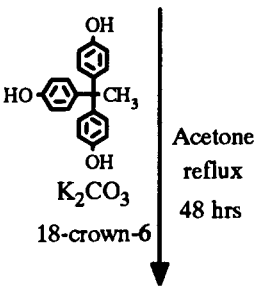

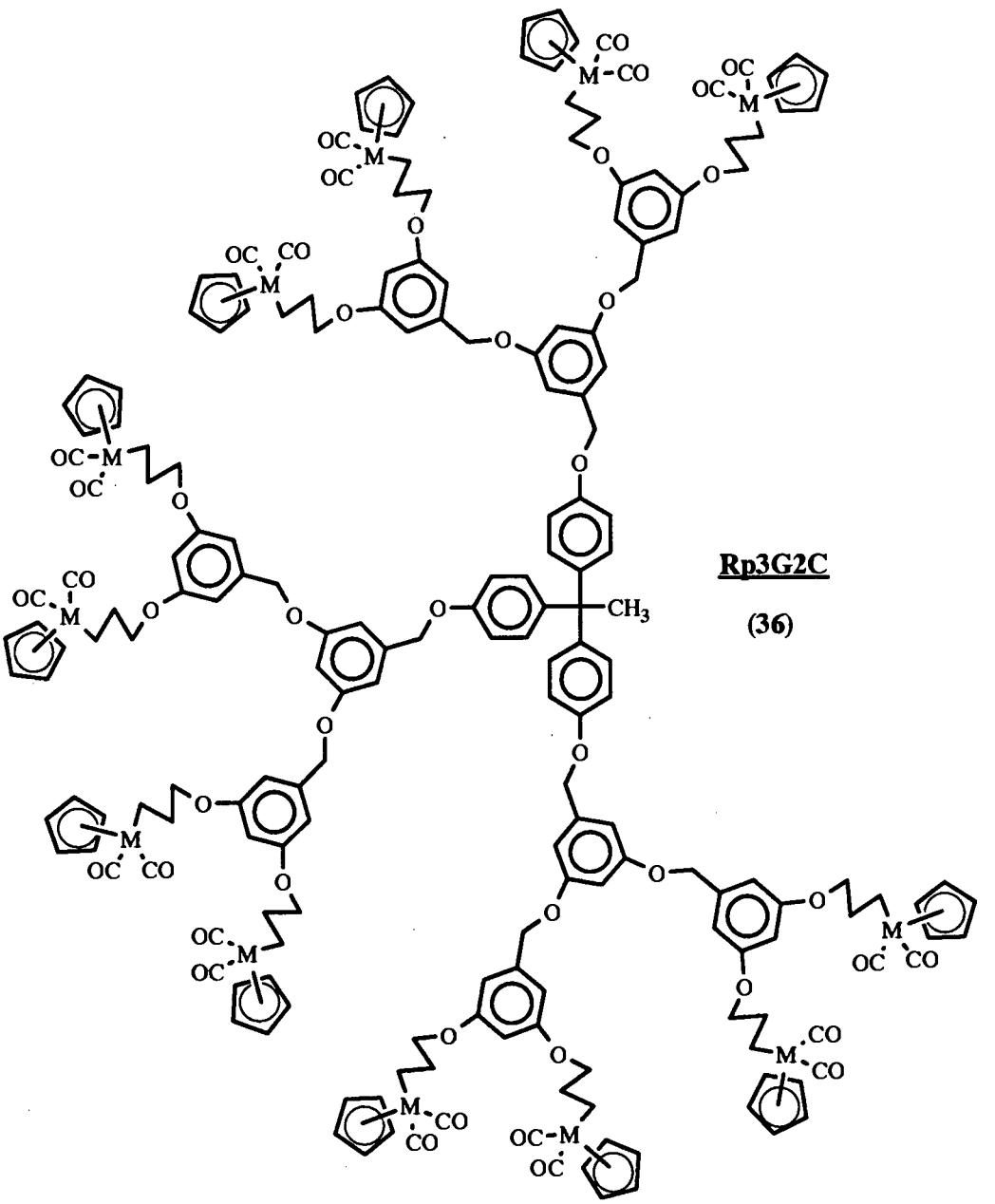

Rp3G2C

(36)

Scheme 4.10

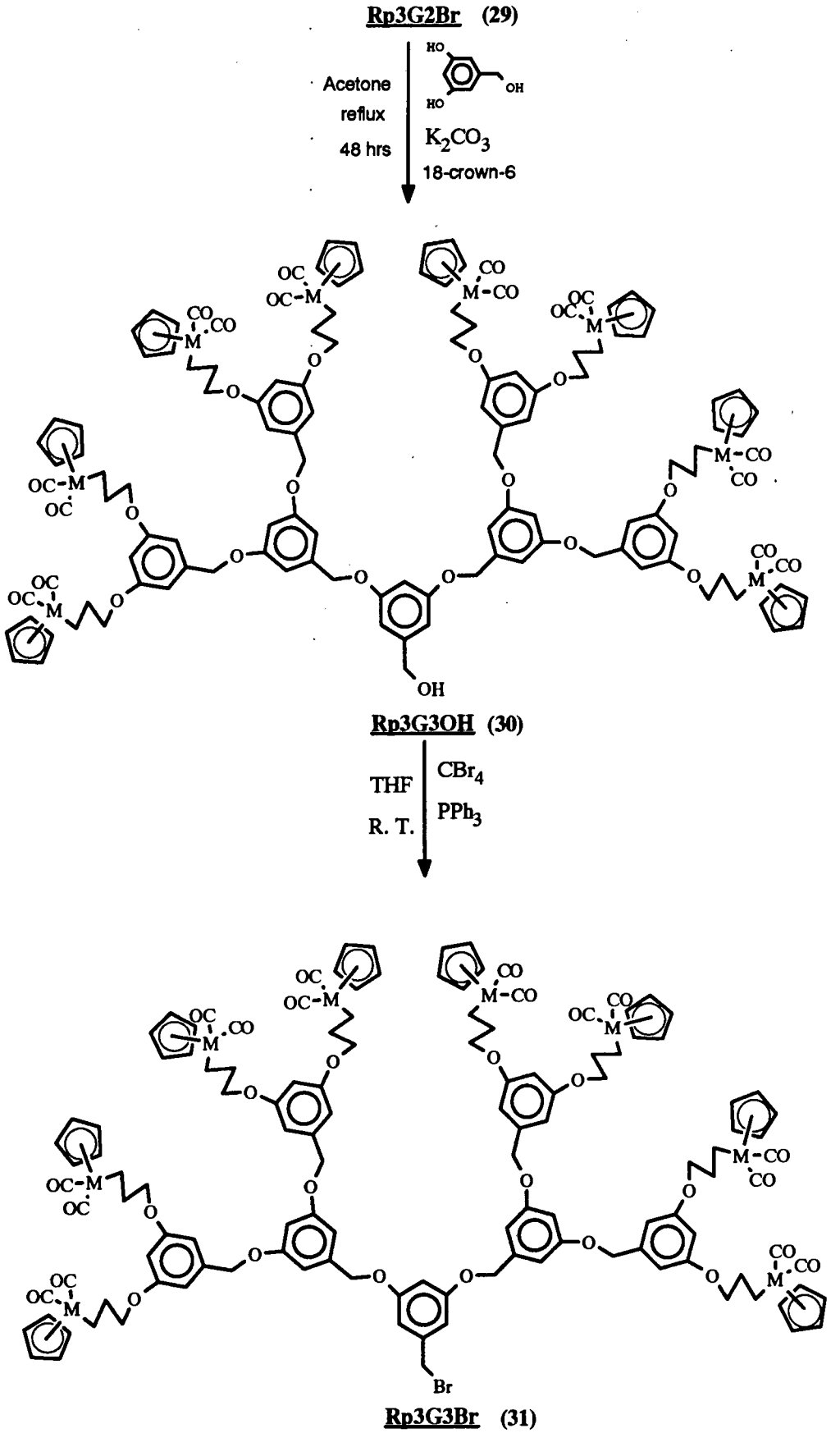
Rp3G2Br (29)
Acetone
reflux
48 hrs
HO
OH
HO
K_2CO_3
18-crown-6
OH
Rp3G3OH (30)
THF
R. T.
CBr_4
PPh_3
Br
Rp3G3Br (31)

Scheme 4.11

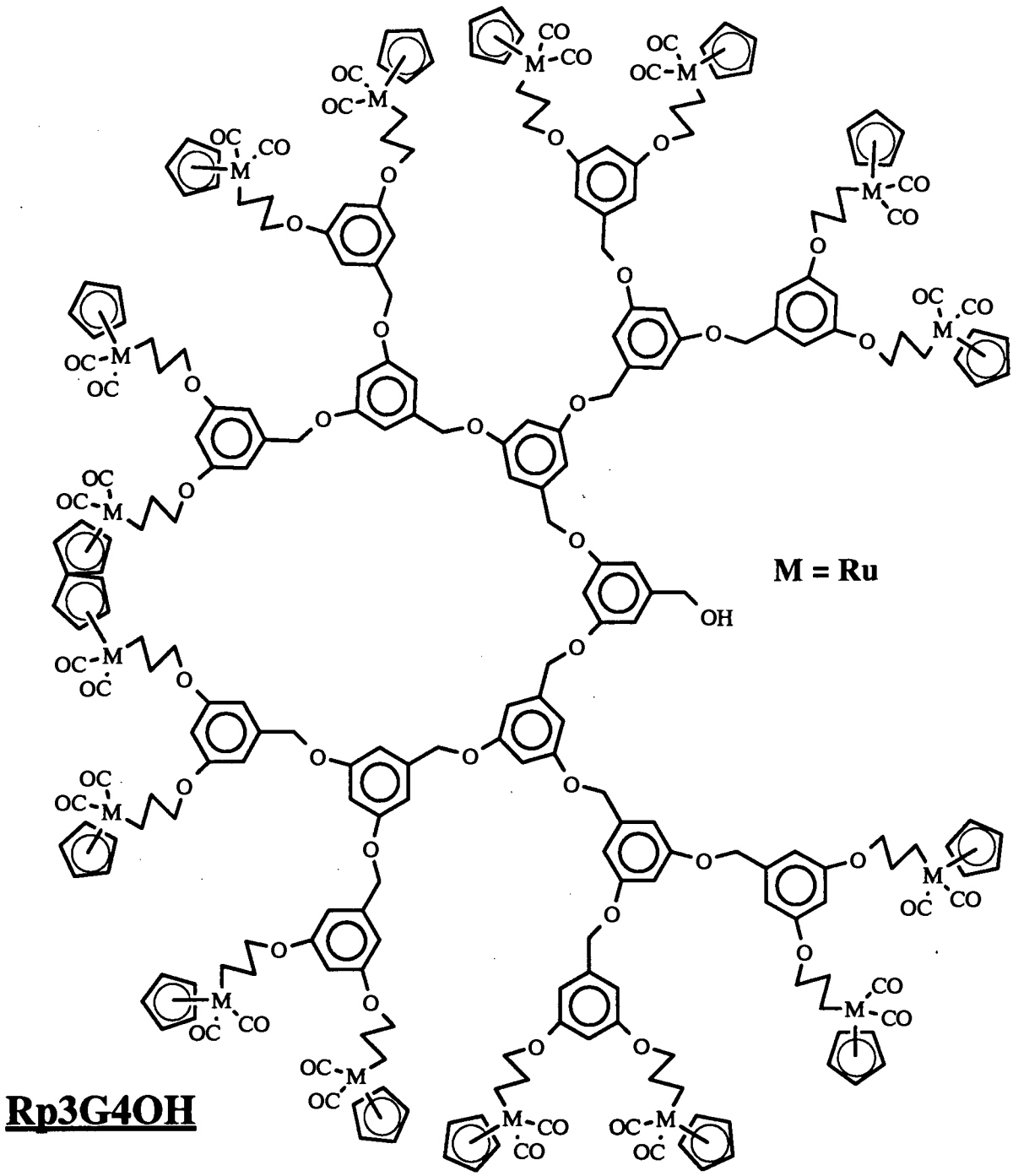

Figure 4.14 A fourth generation ruthenium containing dendritic wedge

In the case of the fourth generation, however the resulting product, Rp3**G**4C **(38)**, and the starting complex, Rp3**G**4Br, could not be separated by column chromatography. This reaction thus became problematic. To solve this, a slight excess of Rp3**G**4Br was used (3.3 equiv.) to react with one molar equivalent of the CORE molecule. Once the reaction was complete (after two days), a large excess of the CORE molecule (*ca.* 15 equiv.) was added to react with any excess of Rp3**G**4Br. The resulting monoalkylated CORE complex still containing two phenolic functional groups, would have very different mobility in column chromatography compared to the desired product Rp3**G**4C. Thus Rp3**G**4C can be purified by column chromatography and obtained in 70% of yield after recrystallization.

As far as we know, Rp3**G**4C is the largest organotransition metal complex ever prepared. It contains 48 ruthenium metal atoms at the chain-ends and has a nominal molecular weight of 18,438 amu.. The diameter of Rp3**G**4C, estimated by a computer assisted molecular model is about 3.2 nm. The structure of Rp3G4C is shown in Figure 4.15.

All these ruthenium dendrimers prepared so far are air stable in the solid state, but slowly decompose in solution within a day on exposure to air.

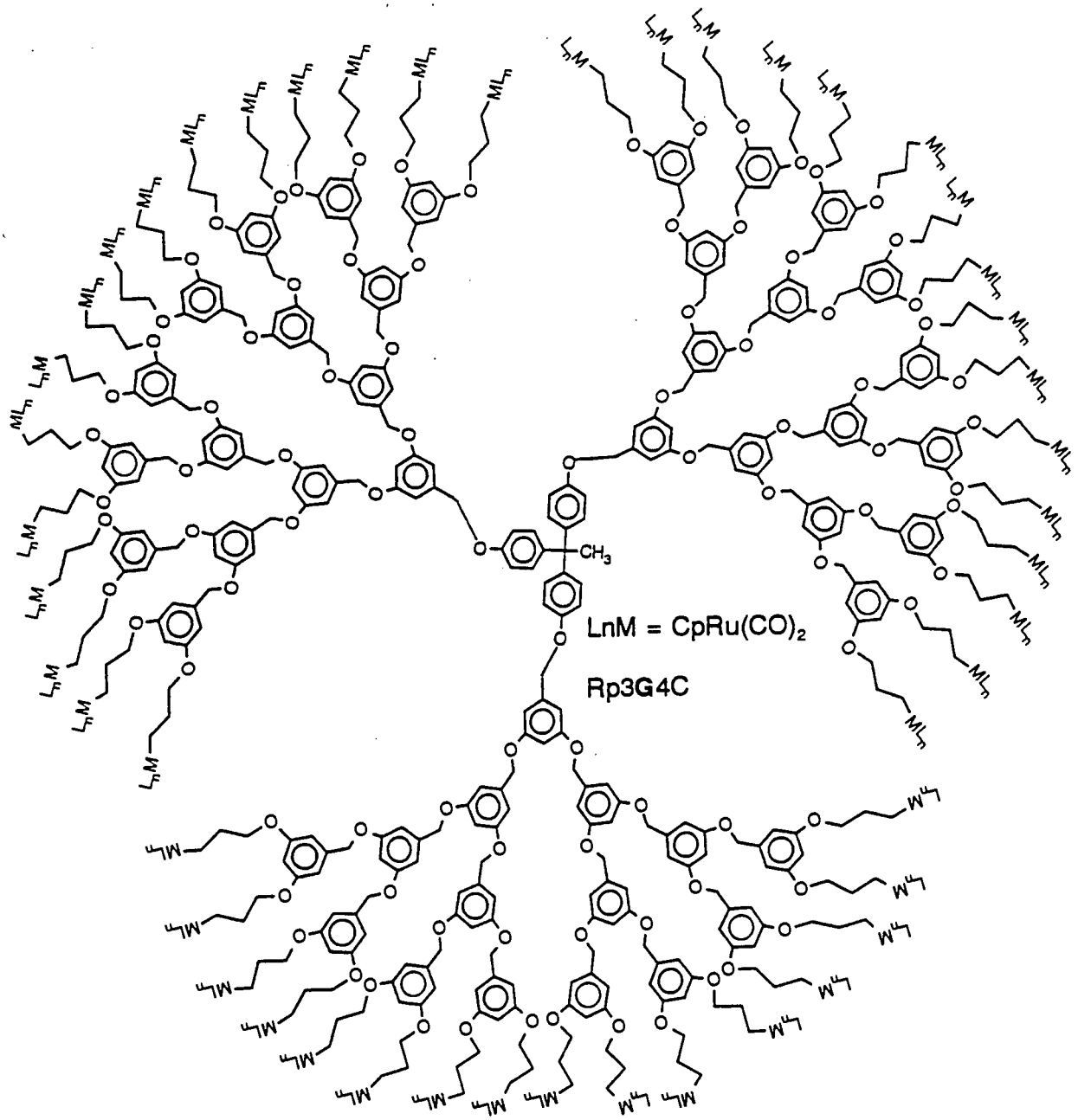

Figure 4.16 An organometallic dendrimer containing 48 ruthenium metal atoms

4.4 CHARACTERIZATION OF NEW ORGANOTRANSITION METAL DENDRIMERS

All the new organotransition metal dendrimers have been characterized by IR, ^{1}H NMR, ^{13}C NMR, mass spectroscopy and elemental analysis. The data are given in the experimental section. The results are discussed in the following text.

4.4.1 IR Spectroscopy

The IR spectra of **(24)** - **(38)** were recorded in a CH_2Cl_2 solution between 2200 and 1600 cm^{-1}. All these ruthenium dendrimers showed two strong absorption bands at 2012 and 1957 cm^{-1}, which are exactly at the same position as for $[CpRu(CO)_2\{(CH_2)_3Br\}]$. It was anticipated that the densely packed chain-ends may have effects on the υ(CO) absorption bands. However neither band shift nor band distortion was observed in any of these dendrimers.

4.4.2 ^{1}H and ^{13}C NMR Spectroscopy

NMR spectroscopy has proved to be invaluable in characterization of the new dendritic compounds [29]. All the dendrimers prepared in this study were characterized by ^{1}H and ^{13}C NMR spectroscopy. A 400 MHz ^{1}H NMR spectrum of Rp3G3OH is shown in Figure 4.17. In all cases, the organometallic functional groups on the periphery of the molecules give four sets of resonances at position: δ 5.23 (Cp), 3.85 (CH_2O), 2.01 (CH_2), and 1.70 ($RuCH_2$) ppm. The triplet observed at δ 3.85 ppm is particularly important, since it confirms the formation of anticipated products at the first stage of construction of the dendrimers, whereas the other peaks indicate that the organometallic functional groups remain in the dendritic structure during the course of the reactions required for their synthesis.

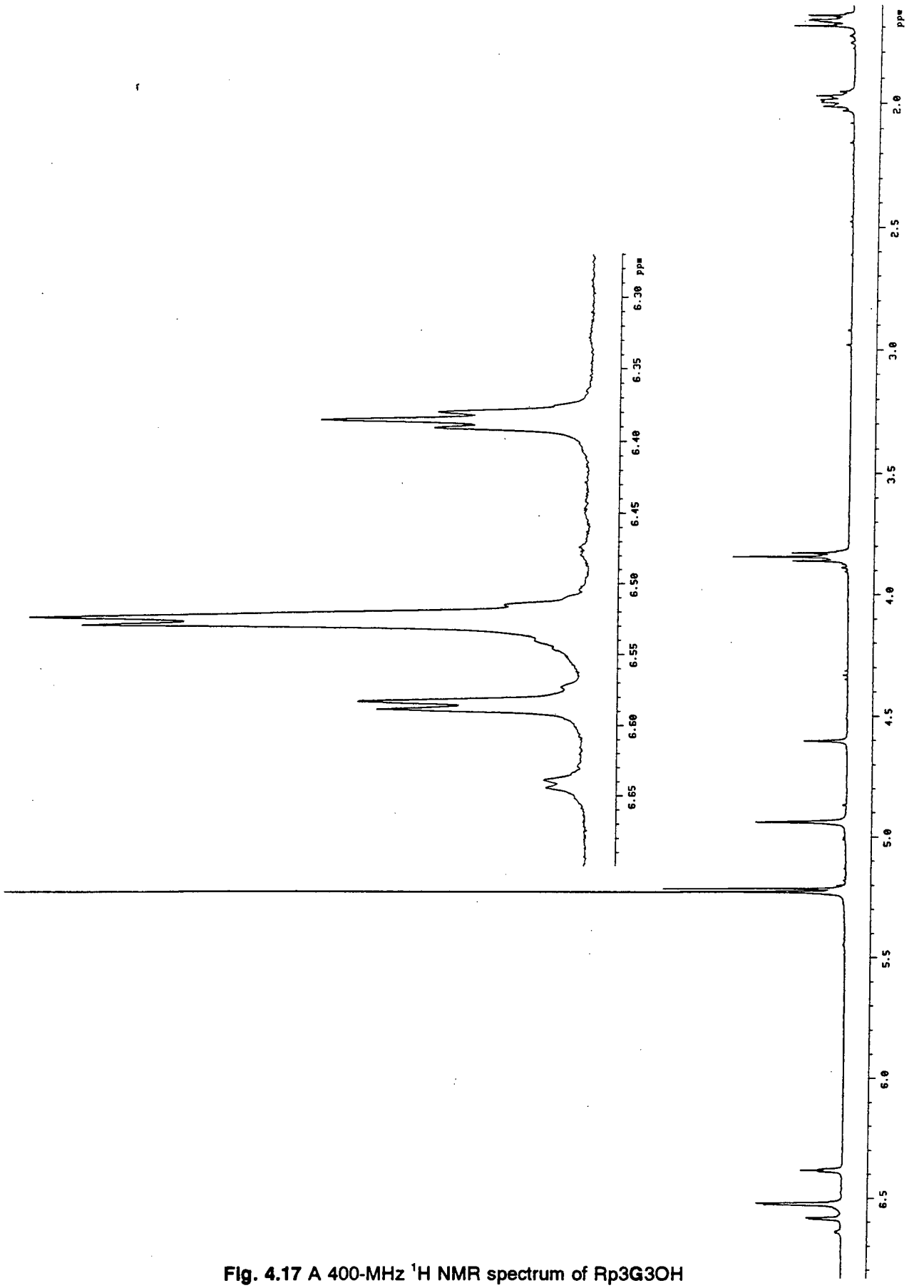

Fig. 4.17 A 400-MHz ^{1}H NMR spectrum of Rp3G3OH

The resonances, occurring in the region of δ 6.3 - 6.7 ppm were assigned to the aromatic protons of the dendritic building blocks. Separate resonances, corresponding to each "layer" of dendritic monomer (with appropriate integrations) were observed. This is demonstrated in Figure 4.17, from which the generation number can be easily identified by the number of doublet peaks (*ie.* three doublets were observed for Rp3**G**3OH).

The resonances in the region of δ 4.3 - 5.0 ppm were assigned to the benzyl CH_2 protons. Again, separate resonances can be seen in the region of δ 4.9 - 5.0 ppm for the different "layers" of dendritic monomers. For example, Figure 4.18 shows the ^1H NMR spectrum of Rp3**G**4OH in the region of 4.5 - 5.1 ppm, from which the different "layers" of dendritic building blocks can clearly be seen.

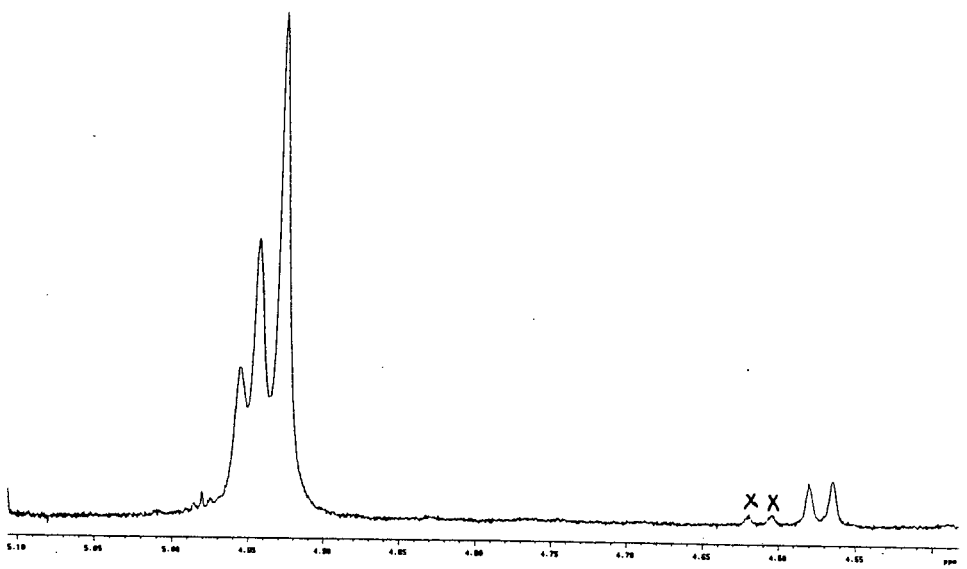

Fig. 4.18 A 400 MHz ^1H NMR spectrum of Rp3**G**4OH in the region of δ 4.5 - 5.1 ppm
X is an impurity

Perhaps the most important information one can obtain from this region is the resonances due to the functional groups at the focal point of dendrimer. The benzyl

alcohol gives a doublet resonance at *ca.* 4.57 ppm, whereas the benzyl bromide shows a singlet resonance at *ca.* 4.40 ppm. A shift from 4.40 to 4.90 ppm of the same CH_2 resonance was observed when dendritic wedges were coupled to the CORE molecule. This was accompanied by a new resonance at 2.01 ppm corresponding to methyl protons of the CORE molecule, while the aromatic protons of the CORE molecule gave two distinguishable doublets at 6.82 and 6.97 ppm. Figure 4.19 shows 400-MHz ^1H NMR spectra of Rp3**G**2OH, Rp3**G**2Br and Rp3**G**2C in the region of 4.4 - 5.0 ppm. The dramatic shift of the focal benzyl CH_2 resonances in the various dendrimers can easily be seen.

In all cases, the integration of resonances was employed to further confirm the generation number and to ascertain whether the reaction of Rp3**G**xBr with CORE molecule (or with 3,5-dihydroxybenzyl alcohol) had gone to completion.

^{13}C NMR spectroscopy was found to be less useful in characterization of various products. This could be due to the limited sensitivity of the ^{13}C nucleus, which cannot distinguish the subtle change of the chemical environment in the dendritic structure. Nevertheless, in the case of the first and second generation dendrimers, the complete assignments of ^{13}C NMR spectra were possible. For example, Figure 4.20 shows the 100-MHz ^{13}C NMR spectrum of Rp3**G**2OH. The different "layers" of aromatic carbons give separate resonances in the region of δ 100 - 180 ppm. Figure 4.21 shows ^{13}C spectra in the region corresponding to the benzyl CH_2 for the various dendrimers. The resonances due to the focal CH_2 groups are clearly distinguishable from the various functional groups, such as CH_2OH (δ 65 ppm), and CH_2Br (δ 34 ppm).

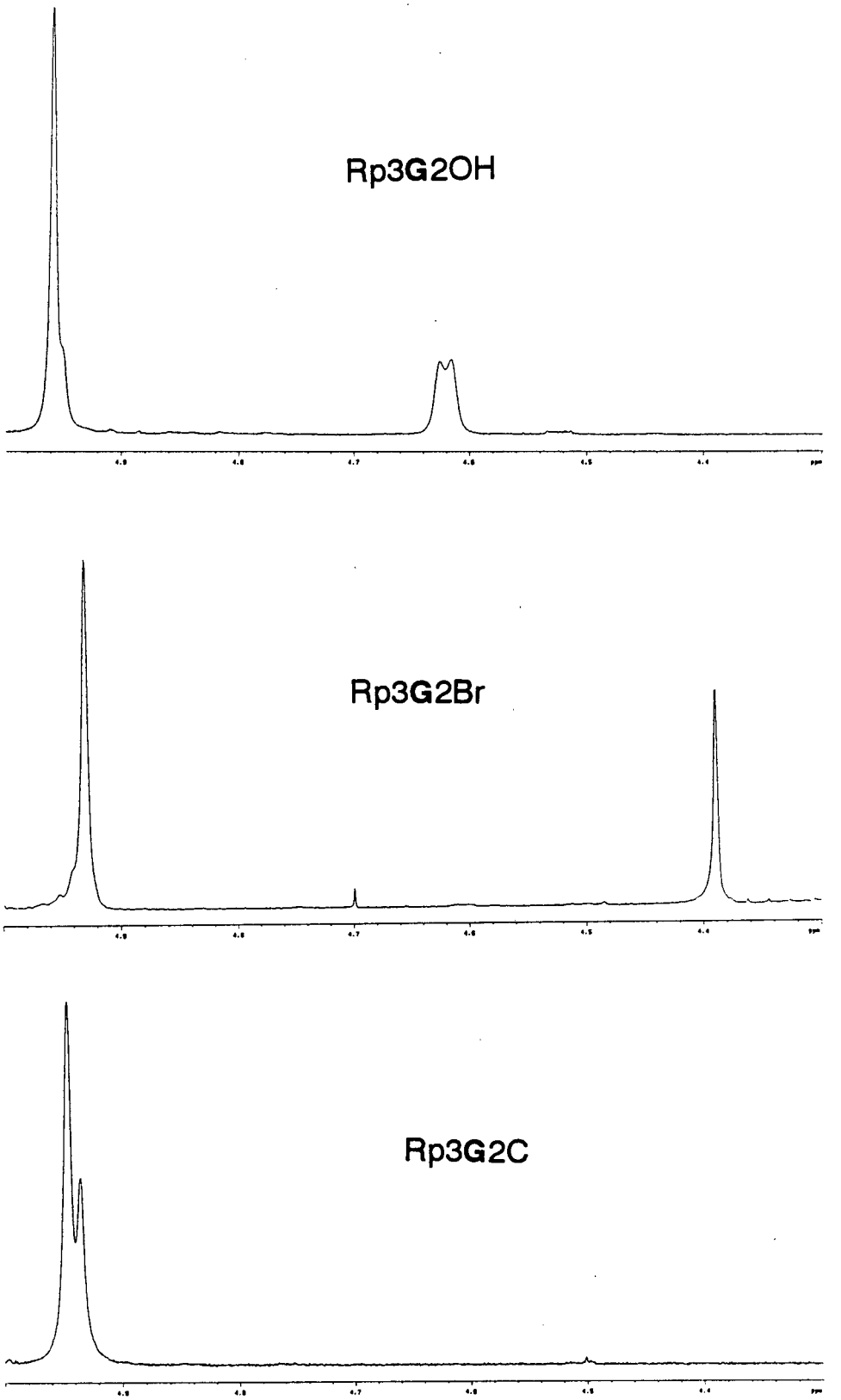

Figure 4.19 The ^{1}H NMR spectra for various types of dendrimer (see Schemes 4.9 and 4.10) in the region of 4.3 - 5.0 ppm; X is an impurity

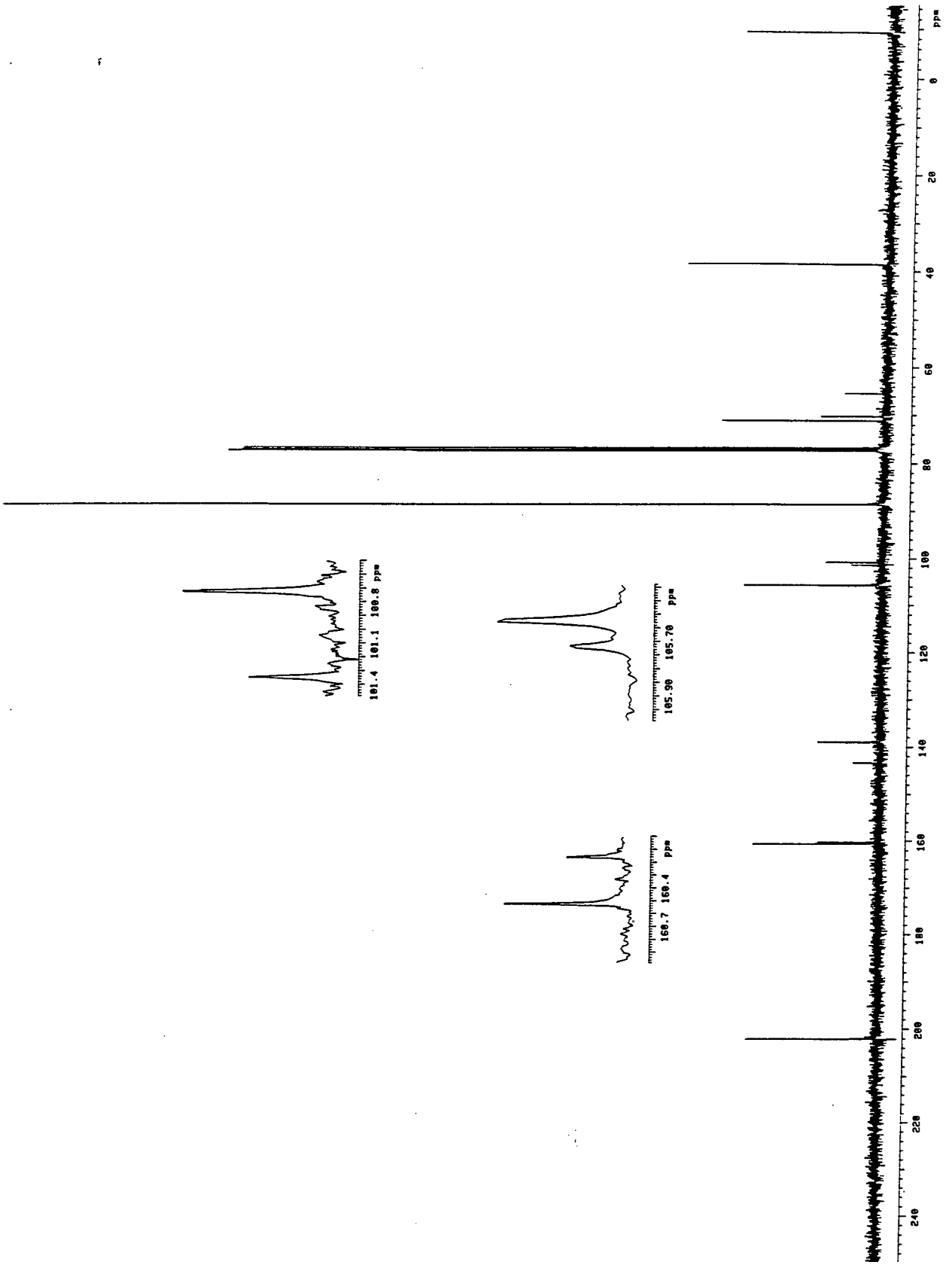

Figure 4.20 A 100-MHz ^{13}C NMR spectrum of Rp3G2OH

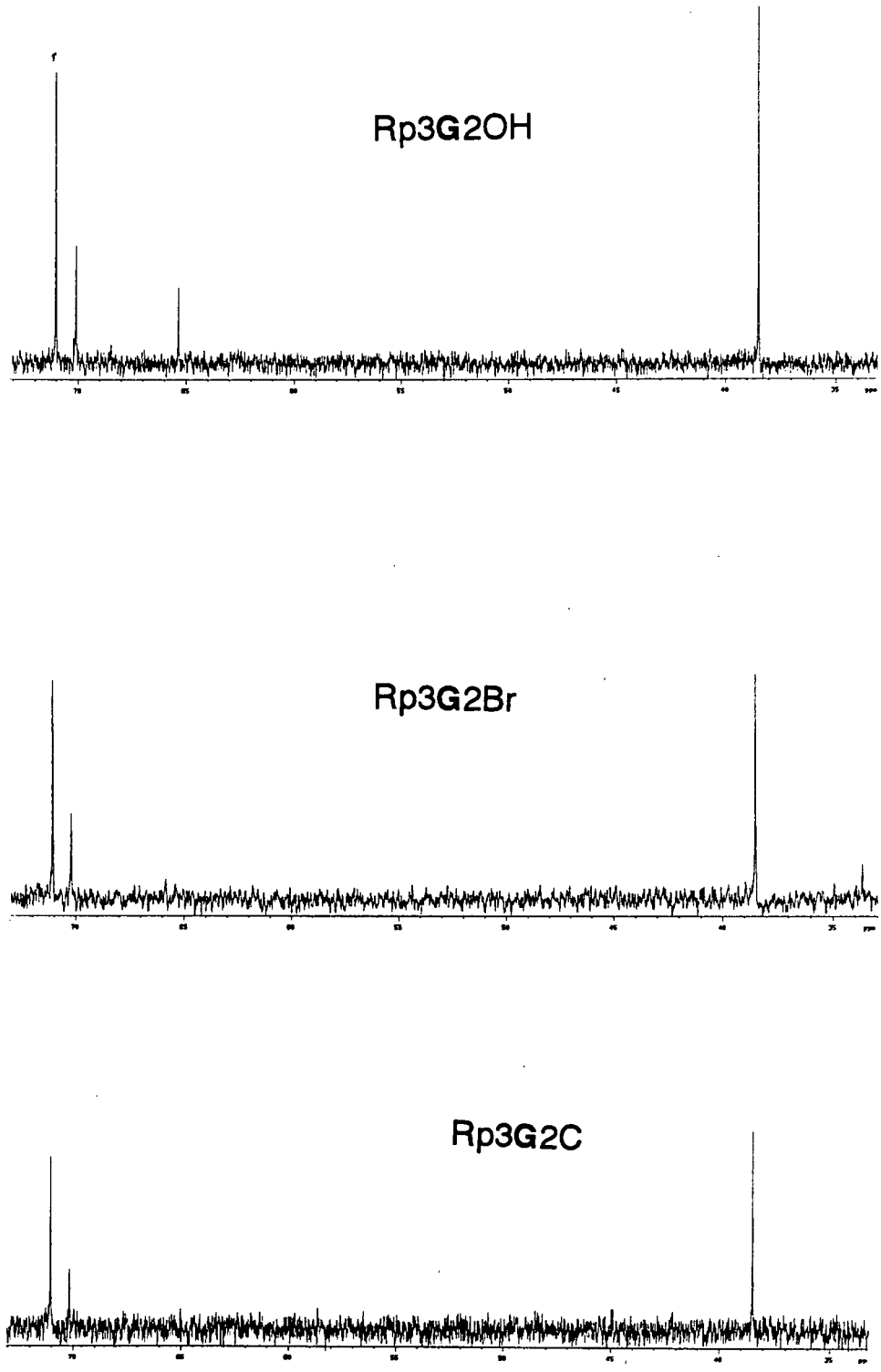

Figure 4.21 The ^{13}C NMR spectra of various type of dendrimers (see Schemes 4.9 and 4.10) in the region of δ 33 - 73 ppm

4.4.3 Mass Spectroscopy

The nominal molecular weights of these new organometallic dendrimers were confirmed by fast atom bombardment (FAB) mass spectroscopy, and the results are given in the experimental section. Unfortunately, due to the limitation of instruments and techniques, we were only able to obtain molecular weights up to about 4,500 for these ruthenium dendrimers.

For the dendrimers with molecular weights below 1,400, the FAB mass spectra showed molecular ion peaks at the anticipated positions. The elemental composition of molecular ion peaks was further confirmed by comparing its isotope pattern with the pattern generated from computer calculation. However, in the cases of high molecular weight dendrimers, we only observed a set of daughter peaks at the anticipated p^+-2CO position. The position of fragments in FAB mass spectra was not completely certain due to the following factors: low intensity of peaks, the complicated isotope pattern of the ruthenium atoms, and the possible overlapping of fragments, such as p^+-2CO-1, p^+-2CO-2 *etc.*

However, we believed that the mass spectra reported here are reasonable, since previous studies in this laboratory have shown that complexes of the type, $[CpM(CO)_2\{(CH_2)_nX\}]$ (where M = Fe, Ru; X = H, Br, I) [46 - 48], give very weak molecular ion peaks in their mass spectra. Also, the ratio of the peak intensities of $(p^+\text{-}2CO)/(p^+)$ is found to increase as the molecular weight of complex increases.

4.4.4 Elemental Analysis

Satisfactory elemental analysis results (C, H) were obtained for most of the new dendrimers (see experimental section). However it was found that the elemental

analysis is not sufficiently accurate to be able to distinguish between certain dendrimers [29]. For example, Rp3**G**2OH requires C = 51.0%, H = 4.2%; while Rp3**G**3Br requires C = 50.8%, H = 4.1%, although these two dendrimers are very different from each other in terms of functional groups at the focal point and generation. However, their differences in elemental analysis, C = 0.2%, H = 0.1% are within the experimental error of the method.

4.5 THERMAL PROPERTIES OF RUTHENIUM CONTAINING DENDRIMERS

Differencial Scanning Calorimetry (DSC) was employed to obtain the glass transition temperatures of these dendrimers. The DSC traces were recorded in the temperature range of -10 to +110 °C. A typical DSC trace for these dendrimers is shown in Figure 4.22. The data obtained and calculation of results are summarized in Table 4.2.

As we have described previously in Section 4.1, the glass transition temperature of dendrimers is related to their chemical composition, chain-end functional groups and molecular weights. In the following text, we shall discuss these factors individually and compare our results with the reported data for the purely organic polybenzylphenylether dendrimers. The difference between the reported polybenzylphenylether dendrimers and the dendrimers prepared in this study is in the chain-end functional groups.

4.5.1 Effects of molecular weight

A plot of T_g against logM was obtained, and is shown in Figure 4.23. The plot indicates that the T_g increases as the molecular weight of dendrimer increases. The "leveling-off" effect is also observed in this study. It is interesting to note that in this case the T_g started leveling off at a molecular weight about 3,000 which is very similar to that observed for the polybenzylphenylether dendrimers [23]. These results thus imply that both types of dendrimers would reach a densely-packed globular structure at a molecular weight above 3,000. Thus the chain-end functional groups seem to have little effect on this characteristic property.

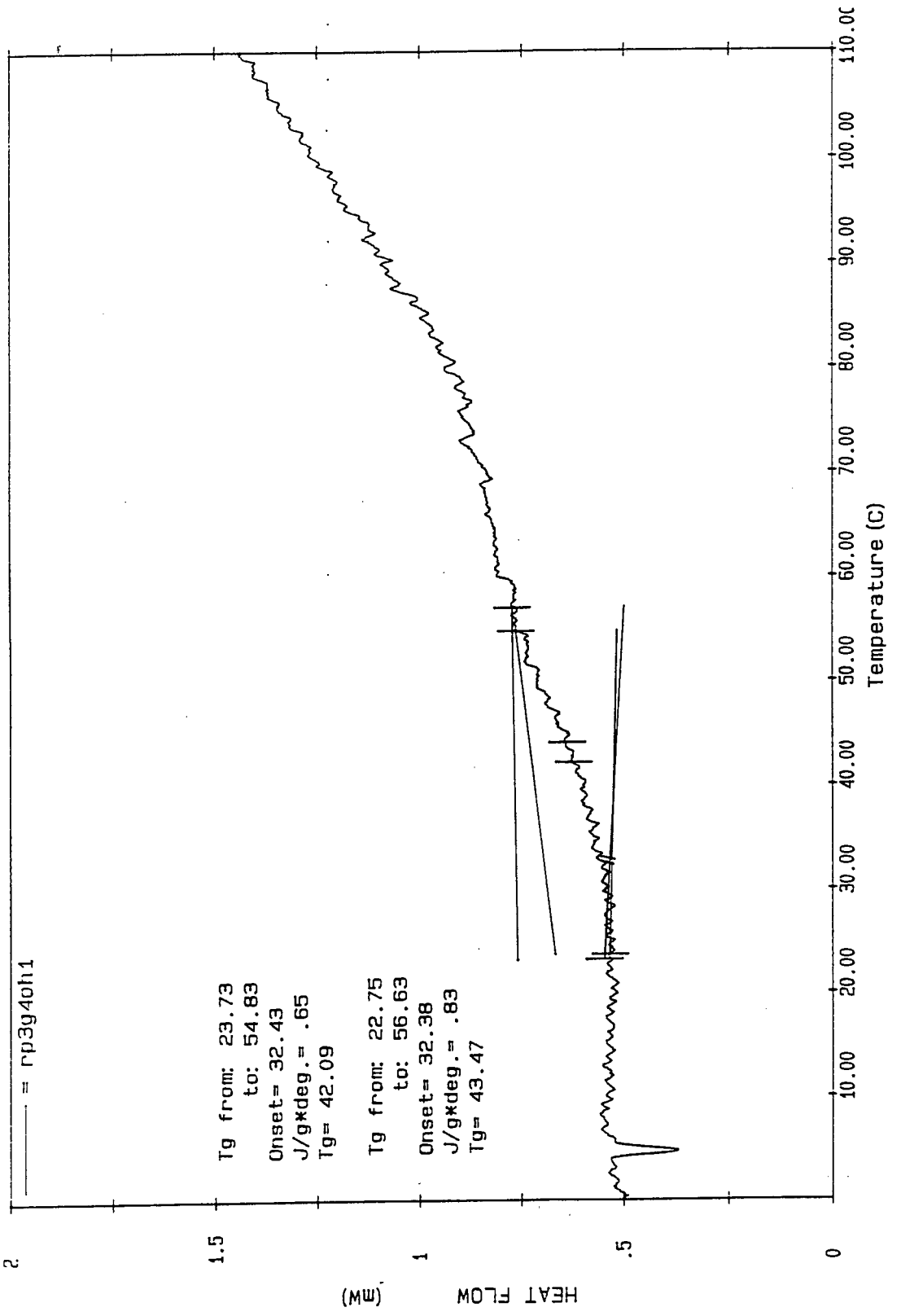

Figure 4.22 A DSC trace of Rp3G4OH

Table 4.2 Thermal data and calculated results for selected ruthenium dendrimers

Complexes	MW	T_g (°C)	log MW	n_e/M	$(n_e/M)_\infty$	$(n_e/M)-(n_e/M)_\infty$	$T_{g\infty}$ (°C)	K
Rp3G1OH	666.66	-3	2.8239	0.003000	0.002595	0.0004.5	48	126000
Rp3G2OH	1437.42	23	3.1576	0.002783	0.002595	0.000188	48	126000
Rp3G3OH	2978.94	37	3.4741	0.002686	0.002595	0.000091	48	126000
Rp3G4OH	6062.00	42	3.7826	0.002639	0.002595	0.000044	48	126000
Rp3G1C	2252.28	34	3.3526	0.002664	0.002595	0.000069	47	208000
Rp3G3C	9189.15	45	3.9633	0.002609	0.002595	0.000014	47	208000
Rp3G4C	18438.31	47	4.2657	0.002603	0.002595	0.000008	47	208000
Rp3G3Br	3041.84	37	3.4831	0.002630	0.002595	0.000035	48	126000

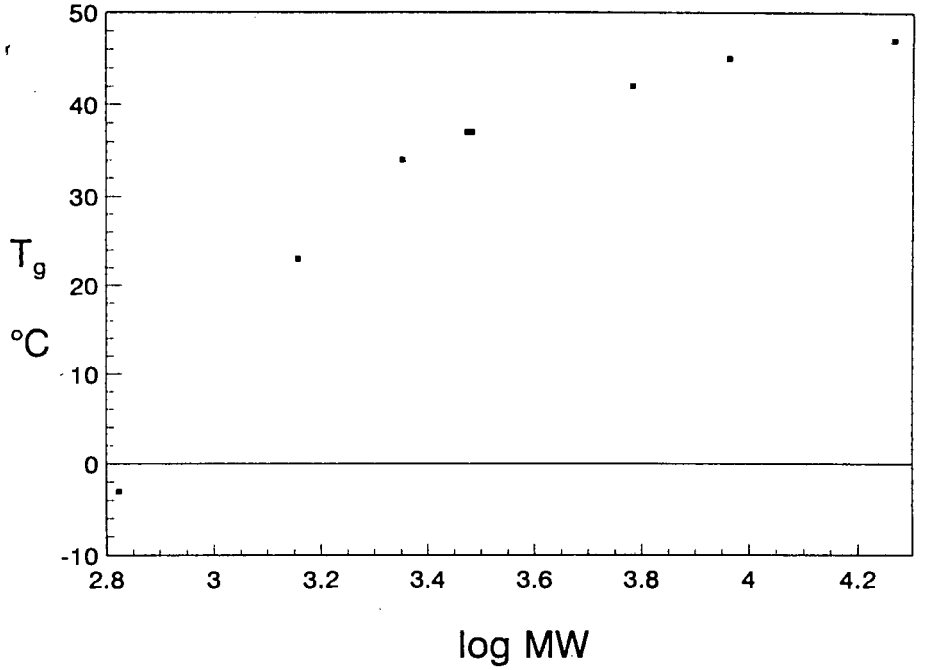

Figure 4.23 A plot of T_g vs logMW for selected ruthenium dendrimers

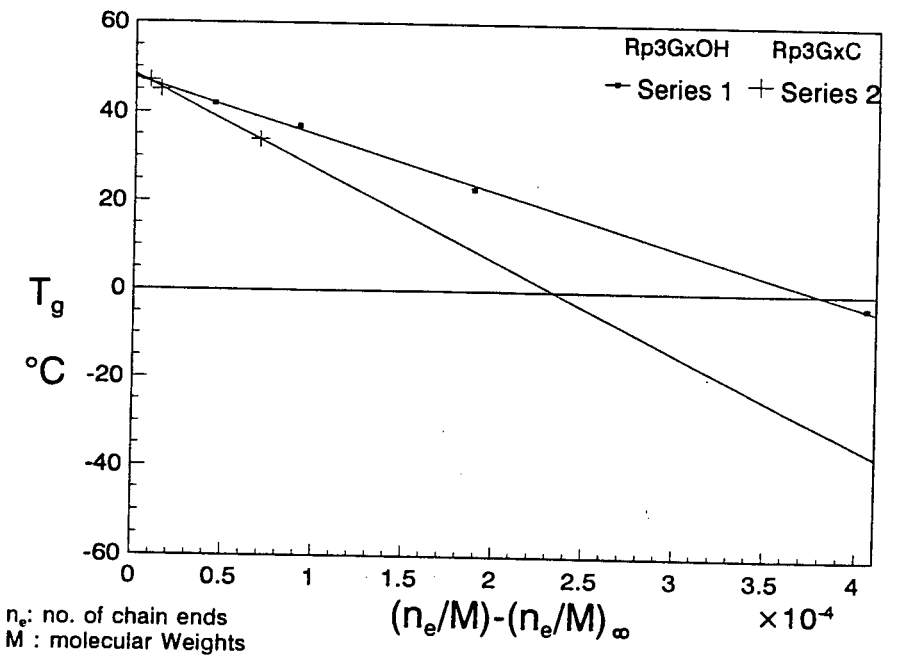

Figure 4.24 A plot of T_g vs $(n_e/M)-(n_e/M)_\infty$ for selected ruthenium dendrimers

Indeed, the computer assisted molecular models for these ruthenium dendrimers do show a transition from a loose, flexible structure to a densely packed globular structure, as shown in the Appendix. For these ruthenium dendrimers, the T_g levels off at the molecular weight corresponding to the third generation dendritic wedges (Rp3**G**3OH or Rp3**G**3Br), whereas in the case of the organic polybenzylphenylether dendrimers, it correspond to a third generation dendrimer (Figure 4.6).

4.5.2 Effects of the chain-end functional groups

The $T_{g\infty}$ and K values were obtained from a plot of T_g vs $[(n_e/M) - (n_e/M)_\infty]$ as shown in Figure 4.24. For the series of dendritic wedges with focal benzyl alcohol functional groups, the n_e values were taken with the assumption that the free volume of the chain-end functional group ($CpRu(CO)_2(CH_2)_3$) is much larger than that of the focal functional group ($PhCH_2OH$). The K values were then calculated from linear regression as the slope of the plot. Indeed, the K values obtained here (*ca.* 126,000) are significantly larger than those reported for the polybenzylphenylether dendrimers with benzyl groups at the chain-ends (ca. 13,600). Since the K values are proportionally related to the chain-end free volume (θ), therefore we were able to support the assumption made for the calculation of the K values.

The K values obtained here for Rp3**G**xOH and Rp3**G**xC are very different (126000 for Rp3**G**xOH and 208000 for Rp3**G**xC). We can ascribe this effect to the increment of the number of chain ends in the Rp3**G**xC series (3, 6, 12, 24, 48) is significantly larger than that in the Rp3**G**xOH series (2, 4, 8, 16).

Also, since the same T_g value was obtained for both Rp3**G**3OH and Rp3**G**3Br, this suggests that the focal functional groups have very little effect on the T_g value.

According to Equation 4.3, the $T_{g\infty}$ values can be obtained from Figure 4.24 as the intercept of Y axis. As expected, the $T_{g\infty}$ values for dendritic wedges (Rp3GxOH) and dendrimers (Rp3GxC) are very similar (48 and 47 °C, respectively). However, in a comparison of the $T_{g\infty}$ values between organic polybenzylphenylether dendrimers (44 °C for dendritic wedges; 43 °C for dendrimers) and the ruthenium dendrimers, no significant difference in $T_{g\infty}$ value was found. This could be due to the fact that $T_{g\infty}$ values are largely dependent on the polarity of chain-ends functional groups, rather than the size of them.

4.6 SCANNING ELECTRON MICROSCOPY

Selected ruthenium dendritic complexes were submited for scanning electron microscopy (SEM). The results, as shown in Figure 4.26, indicate that Rp3G1Br is in the crystalline state and has a thin flaky appearance, whereas the rest of the dendritic complexes are in a polymeric state with a porous glassy appearance, except Rp3G2Br which has a rubbery appearance. This is because the T_g of Rp3G2Br is below room temperature. The porous appearance of these dendritic complexes may be due to the fact that they are very soluble in common organic solvents, which prevent them being separated out from an organic solution as a solid, and thus a porous solid is obtained after evaporation of the solvent molecules.

Rp3G1Br

Rp3G3OH

Rp3G2Br

Rp3G3C

Rp3G1C

Figure 4.26 SEM pictures of selected ruthenium dendrimers

4.7 REFERENCES

1. R. Hoffmann, *New Scientist*, **1990**, *128*, 44.
2. J. M. J. Fréchet, *Science*, **1994**, *263*, 1710.
3. Y. H. Kim, *Adv. Mater.*, **1992**, *4*, 764.
4. *Chem. Brit.*, **1993**, *29*, 460.
5. R. Dagani, *C & EN*, **1993**, Feb. 1, 28.
6. P. Hodge, *Nature*, **1993**, *362*, 18.
7. R. Dagani, *C & EN*, **1993**, Apr. 12, 26.
8. D. A. O'Sullivan, *C & EN*, **1993**, Aug. 16, 20.
9. D. A. Tomalia, A. M. Naylor and W. A. Goddard III, *Angew. Chem. Int. Ed. Engl.*, **1990**, *29*, 138.
10. J. Mulzer *et al.* Ed., *Organic Synthesis Highlights*, pp 378 - 383, VCH, Weinheim, **1991**.
11. H.-B. Mekelburger, W. Jaworek and F. Vögtle, *Angew. Chem. Int. Ed. Engl.*, 1992, *31*, 1571.
12. G. R. Newkome, C. N. Moorefield and G. R. Baker, *Aldrichim. Acta,* **1992**, 25, 31.
13. C. J. Hawker, K. L. Wooley and J. M. J. Fréchet, *Chem. Australia*, **1992**, December, 620.
14. D. A. Tomalia, *Aldrichim. Acta*, **1993**, *26,* 91.
15. V. Balzani, S. Campagna, G. Denti, A. Juris, S. Serroni and M. Venturi, *Coord. Chem. Rev.*, **1994**, *132*, 1.
16. N. J. Turro, J. K. Barton and D. A. Tomalia, *Acc. Chem. Res.*, **1991**, *24*, 332.
17. A. M. Naylor, W. A. Goddard III, G. E. Kiefer and D. A. Tomalia, *J. Am. Chem. Soc.*, **1989**, *111*, 2339.

18. M. F. Ottaviani, S. Bossmann, N. J. Turro and D. A. Tomalia, *J. Am. Chem. Soc.*, **1994**, *116*, 661.

19. G. Caminati, N. J. Turro, D. A. Tomalia, *J. Am. Chem. Soc.*, **1990**, *112*, 8515.

20. K. R. Gopidas, A. R. Leheny, G. Caminati, N. J. Turro and D. A. Tomalia, *J. Am. Chem. Soc.*, **1991**, *113*, 7335.

21. T. H. Mourey, S. R. Turner, M. Rubinstein, J. M. J. Fréchet, C. J. Hawker and K. L. Wooley, *Macromolecules*, **1992**, *25*, 2401.

22. P. G. de Gennes and H. Hervet, *J. de Phys.*, **1983**, *44*, L351.

23. K. L. Wooley, C. J. Hawker, J. M. Pochan and J. M. J. Fréchet, *Macromolecules*, **1993**, *26*, 1514.

24. D. A. Tomalia, H. Baker, J. Dewald, M. Hall, G. Kallos, S. Martin, J. Ryder and P. Smith, *Macromolecules*, **1986**, *19*, 2466.

25. E. Buhleier, W. Wehner, F. Vögtle, *Synthesis*, **1978**, 155.

26. C. Wörner and R. Mülhaupt, *Angew. Chem. Int. Ed. Engl.*, **1993**, *32*, 1306.

27. E. M. M. de Brabander-van den Berg and E. W. Meijer, *Angew. Chem. Int. Ed. Engl.*, **1993**, *32*, 1308.

28. C. Hawker and J. M. J. Fréchet, *J. Chem. Soc., Chem. Commun.*, **1990**, 1010.

29. C. J. Hawker and J. M. J. Fréchet, *J. Am. Chem. Soc.*, **1990**, *112*, 7638.

30. K. L. Wooley, C. J. Hawker and J. M. J. Fréchet, *J. Chem. Soc., Perkin Trans. I*, **1991**, 1059.

31. C. J. Hawker and J. M. J. Fréchet, *J. Am. Chem. Soc.*, **1992**, *114*, 8405.

32. I. Gitsov, K. L. Wooley, C. J. Hawker, P. T. Ivanova and J. M. J. Fréchet, *Macromolecules*, **1993**, *26*, 5621.

33. M. N. Bochkarev., *Organomet. Chem. (USSR)*, **1988**, *1*, 115.

34. S. Serroni, G. Denti, S. Campagna, A. Juris, M. Ciano, V. Balzani, *Angew. Chem. Int. Ed. Engl.*, **1992**, *31*, 1493.

35. G. R. Newkome, F. Cardullo, E. C. Constable, C. N. Moorefield and A. M. W. Cargill Thompson, *J. Chem. Soc., Chem. Commun.*,**1993**, 925.

36. G. R. Newkome, C. N. Moorefield, J. M. Keith, G. R. Baker and G. H. Escamilla, *Angew. Chem. Int. Ed. Engl.*, **1994**, *33*, 666.

37. F. Moulines, L. Djakovitch, R. Boese, B. Gloaguen, W. Thiel, J.-L. Fillaut, M.-H. Delville and D. Astruc, *Angew. Chem. Int. Ed. Engl.*, **1993**, *32*, 1075.

38. A. W. van der Made a.d P. W. N. M. van Leeuwen, *J. Chem. Soc., Chem. Commun.*, **1992**, 1400.

39. L.-L. Zhou and J. Roovers, *Macromolecules*, **1993**, *26*, 963.

40. K. Rengan and R. Engel, *J. Chem. Soc., Perkin Trans. I*, **1991**, 987.

41. K. L. Wooley, C. J. Hawker, J. M. J. Fréchet, F. Wudl, G. Srdanov, S. Shi, C. Li and M. Kao, *J. Am. Chem. Soc.*, **1993**, *115*, 9836.

42. C. J. Hawker, K. L. Wooley and J. M. J. Fréchet, *J. Chem. Soc., Chem. Commun.*, **1994**, 925.

43. R.-H. Jin, T. Aida and S. Inoue, *J. Chem. Soc., Chem. Commun.*, **1993**, 1260.

44. T. Nagasaki, M. Ukon, S. Arimori and S. Shinkai, *J. Chem. Soc., Chem. Commun.*, **1992**, 608.

45. S. Achar and R. J. Puddephatt, *Angew. Chem. Int. Ed. Engl.*, **1994**, *33*, 847.

Appendix Computer Assisted Molecular Models of the Ruthenium Dendrimers

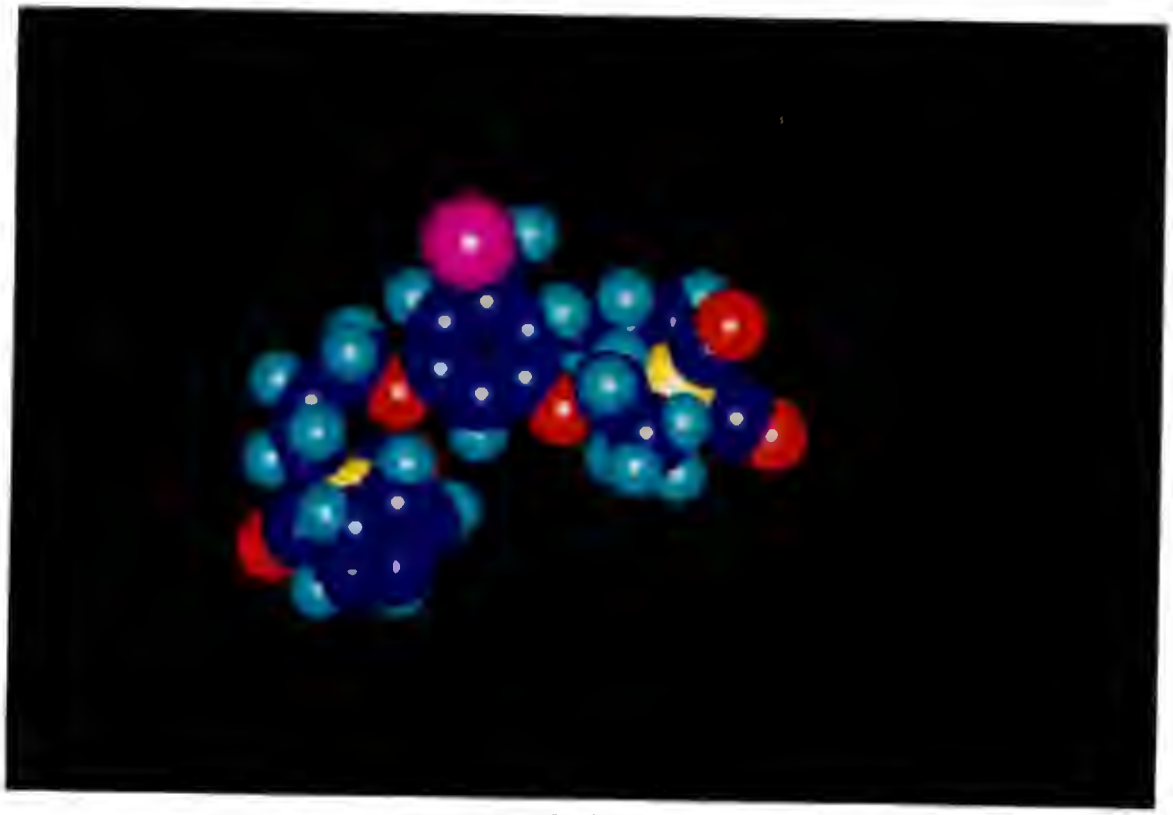

Rp3G1Br

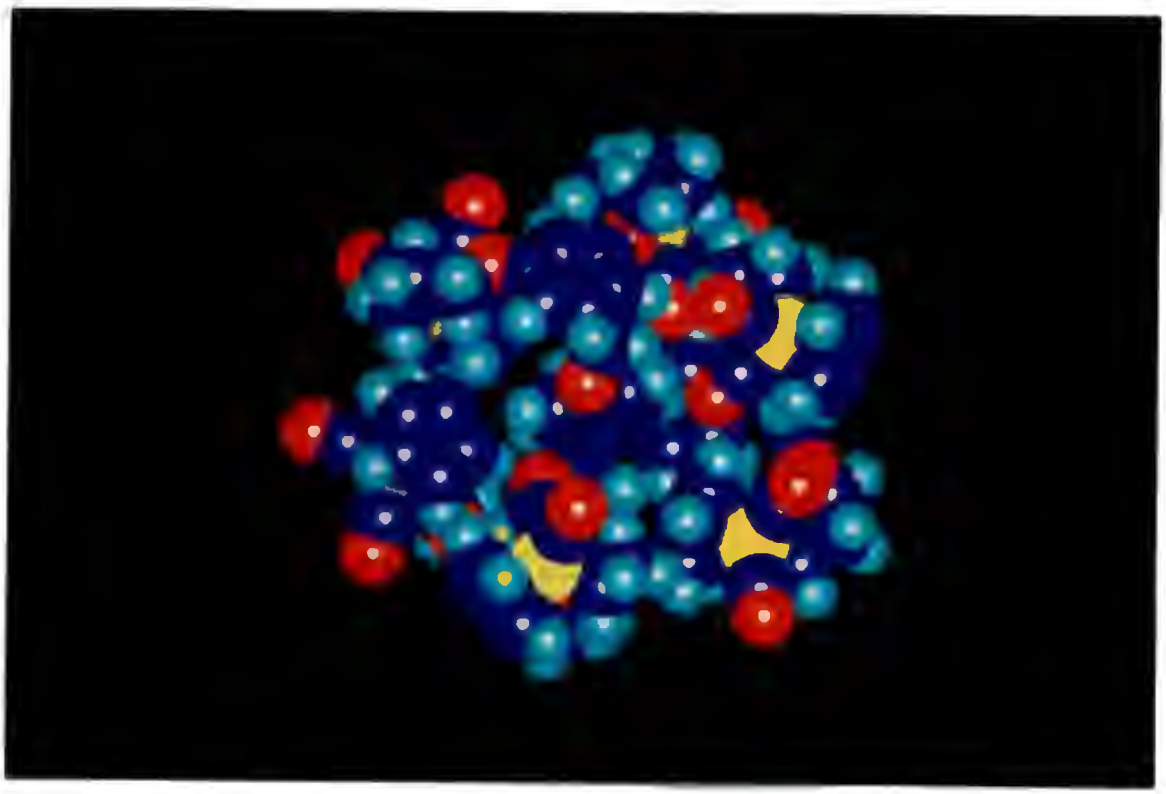

Rp3G1C

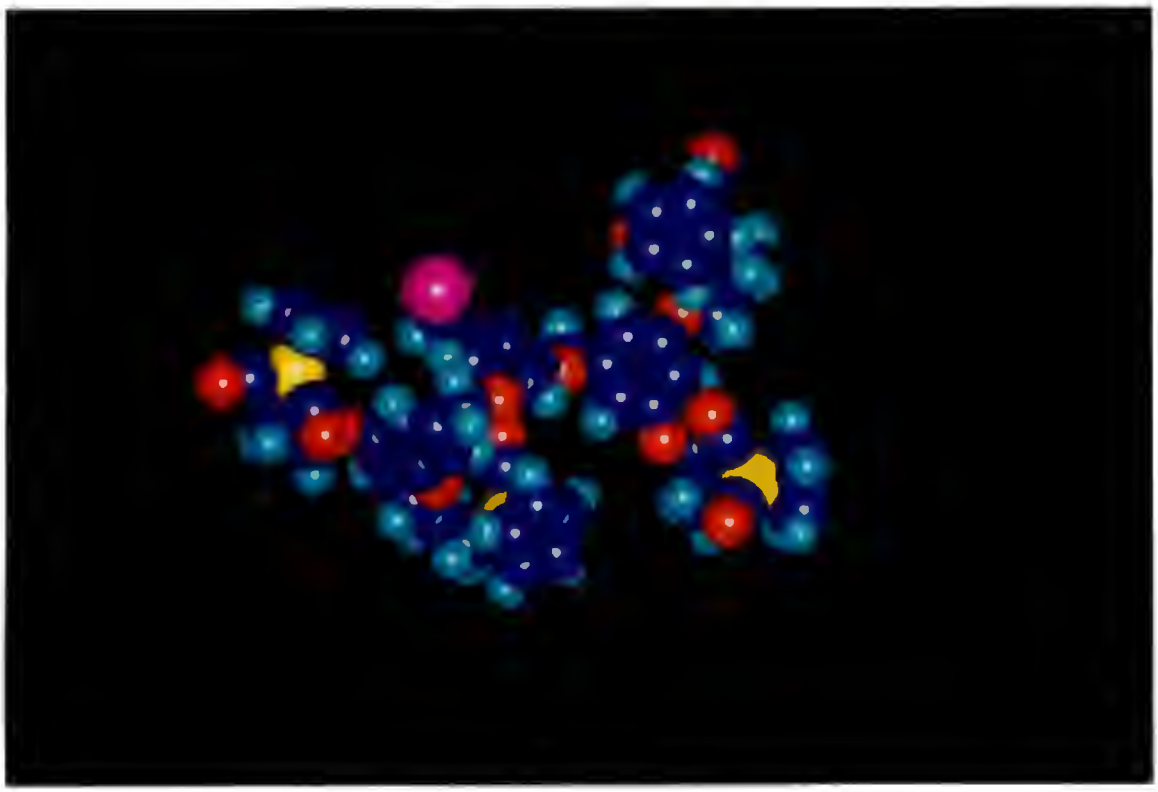

Rp3G2Br

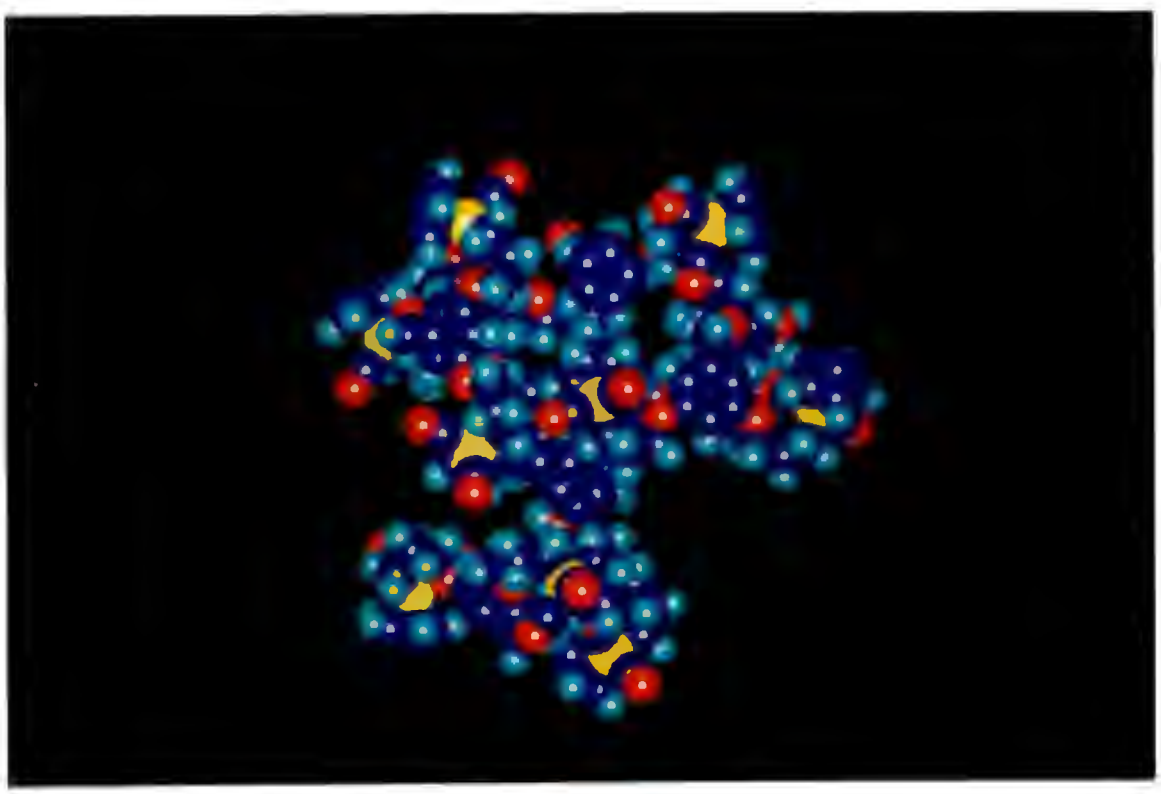

Rp3G2C

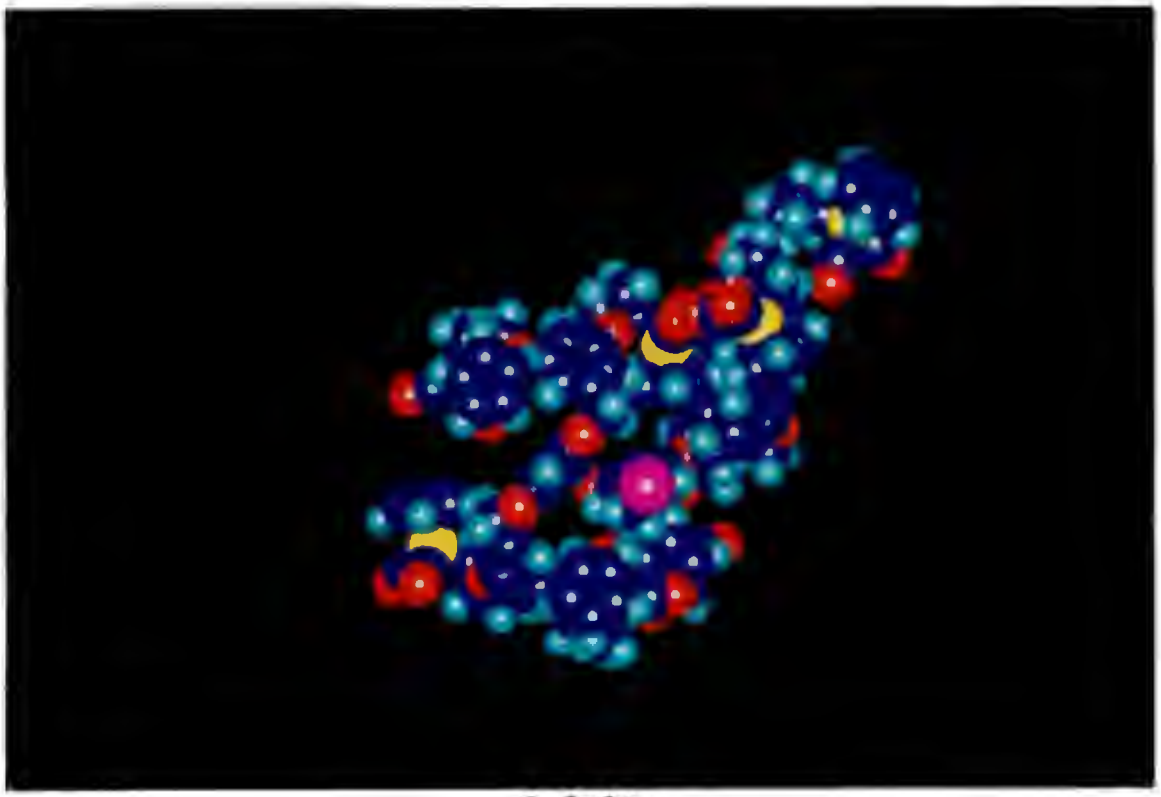

Rp3G3Br

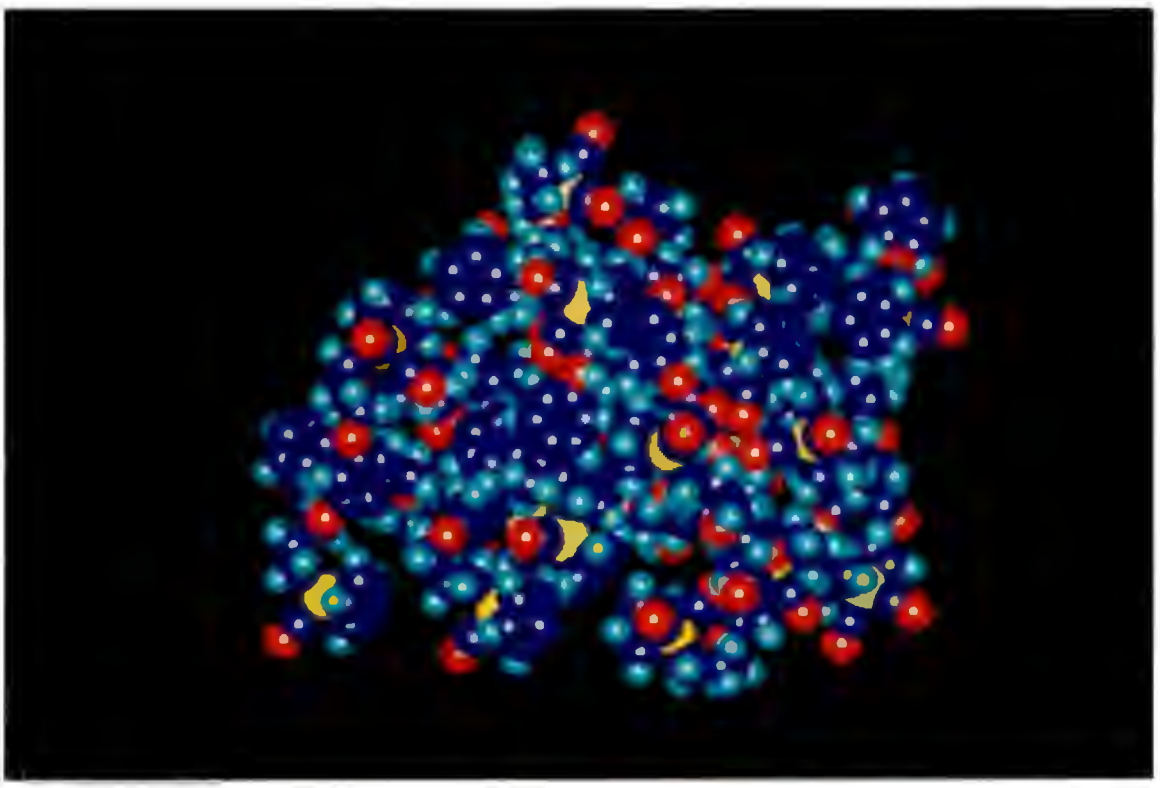

Rp3G3C

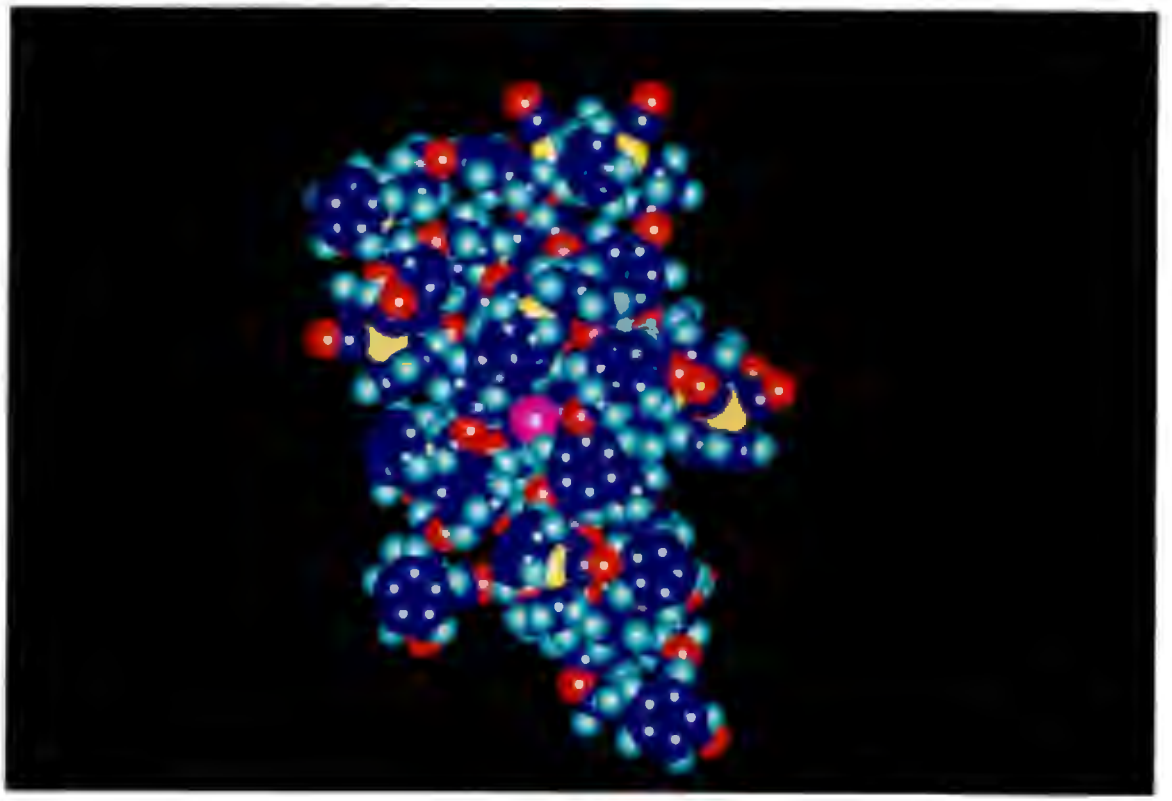

Rp3G4Br

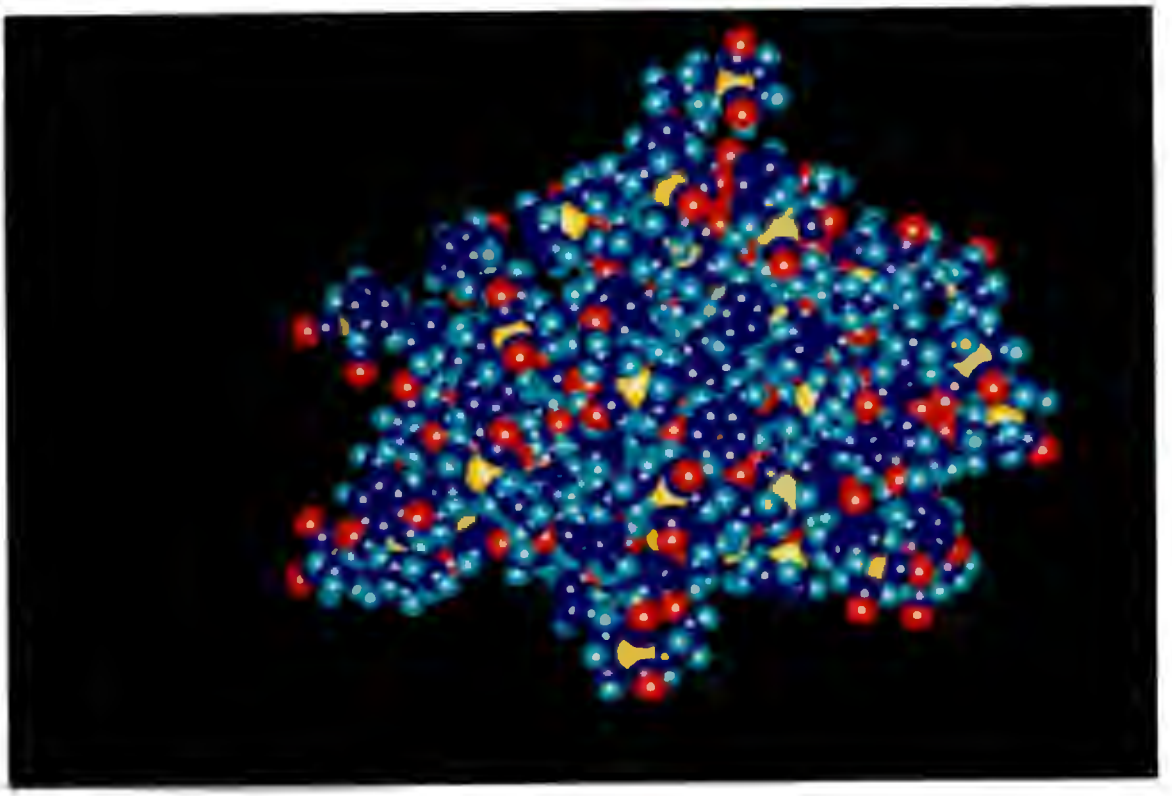

Rp3G4C

CHAPTER 5 EXPERIMENTAL

5.1 GENERAL

All reactions were carried out under a nitrogen atmosphere using standard Schlenk tube techniques.

Solvents were dried as described in the following text. Tetrahydrofuran and diethyl ether were distilled over sodium wire and benzophenone. Hexane, benzene, and toluene were distilled over sodium wire. Carbon tetrachloride and chloroform were distilled before use. Dichloromethane was distilled over anhydrous $CaCl_2$. Acetone was distilled over anhydrous $CaCl_2$ or drierite. Acetonitrile was distilled over P_2O_5. Pyridine and dimethylformamide were distilled over sodium hydroxide pellets. Potassium carbonate and tetrabutylammonium perchlorate were dried under vacuum (0.1 mm Hg) at 90 °C overnight.

$[CpFe(CO)_2]_2$ and $[Cp^*Fe(CO)_2]_2$ were obtained from Strem. $[CpFe(CO)_2\{(CH_2)_3Br\}]$ [1], $[CpFe(CO)_2\{(CH_2)_6Br\}]$ [2], $[CpRu(CO)_2]_2$ [3], $[CpRu(CO)_2\{(CH_2)_3Br\}]$ [4], $[ClCo(DMG)_2(Py)]$ [5], 3,5-dihydroxybenzyl alcohol [6] and 4-nonyloxybenzoyl chloride [7] were prepared by literature methods. Alumina (BDH, active neutral, Brockmann grade 1 or Merk, 90, active, neutral) was deactivated before use. All other reagents were obtained commercially, unless otherwise stated.

Melting points were recorded on a Kofler hot stage microscope (Reichert Thermovar) and are uncorrected. Microanalysis data were obtained from the University of Cape Town Microanalytical Laboratory or Mikroanalytisches Labor Pascher (Germany), or the Division of Energy Technology at the CSIR in Pretoria. Infrared spectra were recorded on a Perkin-Elmer 983 spectrophotometer in solution cells with NaCl

windows or as Nujol mulls between NaCl plates. ^{1}H and ^{13}C NMR spectra were recorded on a Varian VXR 200 or a Varian Unity 400 spectrometer. The chemical shifts are reported according to the proton signal of deuterated solvent. Low resolution electron impact mass spectra were recorded on VG Micromass 16F spectrometer or Kratos MS 80 RFA spectrometer, operated at 70 eV ionising voltage. Fast atom bombardment mass spectra were obtained from the University Chemical Laboratories, Cambridge (England).

Cyclic voltammetry was carried out on a BAS-100B electrochemical analyzer in a one-compartment three electrode system, consisting of Ag/Ag^{+1}(0.01M) as the reference electrode, platinum wire as the auxiliary electrode and a platinum disk electrode as the working electrode. The supporting electrolyte was a solution of 0.1 M tetrabutylammonium perchlorate (TBAP) in dry acetonitrile. The E value was recorded without IR compensation and reported as data obtained. The experiments were performed under an argon atmosphere at room temperature. The Pt disk electrode was polished after each run to ensure the reproducibility of results.

The differential scanning calorimetry (DSC) was carried out on the Perkin Elmer PC series DSC7. Samples were heated under nitrogen from room temperature to 400 °C at a rate of 20 °C/min in a hermetically sealed pan. For the determination of glass transition temperatures of the dendrimers, the sample was sealed hermetically in an aluminium pan and heated under nitrogen from -10 to +110 °C at a rate of 10 °C/min. For the crystalline solid Rp3G1OH, before submitting for DSC, the sample was heated at 110 °C for 5 min. and then quenched in liquid nitrogen in order to freeze the sample to an amorphous state. Scanning electron microscopy are carried out at the Electron Microscopy Unit in University of Cape Town, and the results are obtained from a

Cambridge Stereoscan 200. The computer assisted molecular models for the dendrimers are generated from the Hyperchem®.

5.2 EXPERIMENTAL DETAILS PERTAINING TO CHAPTER 1

5.2.1 Reaction of [CpFe(CO)$_2${(CH$_2$)$_6$Br}] with sodium methoxide

Sodium methoxide was prepared by dissolving sodium (0.322 g; 14 mmol.) in methanol (5 ml). The resulting solution was then added to a solution of [CpFe(CO)$_2${(CH$_2$)$_6$Br}] (0.63 g; 1.8 mmol.) in methanol (10 ml). The reaction mixture was heated at reflux for 2.5 hours. The reaction was monitored by TLC and after this time no starting material was left. The solvent was removed under reduced pressure to give a dark residue. The residue was extracted with hexane (30 ml). After filtration the yellow solution was concentrated and transferred to a short alumina column. The column was first eluted with hexane (50 ml), followed by CH_2Cl_2. The yellow band from CH_2Cl_2 elution was collected. The solvent was removed to give a yellow oil [CpFe(CO)$_2${(CH$_2$)$_6$OCH$_3$}] (0.36 g, 68%). IR (hexane) υ(CO) 2008, 1954 cm^{-1}; ^{1}H NMR δ($CDCl_3$) ppm 4.71 (s, 5H, Cp), 3.36 (t, J = 6 Hz, 2H, CH_2O), 3.33 (s, 3H, OCH_3), 1.2 - 1.7 (m, 10H, CH_2); ^{13}C NMR δ($CDCl_3$) ppm 217.64 (CO), 85.29 (Cp), 73.02 (CH_2O), 58.48 (OCH_3), 3.50 ($FeCH_2$), 38.18, 34.61, 29.71, 25.85 (CH_2); mass spectrum (EI) m/z 293 (P + 1); Found: C 57.7%, H 6.8% Calc for $C_{14}H_{20}O_3Fe$ (M 293.16) C 57.6%, H 6.9%.

5.2.2 Reaction of [CpFe(CO)$_2${(CH$_2$)$_6$Br}] with the cobaloxime anion

[ClCo(DMG)$_2$(Py)] (0.67 g; 1.7 mmol.) and [CpFe(CO)$_2${(CH$_2$)$_6$Br}] (0.58 g; 1.7 mmol.) were mixed with degassed methanol (20 ml). The slurry was stirred at room temperature for 5 min.. $NaBH_4$ (0.16 g; 4.2 mmol.) was added into the mixture in portions, followed by water (1 ml). The orange yellow crystals that formed after 5 min. were collected by filtration. Recrystallization of these crystals from a CH_2Cl_2/hexane solution gave analytically pure [CpFe(CO)$_2${(CH$_2$)$_6$Co(DMG)$_2$(Py)}] (0.64 g, 61%). mp 121 - 124 °C; IR (CH_2Cl_2) υ(CO) 1999, 1937 cm^{-1}; ^{1}H NMR $\delta(CDCl_3)$ ppm 18.12 (br, 2H, OH), 8.60 (d, J = 6 Hz, 2H, Py), 7.84 (t, J = 6 Hz, 1H, Py), 7.29 (m, 2H, Py), 4.70 (s, 5H, Cp), 2.14 (s, 12H, CH_3), 1.4-1.9 (m, 12H, CH_2); ^{13}C NMR δ($CDCl_3$) ppm 217.70 (CO), 149.94, 137.26, 125.06 (Py), 148.97 (C=N), 85.27 (Cp), 38.26, 34.55, 30.63, 30.48, 30.34 (CH_2), 3.88 (Fe-CH_2), 11.98 (CH_3); Found C 47.6%, H 6.1%, N 12.9% Calc for $C_{26}H_{36}O_6N_5FeCo$ (M 629.38) C 47.6%, H 5.9%, N 11.6%.

5.2.3 Reaction of [CpFe(CO)$_2${(CH$_2$)$_6$Br}] with methyl lithium

A solution of methyl lithium (1.5 M) in diethyl ether (1.5 ml; 2.3 mmol.) was slowly added to a -78 °C solution of [CpFe(CO)$_2${(CH$_2$)$_6$Br}] (0.44 g; 1.3 mmol.) in THF (4 ml). The reaction mixture was then slowly warmed up to room temperature over a period of 3 hours and stirred at room temperature for another hour. The solvent was then removed under reduced pressure to give a dark brown residue. The residue was extracted with hexane (30 ml). After filtration, the yellow filtrate was concentrated and transferred to an alumina column. The first yellow fraction was collected on eluting with hexane. Removal of the solvent from this fraction gave

$[CpFe(CO)_2\{(CH_2)_6CH_3\}]$ as a yellow oil. The formulation of $[CpFe(CO)_2\{(CH_2)_6CH_3\}]$ was confirmed by comparing its IR and NMR spectra with those obtained from an authentic sample [8].

5.2.4 Reaction of $[CpFe(CO)_2\{(CH_2)_6Br\}]$ with sodium azide

$[CpFe(CO)_2\{(CH_2)_6Br\}]$ (0.47 g; 1.4 mmol.) in acetonitrile (15 ml) and NaN_3 (0.27 g; 4.15 mmol.) in water (5 ml) were mixed together. The reaction mixture was heated at reflux for 4 hours and monitored by TLC. The reaction was then cooled to room temperature, and the aqueous phase was syringed off. The organic phase was dried over $MgSO_4$, and the solvent was removed under reduced pressure to give a dark yellow residue. The residue was extracted with hexane (50 ml) and filtered. The yellow filtrate was concentrated and transferred to an alumina column. Two yellow bands were developed on eluting with hexane. The solvent was removed from the second yellow band to give $[CpFe(CO)_2\{(CH_2)_6N_3\}]$ as a yellow oil. (0.17 g, 39%) IR (neat) υ(CO) 1997, 1937 υ(N_3) 2096 cm^{-1}; ^1H NMR δ($CDCl_3$) ppm 4.71 (s, 5H, Cp), 3.23 (t, J = 6 Hz, 2H, CH_2N_3), 1.2 - 1.7 (m, 10H, CH_2); ^{13}C NMR δ($CDCl_3$) ppm 217.52 (CO), 85.29 (Cp), 51.51 (CH_2N_3), 3.20 ($FeCH_2$), 37.98, 34.19, 28.70, 26.39 (CH_2); mass spectrum (EI) m/z 303 (P).

5.2.5 Reaction of $[CpFe(CO)_2\{(CH_2)_6Br\}]$ with lithium aluminiumhydride

$LiAlH_4$ (0.32 g; 8.5 mmol.) was added to a THF solution (15 ml) of $[CpFe(CO)_2\{(CH_2)_6Br\}]$ (0.27 g; 0.8 mmol.) and stirred at room temperature for 30 min.. The remaining $LiAlH_4$ was destroyed by adding water (4 ml). The solvent was then removed under reduced pressure. The residue was extracted with hexane (30 ml). After filtration, the yellow filtrate was concentrated and transferred to an alumina

column. The first yellow fraction was collected on eluting with hexane. A yellow oil of [$CpFe(CO)_2\{(CH_2)_6H\}$] was obtained after drying under vacuum (42 mg, 20%). The formulation of the sample was confirmed by comparing its IR and NMR spectra with those obtained from an authentic sample [8].

5.2.6 Reaction of [$CpFe(CO)_2\{(CH_2)_6Br\}$] with magnesium metal

Freshly cleaned magnesium turnings (54 mg; 2.2 mmol.) were placed in a two necked round bottom flask, and covered with THF (4 ml) under N_2. One drop of dibromoethane was added. The mixture was heated at reflux and stirred vigorously for 30 min. A solution of [$CpFe(CO)_2\{(CH_2)_6Br\}$] (0.13 g; 0.36 mmol.) in THF (5 ml) was added to the refluxing reaction solution. After 30 min., another portion of [$CpFe(CO)_2\{(CH_2)_6Br\}$] solution (0.37 g; 1.11 mmol.) in THF (15 ml) was slowly syringed into the reaction. The reaction mixture was kept at reflux overnight. Monitoring by TLC showed that a new species is formed after 2 hours, but that no further change occurred after 6 hours. The resulting dark brown solution was added to a solution of bromobenzene (0.239 g; 1.52 mmol.) in THF (2 ml). The mixture was heated under reflux for another 24 hours and TLC showed no further change. Similar TLC results were obtained when other organic halides were used, including trimethylsilyl chloride, methyl iodide and allyl bromide. The solvent was removed under reduced pressure and the dark residue was extracted with hexane (40 ml). The yellow filtrate was concentrated and transferred to an alumina column. The first two yellow bands were collected on eluting with hexane. The solvents were removed from both portions under reduced pressure to give yellow oils which were investigated by IR and NMR spectroscopy. The spectra showed that the first yellow fraction is

[$CpFe(CO)_2\{(CH_2)_6H\}$] and the second yellow fraction is [$CpFe(CO)_2\{(CH_2)_6Br\}$]. Similar results were obtained when the reaction of [$CpFe(CO)_2\{(CH_2)_6Br\}$] with magnesium was carried out in diethyl ether, but no reaction occurred in hexane after 5 hours at reflux.

5.2.7 Reactions of [$CpFe(CO)_2\{(CH_2)_6Br\}$] with phenol and its derivatives

General procedure A mixture of [$CpFe(CO)_2\{(CH_2)_6Br\}$] (1 equiv.), the appropriate phenol compound (1 equiv. for phenol and 4-hydroxybenzyl alcohol; 0.5 equiv. for resorcinol and 3,5-dihydroxybenzyl alcohol), dry potassium carbonate (1.5 equiv.) and 18-crown-6 (0.1 equiv.) in dry acetone was heated to reflux and stirred vigorously for 24 hours (phenol, 4-hydroxybenzyl alcohol) or 48 hours (resorcinol, 3,5-dihydroxybenzyl alcohol). The reaction was protected from light by aluminium foil, and monitored by TLC. The reaction mixture was then allowed to cool and the solvent was removed under reduced pressure. The work up procedures are outlined in the following text.

[$CpFe(CO)_2\{(CH_2)_6OC_6H_5\}$] The resulting residue was extracted with a 20% CH_2Cl_2/hexane solution. After filtration, the reddish filtrate was concentrated and transferred to an alumina column. The second yellow band was collected on eluting with a 20% CH_2Cl_2/hexane solution. The yellow solution was concentrated and cooled to -78 °C to give a yellow crystalline product [$CpFe(CO)_2\{(CH_2)_6OC_6H_5\}$] (71%). mp 29 - 34 °C; IR (CH_2Cl_2) υ(CO) 1999, 1938 cm^{-1}; ^1H NMR δ($CDCl_3$) ppm 7.28, 6.92 (m, 5H, Ar), 4.72 (s, 5H, Cp), 3.95 (t, J = 6.4 Hz, 2H, CH_2O), 1.2 - 1.9 (m, 10H, CH_2); ^{13}C NMR δ($CDCl_3$) ppm 217.68 (CO), 159.15, 129.37, 120.40, 114.52 (Ar), 85.30 (Cp), 67.92 (CH_2O), 3.44 ($FeCH_2$), 38.16, 34.51, 29.36, 25.76 (CH_2); mass

spectrum (EI) m/z 354 (P).

[{CpFe(CO)$_2$(C$_6$H$_{12}$O)}$_2$C$_6$H$_4$] The resulting residue was extracted with a 20% CH_2Cl_2/hexane solution. After filtration, the reddish filtrate was concentrated and transferred to an alumina column. The second yellow band was collected on eluting with a 70% CH_2Cl_2/hexane solution. The solvent was removed to give [{CpFe(CO)$_2$(C$_6$H$_{12}$O)}$_2$C$_6$H$_4$] as a yellow oil (7%). IR (CH_2Cl_2) υ(CO) 1999, 1938 cm^{-1}; ^{1}H NMR δ($CDCl_3$) ppm 7.15, 6.50, 6.44 (m, 4H, Ar), 4.72 (s, 10H, Cp), 3.93 (t, J = 6 Hz, 4H, CH_2O), 1.2-1.9 (m, 20H, CH_2); ^{13}C NMR δ($CDCl_3$) ppm 217.67 (CO), 160.40, 129.70, 106.65, 101.46 (Ar), 85.30 (Cp), 68.01 (CH_2O), 3.45 ($FeCH_2$), 38.15, 34.50, 29.34, 25.75, (CH_2); mass spectrum (EI) m/z 574 (P - 2CO); Found C 60.6%, H 5.8% Calc for $C_{32}H_{38}O_6Fe_2$ (M 630.34) C 61.0%, H 6.1%.

[CpFe(CO)$_2$(C$_6$H$_{12}$OC$_6$H$_4$CH$_2$OH)] The residue was extracted with a 30% CH_2Cl_2/hexane solution. After filtration, the filtrate was concentrated and transferred to an alumina column. [CpFe(CO)$_2${(CH$_2$)$_6$Br}] was first eluted with a 30% CH_2Cl_2/hexane solution and the second yellow band was collected by eluting with CH_2Cl_2. The solvent was removed to give [CpFe(CO)$_2$(C$_6$H$_{12}$OC$_6$H$_4$CH$_2$OH)] (51%) as a yellow oil. IR (CH_2Cl_2) υ(CO) 1998, 1937 cm^{-1}; ^{1}H NMR δ($CDCl_3$) ppm 7.26 (br, 2H, Ar), 6.88 (br, 2H, Ar), 4.70 (br, 7H, Cp + $ArCH_2O$), 3.94 (br, 2H, CH_2O), 1.5 - 2.0 (br, 10H, CH_2); ^{13}C NMR δ($CDCl_3$) ppm 217.68 (CO), 158.79, 132.90, 128.60, 114.57 (Ar), 85.31 (Cp), 68.11 (CH_2O), 65.00 ($ArCH_2O$), 3.42 ($FeCH_2$), 38.14, 34.49, 29.31, 25.73 (CH_2); mass spectrum (EI) m/z 327 (P - 2CO - 1).

[{CpFe(CO)$_2$(C$_6$H$_{12}$O)}$_2$C$_6$H$_3$CH$_2$OH] The resulting residue was extracted with a 70% CH_2Cl_2/hexane solution. After filtration, the filtrate was concentrated and transferred to an alumina column. The polarity of the eluting solvent was gradually increased from 70% CH_2Cl_2/hexane to CH_2Cl_2. A yellow band was collected after the dark reddish $[CpFe(CO)_2]_2$ band. The solvent was then removed to give [{CpFe(CO)$_2$(C$_6$H$_{12}$O)}$_2$C$_6$H$_3$CH$_2$OH] (36%) as a yellow oil. IR (CH_2Cl_2) υ(CO) 1999, 1938 cm^{-1}; ^{1}H NMR δ($CDCl_3$) ppm 6.43 (d, J = 2 Hz, 2H, Ar), 6.31 (t, J = 2 Hz, 1H, Ar), 4.65 (s, 10H, Cp), 4.55 (d, J = 5 Hz, 2H, C*H*$_2$OH), 3.86 (t, J = 7 Hz, 4H, CH_2O), 1.3 - 1.8 (m, 20H, CH_2); ^{13}C NMR δ($CDCl_3$) ppm 217.68 (CO), 160.56, 143.18, 105.07, 100.58 (Ar), 85.30 (Cp), 68.10 (CH_2O), 65.45 ($ArCH_2O$), 3.43 ($FeCH_2$), 38.14, 34.47, 29.27, 25.73 (CH_2); mass spectrum (EI) m/z 604 (P - 2CO).

5.2.8 Reaction of [CpFe(CO)$_2${(CH$_2$)$_6$Br}] with trityl salt

$[CpFe(CO)_2\{(CH_2)_6Br\}]$ (0.44 g; 1.3 mmol.) was dissolved in CH_2Cl_2 (4 ml). Triphenylcarbenium hexaflorophosphate (CPh_3PF_6) (0.85 g; 2.2 mmol.) was added to the solution, and the reaction mixture was stirred at room temperature for 5 min.. After this time, the solvent was removed under reduced pressure. The solid residue was then recrystallized from acetone/ether to give pure yellow crystalline $[CpFe(CO)_2\{CH_2{=}CH(CH_2)_4Br\}]^+PF_6^-$ (0.51 g, 77%). mp 116 - 119 °C, IR (CH_2Cl_2) υ(CO) 2075, 2037 cm^{-1}, ^{1}H NMR δ(d^6-acetone) ppm 5.88 (s, 5H, Cp), 5.29 (m, 1H, =CH-), 4.07 (d, J = 8 Hz, 1H, *cis*-CH_2=), 3.66 (d, J = 14 Hz, 1H, *trans*-CH_2=), 3.51 (t, J = 6 Hz, 2H, CH_2Br), 2.59 (m, 1H, =CH-C*H*$_2$), 1.63 (m, 1H, =CH-C*H*$_2$), 1.8 - 2.1 (m, 4H, CH_2); ^{13}C NMR δ(d^6-Acetone) ppm 212.03, 209.78 (CO), 90.93

(Cp), 89.05 (=CH-), 55.98 (CH_2=), 36.85, 34.86, 33.42, 32.46 (CH_2); Found C 32.6%, H 3.3% Calc for $C_{13}H_{16}O_2FeBrPF_6$ (M 484.98) C 32.2%, H 3.3%.

5.2.9 Reaction of [CpFe(CO)$_2${(CH$_2$)$_6$Br}] with PPh$_3$

[CpFe(CO)$_2${(CH$_2$)$_6$Br}] (1.01 g; 3.0 mmol.) with PPh_3 (1.91 g; 7.3 mmol.) in a benzene solution (20 ml) was heated under reflux for 6 hours. After this time, the solvent was removed under reduced pressure and the dark residue was extracted with CH_2Cl_2. After filtration, the filtrate was concentrated and transferred to an alumina column. An orange-yellow band was collected on eluting with CH_2Cl_2. The solvent was removed to give an orange-yellow oil. The crystalline sample of [CpFe(CO)(PPh$_3$){CO(CH$_2$)$_6$Br}] (1.67 g; 93%) was obtained when this oil was allowed to stand 5 days at -15 °C. mp 111 - 115 °C; IR (CH_2Cl_2) υ(CO) 1912, 1604 cm^{-1}; ^{1}H NMR δ($CDCl_3$) ppm 7.2 - 7.6 (m, 15H, Ph), 4.40 (s, 5H, Cp), 3.33 (t, J = 7 Hz, CH_2Br), 2.85 (m, 1H, $COCH_2$), 2.52 (m, 1H, $COCH_2$), 0.8 - 1.9 (m, 8H, CH_2); ^{13}C NMR δ($CDCl_3$) ppm 220.36 (d, CO), 136.07, 133.44, 129.63, 127.90 (d, Ph), 85.23 (Cp), 66.01 (d, $COCH_2$), 34.00 (CH_2Br), 32.68, 28.20, 28.03, 24.84 (CH_2); Found C 61.9%, H 5.4% Calc for $C_{31}H_{32}O_2FePBr$ (M 603.32) C 61.7%, H 5.4%.

5.2.10 Reaction of [CpFe(CO)$_2${(CH$_2$)$_6$Br}] with AgBF$_4$/CO

CO was bubbled into a solution of [CpFe(CO)$_2${(CH$_2$)$_6$Br}] (0.53 g: 1.6 mmol.) in CH_2Cl_2 (20 ml), which was pre-cooled in an salt-ice bath. $AgBF_4$ (0.31 g; 1.6 mmol.) was added to the solution and the reaction was maintained at this temperature for 30 min.. Afterwards, the reaction was brought to room temperature. The solvent was removed under reduced pressure and the residue was extracted with a 50%

CH_2Cl_2/hexane solution (50 ml). After filtration, the yellow filtrate was concentrated and transferred to an alumina column. A yellow band was collected on eluting with a 50% CH_2Cl_2/hexane solution. The solvent was removed to give $[CpFe(CO)_2\{CO(CH_2)_6Br\}]$ as a yellow oil (0.12 g, 21%). IR (CH_2Cl_2) υ(CO) 2015, 1955, 1641 cm^{-1}; ^1H NMR δ($CDCl_3$) ppm 4.83 (s, 5H, Cp), 3.38 (t, J = 7 Hz, 2H, CH_2Br), 2.88 (t, J = 7 Hz, 2H, $COCH_2$), 1.2 - 1.9 (m, 8H, CH_2); ^{13}C NMR $\delta(CDCl_3)$ ppm 214.24 (CO), 86.19 (Cp), 66.20 ($COCH_2$), 33.67 (CH_2Br), 32.38, 27.94, 27.75, 24.78 (CH_2); mass spectrum (EI) m/z 370 (P+1); Found C 45.3%, H 4.4% Calc for $C_{14}H_{17}O_3FeBr$ (M 369.04) C 45.6%, H 4.6%.

5.2.11 Thermal decomposition of $[CpFe(CO)_2\{(CH_2)_6Br\}]$ in toluene solution

A solution of $[CpFe(CO)_2\{(CH_2)_6Br\}]$ (*ca.* 70 mg) in toluene (20 ml) was heated to reflux under nitrogen. The reaction was followed by IR spectroscopy. No carbonyl absorptions were observed after 73 hours. The solvent was then removed and the dark residue was extracted with $CDCl_3$ (1 ml). After filtration, the filtrate was submitted for NMR measurements. The ^1H NMR spectrum showed a singlet at δ 4.33 which was assigned to ferrocene.

5.3 EXPERIMENTAL DETAILS PERTAINING TO CHAPTER 2

General procedure for preparation of $[L_mM\{(CH_2)_nOH\}]$ (where L_mM = $CpFe(CO)_2$, $Cp^*Fe(CO)_2$, $CpRu(CO)_2$; n = 2,3,4)

The sodium salt of the metal anions $[L_mM]^-$ (1 equiv.), prepared from $[L_mM]_2$ in THF

solution, was syringed into a THF solution of the appropriate haloalcohol (1 equiv.) at -78 °C for 20 min.. The reaction temperature was then slowly raised to room temperature over a period of 1.5 hours and was kept at room temperature for various lengths of time, depending on the haloalcohol and the metal anion used. After reaction, the solvent was removed under reduced pressure to give a dark brown residue. The residue was then extracted with an 80% CH_2Cl_2/hexane solution to give a reddish solution after filtration. The individual reaction times and work-up procedures are outlined in the following text. The yields of reactions and the characterization data have been given in Chapter 2.

[CpFe(CO)$_2${(CH$_2$)$_2$OH}] This was prepared from the reaction of Na[CpFe(CO)$_2$] with I(CH$_2$)$_2$OH. The reaction mixture was stirred at room temperature for 30 min.. After extraction, the resulting reddish solution was concentrated and the product was separated from the solution at -15 °C as a yellow crystalline solid.

[CpFe(CO)$_2${(CH$_2$)$_3$OH}] This was prepared from the reaction of Na[CpFe(CO)$_2$] with Br(CH$_2$)$_3$OH. The reaction mixture was stirred at room temperature for 2 hours. After extraction, the resulting reddish solution was concentrated and the product was separated from the solution at -15 °C as a yellow crystalline solid.

[CpFe(CO)$_2${(CH$_2$)$_4$OH}] This was prepared from the reaction of Na[CpFe(CO)$_2$] with Cl(CH$_2$)$_4$OH. The reaction mixture was stirred at room temperature overnight. After filtration, the solvent of the resulting reddish solution was removed to give a reddish oil. The oil was dissolved in minium volume of CH_2Cl_2 and transferred to an alumina

column. The major yellow fraction was collected on eluting with CH_2Cl_2. The yellow solution was concentrated and the product was precipitated out as a yellow crystalline solid on the addition of hexane at -78 °C.

*[Cp*Fe(CO)$_2${(CH$_2$)$_2$OH}]* This was prepared from the reaction of Na[Cp*Fe(CO)$_2$] with I(CH$_2$)$_2$OH. The reaction mixture was stirred at room temperature for 1 hour. After filtration, the reddish solution was slowly concentrated at 0 °C under reduced pressure. The product was further crystallized out as a yellow crystalline solid at -15 °C.

*[Cp*Fe(CO)$_2${(CH$_2$)$_3$OH}]* This was prepared from the reaction of Na[Cp*Fe(CO)$_2$] with Br(CH$_2$)$_3$OH. The reaction mixture was stirred at room temperature for 12 hours. After filtration, the reddish solution was concentrated and transferred to an alumina column. The major yellow fraction was collected on eluting with CH_2Cl_2. The solvent of the yellow solution was removed and the yellow crystalline product was precipitated out from a hexane solution at -15 °C.

*[Cp*Fe(CO)$_2${(CH$_2$)$_4$OH}]* This was prepared from the reaction of Na[Cp*Fe(CO)$_2$] with Cl(CH$_2$)$_4$OH. The reaction mixture was stirred at room temperature for 24 hours. The work up procedure of [Cp*Fe(CO)$_2${(CH$_2$)$_4$OH}] is the same as [Cp*Fe(CO)$_2${(CH$_2$)$_3$OH}]. [Cp*Fe(CO)$_2${(CH$_2$)$_4$OH}] was isolated as a yellow crystalline solid.

[CpRu(CO)$_2${(CH$_2$)$_2$OH}] This was prepared from the reaction of Na[CpRu(CO)$_2$] with I(CH$_2$)$_2$OH. The reaction mixture was stirred at room temperature for 2 hours. After

filtration, the reddish brown solution was concentrated and the product was precipitated out as light brown crystals at -15 °C.

[CpRu(CO)$_2${(CH$_2$)$_3$OH}] This was prepared from the reaction of Na[CpRu(CO)$_2$] with Br(CH$_2$)$_3$OH. The reaction mixture was stirred at room temperature for about 3 hours. After filtration, the reddish brown solution was concentrated and transferred to an alumina column. A pale red fraction was collected on eluting with CH_2Cl_2. This pale red solution was concentrated and a white crystalline product was precipitated out on the addition of hexane at -15 °C.

5.4 EXPERIMENTAL DETAILS PERTAINING TO CHAPTER 3

5.4.1 Reaction of [CpFe(CO)$_2${(CH$_2$)$_2$OH] with trimethylsilyl chloride

Excess of trimethylsilyl chloride (1 ml) was added into a -78 °C THF solution (8 ml) of [CpFe(CO)$_2${(CH$_2$)$_2$OH}] (0.21 g; 0.9 mmol.). A yellow precipitate formed immediately after the addition and the reaction temperature was raised to room temperature. The solvent and excess trimethylsilyl chloride were removed under reduced pressure. The resulting yellow solid was dissolved in distilled water (10 ml), and added into an aqueous solution (4 ml) of NH_4PF_6 (0.16 g; 1.0 mmol.) to give a yellow precipitate. The ^{1}H NMR spectrum confirmed that the yellow precipitate is [CpFe(CO)$_2$(η^2-C_2H_4)]$^+PF_6^-$ (0.23 g; 70%).

5.4.2 Reaction of [CpFe(CO)$_2${(CH$_2$)$_3$OH] with trimethylsilyl chloride

Excess of trimethylsilyl chloride (1 ml) was added into a benzene solution (4 ml) of [CpFe(CO)$_2${(CH$_2$)$_3$OH}] (0.22 g; 0.9 mmol.), followed by pyridine (1 ml). The reaction mixture was stirred at room temperature for 30 min. and a white precipitate gradually formed in the solution. The solvent was then removed under reduced pressure, leaving a yellow residue. The residue was extracted with hexane (10 ml) and the solvent of the resulting yellow filtrate was removed to give [CpFe(CO)$_2${(CH$_2$)$_3$OSiMe$_3$}] (0.22 g, 83%) as a yellow oil. IR (hexane) υ(CO) 2009, 1956 cm^{-1}; ^{1}H NMR δ($CDCl_3$) ppm 4.73 (s, 5H, Cp), 3.49 (t, J = 7 Hz, 2H, CH_2O), 1.7 (m, 2H, CH_2), 1.3 (m, 2H, $FeCH_2$), 0.10 (s, 9H, CH_3); ^{13}C NMR δ($CDCl_3$) ppm 217.34 (CO), 85.29 (Cp), 65.68 (CH_2O), 41.01 (CH_2), 0.44 (CH_3), -2.50 ($FeCH_2$), mass spectrum (EI) m/z 308 (P); Found C 50.2%, H 6.2% Calc for $C_{13}H_{20}O_3FeSi$ (M 308.23) C 50.7%, H 6.5%.

5.4.3 Reaction of [CpFe(CO)$_2${(CH$_2$)$_3$OH] with t-butyldimethylsilyl chloride

t-Butyldimethylsilyl chloride (0.19 g; 1.3 mmol.) was added into a DMF solution (6 ml) of [CpFe(CO)$_2${(CH$_2$)$_3$OH}] (0.21 g; 0.9 mmol.), followed by imidazole (82 mg, 1.2 mmol.). The reaction solution was stirred at room temperature for 2 hours and monitored by TLC. The solvent was then removed under high vacuum in a hot water bath. The resulting yellow oil mixed with a white solid was extracted with hexane (10 ml). After filtration, the yellow filtrate was concentrated and transferred to an alumina column. The major yellow fraction was collected on eluting with hexane which was then removed to give [CpFe(CO)$_2${(CH$_2$)$_3$OSiMe$_2$*t*-Bu}] (0.25 g, 79%) as a yellow crystalline solid. mp 47 - 49 °C, IR (hexane) υ(CO) 2009, 1955 cm^{-1}; ^{1}H NMR δ(

$CDCl_3$) ppm 4.71 (s, 5H, Cp), 3.50 (t, J = 7 Hz, 2H, CH_2O), 1.65 (m, 2H, CH_2), 1.32 (m, 2H, $FeCH_2$), 0.89 (s, 9H, CCH_3), 0.04 (s, 6H, $SiCH_3$); ^{13}C NMR δ($CDCl_3$) ppm 217.42 (CO), 85.33 (Cp), 66.33 (CH_2O), 41.19 (CH_2), 26.04 (CCH_3), 18.45 (CCH_3), -2.31 ($FeCH_2$), -5.17 ($SiCH_3$); mass spectrum (EI) m/z 350 (P); Found C 55.0%, H 7.2% Calc for $C_{16}H_{26}O_3SiFe$ (M 350.31) C 54.9%, H 7.2%.

5.4.4 Reaction of [CpFe(CO)$_2${(CH$_2$)$_3$OH}] with t-butyldiphenylsilyl chloride

[CpFe(CO)$_2${(CH$_2$)$_3$OH}] (0.44 g; 1.8 mmol.) with *t*-butyldiphenylsilyl chloride (0.75 g; 2.7 mmol.) was dissolved in DMF (20 ml), followed by imidazole (0.25 g; 3.7 mmol.). The reaction mixture was stirred at room temperature for 24 hours, and monitored by TLC. After reaction, the DMF was removed under high vacuum in a hot water bath to give a yellow oil with a white precipitate. The mixture was extracted with a 20% CH_2Cl_2/hexane solution (30 ml). The solvent was removed under reduced pressure and the resulting yellow oil was redissolved in CH_2Cl_2 (4 ml) and transferred to an alumina column. On eluting with CH_2Cl_2, the first yellow band was collected, and a yellow crystalline [CpFe(CO)$_2${(CH$_2$)$_3$OSiPh$_2$*t*-Bu}] was obtained after recrystallization from CH_2Cl_2/hexane at -15 °C (0.33 g, 39%). mp 73 - 76 °C; IR (hexane) υ(CO) 2009 1955 cm^{-1}; ^1H NMR δ($CDCl_3$) ppm 7.72 (m, 4H, Ar), 7.41 (m, 6H, Ar), 4.70 (s, 5H, Cp), 3.64 (t, J = 7 Hz, 2H, CH_2O), 1.72 (m, 2H, CH_2), 1.33 (m, 2H, $FeCH_2$), 1.10 (s, 9H, CH_3); ^{13}C NMR δ($CDCl_3$) ppm 217.91 (CO), 136.13, 134.87, 129.95, 128.05 (Ar), 85.82 (Cp), 67.53 (CH_2O), 41.39 (CH_2), 27.47 (CH_3), 19.76 (SiC), -1.69 ($FeCH_2$); mass spectrum (EI) m/z 474 (P); Found C 65.9%, H 6.3% Calc for $C_{26}H_{30}O_3SiFe$ (M 474.45) C 65.8%, H 6.4%.

5.4.5 Reaction of [CpFe(CO)$_2${(CH$_2$)$_3$OH}] with PPh$_3$/CBr$_4$

[CpFe(CO)$_2${(CH$_2$)$_3$OH}] (0.21 g; 0.9 mmol.) with CBr_4 (0.32 g; 1.0 mmol.) was dissolved in minimum amount of THF (*ca.* 2 ml), followed by PPh_3 (0.24 g; 0.9 mmol.). The reaction mixture was stirred at room temperature for 20 min.; an orange colorred precipitate formed after 5 min.. The reaction was monitored by TLC, eluting with hexane. The reaction mixture was then partitioned in a mixture of hexane and water; the hexane layer was collected, giving a yellow solution. After drying over anhydrous $MgSO_4$, the yellow filtrate was concentrated and transferred to an alumina column. A yellow band was collected on eluting with hexane and a yellow oil was obtained after removing the solvent. The ^{1}H NMR spectrum of this yellow oil was compared with that obtained from an authentic sample [CpFe(CO)$_2${(CH$_2$)$_3$Br}], confirming the structure.

5.4.6 Reaction of [CpFe(CO)$_2${(CH$_2$)$_3$OH}] with trityl chloride

[CpFe(CO)$_2${(CH$_2$)$_3$OH}] (0.31 g, 1.3 mmol.) with Ph_3CCl (0.37 g, 1.3 mmol.) was dissolved in benzene (25 ml), followed by pyridine (0.23 g, 2.8 mmol.). The reaction mixture was stirred at room temperature for 3 days and protected from light. The reaction was monitored by TLC and a white precipitate gradually formed in the reaction solution. The precipitate was filtered off after reaction, leaving a yellow filtrate. The solvent was removed from the yellow filtrate to give a yellow oil. The yellow oil was dissolved in CH_2Cl_2 (4 ml) and transferred to an alumina column. The first yellow band was collected on eluting with CH_2Cl_2. The resulting yellow solution was concentrated and a yellow crystalline product [CpFe(CO)$_2${(CH$_2$)$_3$OCPh$_3$}] was obtained on the addition of hexane at -15 °C (0.37 g, 61%). mp 116 - 120 °C; IR

(CH_2Cl_2) υ(CO) 2002, 1942 cm^{-1}; ^1H NMR δ($CDCl_3$) ppm 7.48 (m, 6H, Ar), 7.29 (m, 9H, Ar), 4.71 (s, 5H, Cp), 3.02 (t, J = 6 Hz, 2H, CH_2O), 1.78 (m, 2H, CH_2), 1.36 (m, 2H, $FeCH_2$); ^{13}C NMR δ($CDCl_3$) ppm 217.46 (CO), 144.69, 128.79, 127.71, 126.80 (Ar), 86.10 (CPh_3), 85.37 (Cp), 67.07 (CH_2O), 38.21 (CH_2), -1.62 ($FeCH_2$), mass spectrum (EI) m/z 422 (P - 2CO), Found C 72.8%, H 5.8% Calc for $C_{29}H_{26}O_3Fe$ (M 478.37) C 72.8%, H 5.5%.

5.4.7 Reaction of [CpFe(CO)$_2${(CH$_2$)$_3$OH}] with 4-nonyloxybenzoyl chloride

[$CpFe(CO)_2\{(CH_2)_3OH\}$] (0.31 g, 1.3 mmol.) with 4-nonyloxybenzoyl chloride was dissolved in THF (14 ml), followed by pyridine (213 μl, 2.6 mmol.). The reaction mixture was stirred at room temperature overnight and a white precipitate formed gradually in the solution. The precipitate was filtered off, leaving a yellow filtrate. The solvent was removed from the yellow filtrate to give a yellow oil. The yellow oil was dissolved in CH_2Cl_2 (4 ml) and transferred to an alumina column. The first yellow band was collected on eluting with a 50% CH_2Cl_2/hexane solution. The yellow solution was concentrated and [$CpFe(CO)_2\{(CH_2)_3O_2C(C_6H_4)OC_9H_{19}\}$] was obtained as a yellow crystalline product after cooling the yellow concentrate at -78 °C (0.28 g, 44%). mp 34 - 37 °C; IR (CH_2Cl_2) υ(CO) 2003, 1943, 1700 cm^{-1}; ^1H NMR δ($CDCl_3$) ppm 7.92 (d, J = 9 Hz, 2H, Ar), 6.83 (d, J = 9 Hz, 2H, Ar), 4.68 (s, 5H, Cp), 4.14 (t, J = 7 Hz, 2H, CH_2OPh), 3.93 (t, J = 7 Hz, 2H, CH_2O_2C), 1.1 - 1.9 (m, 14H, CH_2), 0.82 (t, J = 7 Hz, 3H, CH_3); ^{13}C NMR δ($CDCl_3$) ppm 217.21 (CO), 166.44 (CO_2), 162.77, 131.44, 122.81, 113.96 (Ar), 85.31 (Cp), 68.13, 67.32 (CH_2O), 36.67, 31.80, 29.45, 29.30, 29.18, 29.07, 25.93, 22.61 (CH_2), 14.04 (CH_3), -2.82 ($FeCH_2$); mass spectrum (EI) m/z 482 (P); Found C 64.8%, H 6.8 % Calc for $C_{26}H_{34}O_5Fe$

(M 482.40) C 64.7%, H 7.1%.

5.4.8 Reaction of [CpFe(CO)$_2${(CH$_2$)$_3$OH}] with PPh$_3$

[CpFe(CO)$_2${(CH$_2$)$_3$OH}] (0.13 g, 0.6 mmol.) with PPh$_3$ (0.15 g, 0.6 mmol.) was dissolved in benzene (10 ml). The reaction was heated at reflux for 5 hours and monitored by TLC. The solvent was removed and the resulting brown residue was extracted with ether (20 ml). After filtration, the yellow filtrate was concentrated and transferred to an alumina column. The orange colored band was collected on eluting with ether. An orange-yellow crystalline product, [CpFe(CO)(PPh$_3$){CO(CH$_2$)$_3$OH}] was obtained after removing the solvent under reduced pressure (0.10 g, 37%). mp 124 - 126 °C; IR (CH_2Cl_2) υ(CO) 1914, 1601 cm^{-1}; ^{1}H NMR δ($CDCl_3$) ppm 7.3 - 7.6 (m, 15H, Ph), 4.42 (s, 5H, Cp), 3.27 (br, 2H, CH_2O), 3.05 (m, 1H, $COCH_2$), 2.70 (m, 1H, $COCH_2$), 2.53 (br, 1H, OH), 1.29 (m, 2H, CH_2); ^{13}C NMR δ($CDCl_3$) ppm 220.00 (d, CO), 136.64, 133.20, 129.80, 128.17 (d, Ph), 85.31 (Cp), 64.06 (CO*C*H$_2$), 63.05 (CH_2O), 28.45 (CH_2).

5.5 EXPERIMENTAL DETAILS PERTAINING TO CHAPTER 4

5.5.1 Preparation of Fp3G1OH and Rp3GxOH (where x = 1, 2, 3, 4)

General procedure A mixture of the appropriate Fp3G0Br or Rp3GxBr (2 equiv.), 3,5-dihydroxybenzyl alcohol (1 equiv.), potassium carbonate (3 equiv.), and 18-crown-6 (0.2 equiv.) in acetone was heated at reflux and stirred vigorously for 48 hours. The reaction was monitored by TLC, eluting with a 70% CH_2Cl_2/hexane

solution. After reaction, the solvent was removed under reduced pressure to give a yellow residue (or a dark reddish residue for Fp3**G**1OH). The residue was then extracted with a 70% CH_2Cl_2/hexane solution. After filtration, the filtrate was concentrated and transferred to an alumina column. The polarity of the eluting solvent was gradually increased from 70% CH_2Cl_2/hexane to CH_2Cl_2. The purification procedure for each individual complex is outlined in the following text.

*Fp3**G**1OH* This was prepared from [$CpFe(CO)_2\{(CH_2)_3Br\}$] and purified by column chromatography. The major yellow band was collected and the solvent was removed to give a yellow oil (40%). IR (CH_2Cl_2) υ(CO) 1999, 1938 cm^{-1}; ^1H NMR $\delta(CDCl_3)$ ppm 6.42 (d, J = 2 Hz, 2H, Ar), 6.31 (t, J = 2 Hz, 1H, Ar), 4.69 (s, 10H, Cp), 4.52 (br, 2H, $ArCH_2$), 3.80 (t, J = 7 Hz, 4H, CH_2O), 1.82 (m, 4H, CH_2), 1.38 (m, 4H, $FeCH_2$); ^{13}C NMR δ($CDCl_3$) ppm 217.30 (CO), 160.54, 143.20, 105.07, 100.50 (Ar), 85.36 (Cp), 70.90 (CH_2O), 65.39 ($ArCH_2$), 37.13 (CH_2), -2.55 ($FeCH_2$); mass spectrum (EI) m/z 548 (P - CO)

*Rp3**G**1OH* This was prepared from [$CpRu(CO)_2\{(CH_2)_3Br\}$] and purified by column chromatography. A colorless band was collected and the solvent was removed to give a colorless oil. The white crystalline product was obtained after recrystallization from an ether/hexane mixture at -15 °C (70%). mp 81 - 84 °C; IR (CH_2Cl_2) υ(CO) 2012, 1948 cm^{-1}; ^1H NMR δ($CDCl_3$) ppm 6.49 (d, J = 2 Hz, 2H, Ar), 6.38 (t, J = 2 Hz, 1H, Ar), 5.25 (s, 10H, Cp), 4.61 (d, J = 6 Hz, 2H, $ArCH_2$), 3.86 (t, J = 7 Hz, 4H, CH_2OAr), 2.01 (m, 4H, CH_2), 1.69 (m, 4H, $RuCH_2$); ^{13}C NMR δ($CDCl_3$) ppm 202.09 (CO), 160.60, 143.14, 105.07, 100.51 (Ar), 88.54 (Cp), 71.05 (CH_2OAr),

65.53 ($ArCH_2$), 38.50 (CH_2), -9.33 ($RuCH_2$); mass spectrum (EI) m/z 638 (P - CO); Found C 48.8%, H 4.3% Calc for $C_{27}H_{28}O_7Ru_2$ (M 666.66) C 48.7%, H 4.2%.

Rp3G2OH This was prepared from Rp3G1Br and purified by column chromatography. The major colorless band was collected and the solvent was removed to give a pale yellow oil. A colorless oil was then separated out from CH_2Cl_2/hexane at -15 °C. The final white rubbery product was obtained after drying the oil under high vacuum (70%). IR (CH_2Cl_2) υ(CO) 2012, 1948 cm^{-1}; ^1H NMR δ($CDCl_3$) ppm 6.61 (d, J = 2 Hz, 2H, Ar), 6.55 (d, J = 2 Hz, 5H, Ar), 6.41 (t, J = 2 Hz, 2H, Ar), 5.25 (s, 20H, Cp), 4.96 (s, 4H, $ArCH_2$), 4.62 (d, J = 4 Hz, 2H, CH_2OH), 3.86 (t, J = 7 Hz, 8H, CH_2OAr), 2.01 (m, 8H, CH_2), 1.69 (m, 8H, $RuCH_2$); ^{13}C NMR δ($CDCl_3$) ppm 202.06 (CO), 160.52, 160.16, 143.31, 138.95, 105.72, 105.63, 101.35, 100.72 (Ar), 88.52 (Cp), 71.02 (CH_2OAr), 70.10 ($ArCH_2O$), 65.35 ($ArCH_2OH$), 38.46 (CH_2), -9.34 ($RuCH_2$); mass spectrum (FAB) m/z 1439 (P + 1); Found C 51.1%, H 4.4% Calc for $C_{61}H_{60}O_{15}Ru_4$ (M 1437.42) C 51.0%, H 4.2%.

Rp3G3OH This was prepared from Rp3G2Br and purified by column chromatography. The major colorless band was collected and the solvent was removed to give a pale yellow oil. A colorless oil separated out from CH_2Cl_2/hexane at -15 °C. A white glassy solid was obtained after drying the oil under high vacuum (74%). IR (CH_2Cl_2) υ(CO) 2012, 1948 cm^{-1}; ^1H NMR δ($CDCl_3$) ppm 6.66 (d, J = 2 Hz, 4H, Ar), 6.59 (d, J = 2 Hz, 2H, Ar), 6.54 (d, J = 2 Hz, 11H, Ar), 6.40 (t, J = 2 Hz, 4H, Ar), 5.23 (s, 40H, Cp), 4.96 (s, 4H, $ArCH_2O$), 4.95 (s, 8H, $ArCH_2O$), 4.62 (d, J = 6 Hz, 2H, CH_2OH), 3.85 (t, J = 7 Hz, 16H, CH_2O), 2.00 (m, 16H, CH_2), 1.69 (m, 16H, $RuCH_2$); ^{13}C

NMR δ($CDCl_3$) ppm 202.10 (CO), 160.54, 160.16, 160.10, 138.94, 106.37, 105.69, 100.80 (Ar), 88.55 (Cp), 71.06, 70.18 (CH_2O), 38.47 (CH_2), -9.31 ($RuCH_2$); mass spectrum (FAB) m/z 2922 (P - 2CO), Found C 51.4%, H 4.2% Calc for $C_{129}H_{124}O_{31}Ru_8$ (M 2979.09) C 52.0%, H 4.2%.

Rp3G4OH This was prepared from Rp3**G**3Br and purified by column chromatography. The major colorless band was collected and the solvent was removed to give a pale yellow oil. A colorless oil separated out from CH_2Cl_2/hexane at -15 °C. The final white glassy solid was obtained after drying the oil under high vacuum (66%). IR (CH_2Cl_2) υ(CO) 2012, 1948 cm^{-1}; ^1H NMR δ($CDCl_3$) ppm 6.66 (d, J = 2 Hz, 12H, Ar), 6.59 (d, J = 2 Hz, 2H, Ar), 6.53 (d, J = 2 Hz, 23H, Ar), 6.38 (t, J = 2 Hz, 8H, Ar), 5.21 (s, 80H, Cp), 4.96 (s, 4H, $ArCH_2O$), 4.94 (s, 8H, $ArCH_2O$), 4.93 (s, 16H, $ArCH_2O$), 4.57 (d, J = 6 Hz, 2H, $ArCH_2OH$), 3.83 (t, J = 6 Hz, 32H, CH_2O), 1.98 (m, 32H, CH_2), 1.67 (m, 32H, $RuCH_2$); ^{13}C NMR δ($CDCl_3$) ppm 202.13 (CO), 177.24, 160.54, 160.15, 160.10, 139.13, 138.92, 106.48, 106.46, 106.43, 105.71, 100.79 (Ar), 88.56 (Cp), 71.04, 70.17, 70.07 ($ArCH_2O$), 38.47 (CH_2), -9.37 ($RuCH_2$); Found C 52.7%, H 4.5% Calc for $C_{265}H_{252}O_{63}Ru_{16}$ (M 6062.00) C 52.5%, H 4.2%.

5.5.2 Preparation of Fp3G1Br and Rp3GxBr (where x = 1, 2, 3, 4)

General procedure The appropriate Fp3**G**1OH or Rp3**G**xOH (1 equiv.) with CBr_4 (1.25 equiv.) was dissolved in the minimum volume of THF, followed by PPh_3 (1.25 equiv.). The reaction mixture was stirred at room temperature and monitored by TLC (eluting with 30% CH_2Cl_2/hexane). For the latter generation complexes, a large excess of CBr_4 and PPh_3 was required to drive the reaction to completion. This was

achieved by adding PPh_3 and CBr_4 at a rate of 1.25 equiv. every 10 min., until TLC showed no more starting material. After the reaction was completed, distilled water was added to the reaction mixture, and the aqueous phase was extracted with CH_2Cl_2 twice. The organic phase was then collected and dried over anhydrous $MgSO_4$. After filtration, CH_2Cl_2 was removed under reduced pressure to give a yellow oil. The crude product was purified by column chromatography, eluting with appropriate solvents. The purification details for each individual complex are given in the following text.

Fp3G1Br This was prepared from Fp3G1OH and purified by column chromatography on eluting with a 30% CH_2Cl_2/hexane solution. The major yellow band was collected and the solvent was removed to give a dark yellow oil (72%). The sample appeared to be very unstable. It started decomposing within 20 min. under high vacuum. IR (CH_2Cl_2) υ(CO) 1999, 1938 cm^{-1}; ^1H NMR δ($CDCl_3$) ppm 6.49 (br, 2H, Ar), 6.35 (br, 1H, Ar), 4.75 (s, 10H, Cp), 4.39 (s, 2H, CH_2Br), 3.85 (br, 4H, CH_2O), 1.88 (br, 4H, CH_2), 1.43 (br, 4H, $FeCH_2$); ^{13}C NMR δ($CDCl_3$) ppm 217.30 (CO), 160.45, 139.44, 107.43, 101.42 (Ar), 85.38 (Cp), 70.96 (CH_2O), 37.09 (CH_2), 33.89 (CH_2Br), -2.58 ($FeCH_2$).

Rp3G1Br This was prepared from Rp3G1OH and purified by column chromatography on eluting with a 30% CH_2Cl_2/hexane solution. The major colorless fraction was collected and the solution was concentrated to give a white crystalline solid at -15 °C (65%). mp 107 - 109 °C; IR (CH_2Cl_2) υ(CO) 2012, 1948 cm^{-1}; ^1H NMR δ($CDCl_3$) ppm 6.45 (d, J = 2 Hz, 2H, Ar), 6.31 (t, J = 2 Hz, 1H, Ar), 5.19 (s, 10H, Cp), 4.34 (s, 2H, CH_2Br), 3.79 (t, J = 7 Hz, 4H, CH_2O), 1.95 (m, 4H, CH_2), 1.61 (m,

4H, $RuCH_2$); ^{13}C NMR δ($CDCl_3$) ppm 202.05 (CO), 160.47, 139.45, 107.44, 101.42 (Ar), 88.53 (Cp), 71.09 (CH_2O), 38.44 (CH_2), 33.89 (CH_2Br), -9.39 ($RuCH_2$); mass spectrum (FAB) m/z 731 (P + 1); Found C 43.9%, H 3.6%, Br 11.7% Calc for $C_{27}H_{27}O_6BrRu_2$ (M 729.55) C 44.4%, H 3.7%, Br 11.0%.

Rp3G2Br This was prepared from Rp3**G**2OH and purified by column chromatography. The polarity of the eluting solvent was gradually increased from 30% CH_2Cl_2/hexane to 50% CH_2Cl_2/hexane. The major colorless fraction was collected, concentrated and cooled to -15 °C. A colorless oil separated out and a white rubbery solid was obtained after drying the oil under high vacuum. IR (CH_2Cl_2) υ(CO) 2012, 1948 cm^{-1}; ^1H NMR δ($CDCl_3$) ppm 6.55 (d, J = 2 Hz, 2H, Ar), 6.47 (d, J = 2 Hz, 5H, Ar), 6.34 (t, J = 2 Hz, 2H, Ar), 5.18 (s, 20H, Cp), 4.88 (s, 4H, $ArCH_2O$), 4.34 (s, 2H, CH_2Br), 3.80 (t, J = 7 Hz, 8H, CH_2OAr), 1.94 (m, 8H, CH_2), 1.63 (m, 8H, $RuCH_2$); ^{13}C NMR δ($CDCl_3$) ppm 202.08 (CO), 160.57, 160.06, 139.66, 138.74, 108.16, 105.69, 102.24, 100.82 (Ar), 88.55 (Cp), 71.06 (CH_2OAr), 70.22 ($ArCH_2O$), 38.47 (CH_2), 33.66 (CH_2Br), -9.32 ($RuCH_2$); mass spectrum (FAB) m/z 1445 (P - 2CO); Found C 48.3%, H 4.0%, Br 5.2% Calc for $C_{61}H_{59}O_{14}BrRu_4$ (M 1500.32) C 48.8%, H 4.0%, Br 5.3%.

Rp3G3Br This was prepared from Rp3**G**3OH and purified by column chromatography. The polarity of the eluting solvent was gradually increased from 50% CH_2Cl_2/hexane to 70% CH_2Cl_2/hexane. The major colorless fraction was collected and concentrated. A pale yellow oil separated out from the solution at -15 °C and a white glassy solid was obtained after drying the oil under high vacuum (73%). IR (CH_2Cl_2) υ(CO)

2012, 1948 cm^{-1}; ^1H NMR δ($CDCl_3$) ppm 6.66 (d, J = 2 Hz, 4H, Ar), 6.62 (d, J = 2 Hz, 2H, Ar), 6.57 (t, J = 2 Hz, 3H, Ar), 6.55 (d, J = 2 Hz, 8H, Ar), 6.40 (t, J = 2 Hz, 4H, Ar), 5.23 (s, 40H, Cp), 4.96 (s, 12H, $ArCH_2O$), 4.41 (s, 2H, CH_2Br), 3.86 (t, J = 7 Hz, 16H, CH_2O), 2.01 (m, 16H, CH_2), 1.69 (m, 16H, $RuCH_2$); ^{13}C NMR δ($CDCl_3$) ppm 202.10 (CO), 160.56, 160.18, 138.92 106.46, 105.70, 100.80 (Ar), 88.55 (Cp), 71.05 (CH_2O), 70.21, 70.11 ($ArCH_2O$), 38.48 (CH_2), -9.30 ($RuCH_2$); mass spectrum (FAB) m/z 2988 (P - 2CO); Found C 50.5%, H 4.4% Calc for $C_{129}H_{123}O_{30}BrRu_8$ (M 3041.84) C 50.8%, H 4.1%.

Rp3G4Br This was prepared from Rp3G4OH and purified by column chromatography, eluting with a 50% CH_2Cl_2/hexane solution. The major colorless band was collected and concentrated. A pale yellow oil separated out from the solution at -15 °C and the final white glassy solid was obtained after drying the oil under high vacuum (66%). IR (CH_2Cl_2) 2012, 1948 cm^{-1}. ^1H NMR δ($CDCl_3$) ppm 6.67 (d, J = 2 Hz, 8H, Ar), 6.63 (d, J = 2 Hz, 4H, Ar), 6.54 (d, J = 2 Hz, 25H, Ar), 6.40 (t, J = 2 Hz, 8H, Ar), 5.22 (s, 80H, Cp), 4.96, 4.94 (s, 30H, $ArCH_2O$), 4.38 (s, 2H, CH_2Br), 3.85 (t, J = 7 Hz, 32H, CH_2O), 2.00 (m, 32H, CH_2), 1.68 (m, 32H, $RuCH_2$); ^{13}C NMR δ($CDCl_3$) ppm 202.11 (CO), 160.54, 160.16, 139.08, 138.92, 106.49, 105.70, 100.79 (Ar), 88.55 (Cp), 71.02 (CH_2O), 70.16 70.07 ($ArCH_2O$), 38.46 (CH_2), -9.30 ($RuCH_2$); Found C 52.1%, H 4.2% Calc for $C_{265}H_{251}O_{62}BrRu_{16}$ (M 6124.89) C 52.0%, H 4.1%.

5.5.3 Preparation of Rp3GxC (where x = 0, 1, 2, 3)

General procedure A mixture of the appropriate Rp3GxBr (3 equiv.), 1,1,1-tris(4-hydroxyphenyl)ethane (1 equiv.), potassium carbonate (5 equiv.) and 18-crown-6 (0.3 equiv.) in acetone was heated at reflux and stirred vigorously for 48 hours. The reaction was monitored by TLC, eluting with a 60% CH_2Cl_2/hexane solution. After reaction, the solvent was removed to give a pale yellow residue. The residue was then extracted with a 70% CH_2Cl_2/hexane solution. After filtration, the filtrate was concentrated and transferred to an alumina column. The purification procedure for each individual complex is outlined in the following text.

Rp3G0C This was prepared from $[CpRu(CO)_2\{(CH_2)_3Br\}]$ and purified by column chromatography, eluting with a 50% CH_2Cl_2/hexane solution. The colorless band was collected and concentrated. A pale yellow oil separated out from the solution at -15 °C, and the final white glassy solid was obtained after drying the oil under high vacuum (32%). IR (CH_2Cl_2) 2012, 1948 cm^{-1}; ^1H NMR δ($CDCl_3$) ppm 6.92 (d, J = 9 Hz, 6H, Ar^{CORE}), 6.71 (d, J = 9 Hz, 6H, Ar^{CORE}), 5.19 (s, 15H, Cp), 3.79 (t, J = 7 Hz, 6H, CH_2O), 2.04 (m, 9H, CH_2 + CH_3), 1.68 (m, 6H, $RuCH_2$); ^{13}C NMR δ($CDCl_3$) ppm 202.07 (CO), 157.11, 141.63, 129.57, 113.59 (Ar^{CORE}), 88.53 (Cp), 70.94 (CH_2O), 50.55 (*C*CH3), 38.59 (CH_2), 30.77 (C*C*H3), -9.02 ($RuCH_2$); mass spectrum (FAB) m/z 1097 (P + 1); Found C 55.1%, H 4.2% Calc for $C_{50}H_{48}O_9Ru_3$ (M 1096.14) C 54.8%, H 4.4%.

Rp3G1C This was prepared from Rp3G1Br and purified by column chromatography, eluting with a 50% CH_2Cl_2/hexane solution. The major colorless fraction was collected and concentrated. A pale yellow oil separated out from the solution at -15 °C, and the

final white glassy solid was obtained after drying the oil under high vacuum (70%). IR (CH_2Cl_2) υ(CO) 2012, 1948 cm^{-1}; ^1H NMR δ($CDCl_3$) ppm 6.98 (d, J = 9 Hz, 6H, Ar^{CORE}), 6.85 (d, J = 9 Hz, 6H, Ar^{CORE}), 6.56 (d, J = 2 Hz, 6H, Ar), 6.40 (t, J = 2 Hz, 3H, Ar), 5.25 (s, 30H, Cp), 4.96 (s, 6H, $ArCH_2O$), 3.86 (t, J = 7 Hz, 12H, CH_2O), 2.10 (s, 3H, CH_3), 2.01 (m, 12H, CH_2), 1.69 (m, 12H, $RuCH_2$), ^{13}C NMR δ($CDCl_3$) ppm 202.10 (CO), 160.54, 139.33, 105.69, 100.71 (Ar), 156.87, 142.01, 129.63, 114.02 (Ar^{CORE}), 88.56 (Cp), 71.05 (CH_2O), 70.11 ($ArCH_2O$), 50.66 (CCH_3), 38.49 (CH_2), 30.10 (CCH_3), -9.31 ($RuCH_2$); mass spectrum (FAB) m/z 2192 (P-60); Found C 54.15, H 4.4% Calc for $C_{101}H_{96}O_{21}Ru_6$ (M 2252.28) C 53.9%, H 4.3%.

Rp3G2C This was prepared from Rp3G2Br and purified by column chromatography. The polarity of the eluting solvent was gradually increased from 50% CH_2Cl_2/hexane to 70% CH_2Cl_2/hexane. The major colorless fraction was collected and concentrated. A pale yellow oil separated out from the solution at -15 °C and the white glassy solid was obtained after drying the oil under high vacuum (76%). IR (CH_2Cl_2) υ(CO) 2012, 1948 cm^{-1}; ^1H NMR δ($CDCl_3$) ppm 7.01 (d, J = 9 Hz, 6H, Ar^{CORE}), 6.86 (d, J = 9 Hz, 6H, Ar^{CORE}), 6.67 (d, J = 2 Hz, 6H, Ar), 6.55 (d, J = 2 Hz, 15H, Ar), 6.40 (t, J = 2 Hz, 6H, Ar), 5.22 (s, 60H, Cp), 4.95 (s, 12H, $ArCH_2O$), 4.94 (s, 18H, $ArCH_2O$), 3.86 (t, J = 7 Hz, 24H, CH_2O), 2.11 (s, 3H, CCH_3), 2.01 (m, 24H, CH_2), 1.68 (s, 24H, $RuCH_2$); 13C NMR δ($CDCl_3$) ppm 202.11 (CO), 160.55, 160.14, 138.93, 129.67, 114.01, 106.51, 106.49, 105.71, 100.79 (Ar + Ar^{CORE}), 88.55 (Cp), 71.04 (CH_2O), 70.18 ($ArCH_2O$), 38.47 (CH_2), -9.31 ($RuCH_2$); mass spectrum (FAB) m/z 4509 (P - 2CO); Found C 53.3%, H 4.0% Calc for $C_{203}H_{192}O_{45}Ru_{12}$

(M 4564.57) C 53.4%, H 4.2%.

Rp3G3C This was prepared from Rp3G3Br and purified by column chromatography, eluting with a 60% CH_2Cl_2/hexane solution. The major colorless fraction was collected and concentrated. A pale yellow oil separated out from solution at -15 °C and the final white glassy solid was obtained after drying the oil under high vacuum (54%). IR (CH_2Cl_2) υ(CO) 2012, 1948 cm^{-1}; ^1H NMR δ($CDCl_3$) ppm 7.01 (d, J = 9 Hz, 6H, Ar^{CORE}), 6.87 (d, J = 9 Hz, 6H, Ar^{CORE}), 6.69 (d, J = 2 Hz, 6H, Ar), 6.67 (d, J = 2 Hz, 12H, Ar), 6.54 (d, J = 2 Hz, 33H, Ar), 6.39 (t, J = 2 Hz, 12H, Ar), 5.21 (s, 120H, Cp), 4.94 (s, 42H, $ArCH_2O$), 3.84 (t, J = 7 Hz, 48H, CH_2O), 2.04 (s, 3H, CCH_3), 1.99 (m, 48H, CH_2), 1.67 (m, 48H, $RuCH_2$); ^{13}C NMR δ($CDCl_3$) ppm 202.13 (CO), 160.54, 160.16, 139.09, 138.92, 106.53, 105.70, 100.79 (Ar + Ar^{CORE}), 88.56 (Cp), 71.03, 70.17 ($ArCH_2O$), 38.47 (CH_2), -9.30 ($RuCH_2$); Found C 53.3%, H 4.4% Calc for $C_{407}H_{384}O_{93}Ru_{24}$ (M 9189.15) C 53.2%, H 4.2%.

5.5.4 Preparation of Rp3G4C

A mixture of Rp3G4Br (110 mg, 0.018 mmol.), 1,1,1-tris(4-hydroxyphenyl)ethane (1.8 mg, 0.0058 mmol.), potassium carbonate (320 mg, excess), and 18-crown-6 (49 mg, excess) in acetone (30 ml) was stirred vigorously and heated at reflux for 48 hours. The reaction was monitored by TLC and no change was observed during the reaction. After this time, another portion of 1,1,1-tris(4-hydroxyphenyl)ethane (22 mg, excess) was added into the reaction, and the reaction mixture was stirred and heated at reflux for another 24 hours. The solvent was then removed under reduced pressure to give a pale yellow residue. The residue was extracted with CH_2Cl_2 (*ca.* 20 ml) and

the white precipitate was filtered off. The pale yellow filtrate was concentrated and transferred to an alumina column, eluting with a 60% CH_2Cl_2/hexane solution. The major colorless fraction was collected and concentrated. A pale yellow oil was separated out from the solution at -15 °C and the final white glassy solid was obtained after drying this oil under high vacuum (70 mg, 66%). IR (CH_2Cl_2) υ(CO) 2012, 1948 cm^{-1}; ^1H NMR δ($CDCl_3$) ppm 7.01 (br d, 6H, Ar^{CORE}), 6.84 (br d, 6H, Ar^{CORE}), 6.65 (br, 42H, Ar), 6.52 (br, 69H, Ar), 6.37 (br, 24H, Ar), 5.17 (s, 240H, Ar), 4.91 (br, 90H, $ArCH_2O$), 3.82 (br, 96H, CH_2O), 1.96 (m, 99H, CH_2 and CH_3), 1.66 (m, 96H, $RuCH_2$); ^{13}C NMR δ($CDCl_3$) ppm 202.13 (CO), 160.53, 160.13, 138.93, 106.51, 105.70, 101.63, 100.80 (Ar + Ar^{CORE}), 88.56 (Cp), 71.03, 70.17 ($ArCH_2O$), 38.47 (CH_2), -9.29 ($RuCH_2$); Found C 52.9%, H 4.3% Calc for $C_{815}H_{768}O_{189}Ru_{48}$ (M 18438.31) C 53.1%, H 4.2%.

5.6 REFERENCES

1. J. R. Moss, *J. Organomet. Chem.*, **1982**, *231*, 229.
2. H. B. Friedrich, P. A. Makhesha, J. R. Moss and B. K. Williamson, *J. Organomet. Chem.*, **1990**, *384*, 325.
3. N. M. Doherty, S. A. R. Knox, *Inorg. Synth.*, **1985**, *25*, 179.
4. H. B. Friedrich, K. P. Finch, M. A. Gafoor and J. R. Moss, *Inorg. Chim. Acta*, **1993**, *206*, 225.
5. G. N. Schrauzer, *Inorg. Synth.*, **1968**, *11*, 61.
6. C. G. Pitt, H. H. Seltzman, Y. Sayed, C. E. Twine Jr. and D. L. Williams, *J. Org. Chem.*, **1979**, *44*, 677.
7. A. I. Vogel, *Vogel's Textbook of Pratical Organic Chemistry*, 5th Ed., pp 1073, Longman, London, **1989**.
8. A. Emeran, M. A. Gafoor, J. K. I. Goslett, Y.-H. Liao, L. Pimble and J. R. Moss, *J. Organomet. Chem.*, **1991**, *405*, 237.